Universität Rostock Traditio et Innovatio

Model-based Generation of High-Resolution Flood Flow Characteristics for Small Ungauged Streams in the Northeast German Lowlands

An Automated Approach Based on Available Geodata

Kumulative Dissertation

zur Erlangung des akademischen Grades
Doktor der Ingenieurwissenschaften (Dr.-Ing.)

an der Agrar- und Umweltwissenschaftlichen Fakultät
der Universität Rostock

vorgelegt von M.Sc. Frauke Kachholz

Rostock, 2023

https://doi.org/10.18453/rosdok_id00004530

Gutachter:

Prof. Dr. Jens Tränckner, Universität Rostock, Institut für Wasserwirtschaft

Prof. Dr. Malte Henrichs, Fachhochschule Münster, Institut für Infrastruktur, Wasser, Ressourcen und Umwelt

Prof. Dr. Robert Jüpner, Rheinland-Pfälzische Technische Universität Kaiserslautern Landau, Fachbereich Bauingenieurwesen

Jahr der Einreichung: 2023

Jahr der Verteidigung: 2023

Zusammenfassung

Ein intensivierter Wasserkreislauf aufgrund des Klimawandels und eine beobachtbare Zunahme der Flächenversiegelung infolge der Urbanisierung führen zu häufigeren und stärkeren Hochwasserereignissen. Um den daraus resultierenden Herausforderungen für die Stadt- und Raumplanung gerecht zu werden, ist die Kenntnis gewässerabschnittsspezifischer hydrologischer und hydraulischer Hochwasserkennwerte unerlässlich. Doch gerade für die zahlreichen kleinen Flüsse und Bäche sind diese aufgrund fehlender Messstellen nur selten verfügbar. Es müssen also Wege gefunden werden, um diese Informationslücken flächendeckend zu schließen. Für das Untersuchungsgebiet Rostock und die angrenzenden Gemeinden im Nordostdeutschen Tiefland existieren zwar teilweise bereits statistisch ermittelte Hochwasserkennwerte, jedoch unterliegen diese einem limitierten Gültigkeitsbereich. Um einer ganzheitlichen Betrachtung der Gewässer und ihrer Einzugsgebiete gerecht zu werden, scheint die Nutzung gekoppelter hydrologisch/hydraulischer Fließgewässermodelle ein geeignetes Mittel zu sein. Die besondere Herausforderung hierbei besteht jedoch darin belastbare Modelle aufzustellen, obwohl keine oder nur wenige Messdaten für die Kalibrierung und Validierung zur Verfügung stehen. Anhand eines beobachteten Einzugsgebietes mit vorhandenen Messdaten wurde daher ein Verfahren entwickelt, mit dem größtenteils physikalische Modellparameter auf der Basis verfügbarer Geodaten abgeleitet und deren Zusammenhänge anschließend automatisiert auf unbeobachtete Gebiete übertragen werden können. Auf diese Weise werden räumlich und zeitlich hoch aufgelöste Hochwasserkennwerte für eine ganze Region berechnet. Zwar ist mit der Methode grundsätzlich eine Abnahme der Modellgüte verbunden, jedoch liegt diese im akzeptablen Bereich (Kalibrierungsgebiet: MAE = 0,032 m^3s^{-1}, R = 0,84, NSE = 0,84; Validierungsgebiet: MAE = 0,045 m^3s^{-1}, R = 0,88, NSE = 0,59). Während Basisdurchflüsse und kleine bis moderate Regenereignisse vom Modell gut widergegeben werden, werden die durch Starkregenereignisse hervorgerufenen Spitzendurchflüsse überschätzt. Für die schwächere Modellanpassung kann z. T. der verwendete Input-Niederschlag verantwortlich gemacht werden, da dieser außerhalb des Einzugsgebietes gemessen wurde. Aufbauend auf den generierten Hochwasserkennwerten wurde eine in ein Entscheidungsunterstützungssystem eingebettete GIS-Routine entwickelt, um interaktiv Hochwasserparameter für geplante Landnutzungsänderungen (verbunden mit Bodenversiegelung) zu prognostizieren. Die GIS-Routine verwendet eine vereinfachte Methode zur Abfluss-

und Durchflussberechnung, bietet aber den entscheidenden Vorteil, dass sie ohne Modellierungskenntnisse anwendbar ist. Für Blockregen > 3 h werden auf diese Weise gute bis sehr gute Ergebnisse erzielt, während bei kürzeren, dynamischen Regenereignissen Abweichungen im berechneten Abfluss um bis zu 30 % zu verzeichnen sind.

Abstract

An intensifying water cycle due to climate change and an observable increase in land sealing as a result of urbanization will lead to more frequent and more severe flood events. In order to meet the resulting challenges for urban and land use planning, the knowledge of stream section-specific hydrological and hydraulic flood characteristics is essential. But especially for the numerous small rivers and streams, these are rarely available due to the lack of monitoring stations. Therefore, it is necessary to find ways to close these information gaps comprehensively. For the study area of Rostock and the neighbouring municipalities in the northeast German lowlands, statistically determined flood characteristics already exist in part, but these are subject to a limited range of validity. In order to take a holistic view of the streams and their catchments, the use of coupled hydrological/hydraulic models seems to be suitable. The particular challenge, however, is to establish robust models, although no or only few measured data are available for calibration and validation. Therefore, a method was developed by means of a gauged catchment, with which mostly physical model parameters are derived on the basis of available geodata. These relations are then automatically transferred to unobserved areas. In this way, high spatial and temporal resolution flood characteristics are calculated for an entire region. Although this method is generally associated with a decrease in model fit, the decrease lies within an acceptable range (calibration site: MAE = 0.032 m^3s^{-1}, R = 0.84, NSE = 0.84; validation site: MAE = 0.045 m^3s^{-1}, R = 0.88, NSE = 0.59). While base flows and small to moderate rainfall events are well reproduced by the model, peak flows caused by heavy rainfall are overestimated. However, the input rainfall may be partly responsible for the poorer model fit, since it was measured outside the catchment. Building on the generated flood characteristics, a GIS routine embedded in a decision support system was developed to interactively forecast flood parameters for planned land use changes associated with soil sealing. The GIS routine uses a simplified method for runoff and flow calculation, but has the decisive advantage of being applicable without modelling knowledge. For block rains > 3 h, good to very good results are achieved, while for shorter, dynamic rain events, deviations in the calculated runoff of up to 30 % are recorded.

Danksagung

Zuallererst danke ich Prof. Dr. Jens Tränckner, ohne den diese Arbeit nicht entstanden wäre. Ich danke Dir für die guten Ratschläge, für die Motivation, die konstruktive Kritik und den Raum, den du mir gegeben hast, um eigene Ideen zu entwickeln.

Ebenso möchte ich mich bei der gesamten Arbeitsgruppe Wasserwirtschaft und der Arbeitsgruppe Hydrologie und Angewandte Meteorologie für die freundschaftliche Arbeitsatmosphäre und den interdisziplinären Austausch bedanken. Mit euch hat das Arbeiten (und alles drumherum) wirklich Spaß gemacht.

Mein Dank gilt ebenso Herrn Prof. Dr. Mathias Uhl, Birgitta Hörnschemeyer und Prof. Dr. Malte Henrichs, die die Softwareerweiterung SWMM-UrbanEVA ohne zu zögern bereitgestellt haben und auch für Fragen bereitwillig zur Verfügung standen.

Ich möchte auch den ehemaligen Masterstudentinnen Julia Gehrke (ehemals Ewert) und Kerstin Rautenberg danken, deren Ergebnisse in diese Arbeit eingeflossen sind.

Besonderer Dank gilt zudem Prof. Dr. Konrad Miegel, der mich schon früh im Studium für sein Fachgebiet der Hydrologie an der Schnittstelle zur Wasserwirtschaft begeistert hat.

Table of Content

List of Figures

List of Tables

List of Abbreviations and Symbols

Δt	simulation time step
Ψ_p	peak runoff coefficient
A_b	wetted part of the leaf A_b
ADCP	acoustic doppler current profiler
A_{new}	area of new land use polygon
A_{SC}	area of subcatchment
BauNVO	Baunutzungsverordnung (engl. building use ordinance)
calc	calculated
CP	cross profile
D	thickness of soil layer
DEM	digital elevation model
DSS	decision support system
DWA	Deutsche Vereinigung für Wasserwirtschaft, Abwasser und Abfall e.V.
$E_{I,a}$	actual interception
$E_{I,p}$	potential interception
EPA	United States Environmental Protection Agency
E_{peak}	peak error
$E_{S,a}$	actual soil evaporation
$E_{S,p}$	potential soil evaporation
$E_{STI,a}$	actual vegetation-specific evapotranspiration
$E_{STI,p}$	potential plant-specific evapotranspiration
ET	evapotranspiration
$E_{T,a}$	actual transpiration
$E_{T,p}$	potential transpiration
ET_0	potential grass reference evapotranspiration
E_{Vol}	volume error
$E_{W,a}$	actual evaporation of free water surface
$E_{W,p}$	potential evaporation of free water surface
GIS-DSS	GIS-based expert support system
GPS	Global Positioning System
GPS_meas.	measured terrestrially with GPS
GW	groundwater
H_{CB}	height of channel bottom above aquifer bottom
HEC	US Army Corps of Engineers - Hydrologic Engineering Center
H_{GW}	groundwater level above aquifer bottom
HMS	Hydrologic Modeling System
h_{pond}	height of ponding surface water
H_{SW}	height of surface water at receiving node above aquifer bottom
I	potential interception height
Kc	crop factor
KOSTRA	heavy rainfall regionalization for Germany (German: Koordinierte Starkniederschlagsregionalisierung und -auswertung)
LAI	leaf area index
LAI_{doy}	LAI corresponding to day of year

LID	low impact development
MAE	mean absolute error
n	number of measurement data
NSE	Nash-Sutcliffe efficiency
obs	observed (measured)
P	precipitation
P_{net}	precipitation subtracted by interception losses
Q_{calc}	calculated flow
Q_{diff}	aggregated runoff difference
Q_{free}	flow rate that would additionally fit into the cross profile at maximum flow
$Q_{free,plan}$	flow that would still fit in profile in plan state
Q_{full}	maximum possible flow at normal flow (water level gradient = bottom gradient)
Q_{GW}	lateral groundwater flow
$Q_{max,act}$	maximum flow in actual state
$Q_{max,plan}$	maximum flow in plan state
$Q_{max,SWMM}$	maximum flow calculated with SWMM
$Q_{max,SWR}$	maximum flow calculated with the SWR
Q_{obs}	observed flow
R	correlation coefficient
RAS	River Analysis System
r_{diff}	runoff rate difference per pixel
ri_{max}	maximum rainfall intensity per area
r_{max}	maximum runoff rate per area
$R_{max,act}$	maximum direct runoff (surface runoff)
$r_{max,act}$	maximum runoff rate per pixel in actual state
$R_{max,plan}$	maximum runoff rate in plan state
$r_{max,plan}$	maximum runoff rate per pixel in plan state
SCF	vegetation-covered fraction
SCS	Soil Conservation Service
$S_{I,a}$	actual intercept height
S_L	leaf storage coefficient
S_{max}	max. interception height
SWAT	Soil & Water Assessment Tool
SWMM	Storm Water Management Model
SWR	Storm Water Routine
WIN	watercourse identification number
W_{rel}	relative soil moisture
θ	actual moisture content
θ_{FK}	moisture content at field capacity
θ_{WP}	moisture content at wilting point
Ψ_p	peak runoff coefficient

1 Introduction

1.1 Preface

Floods have the potential to cause fatalities, relocation of people, environmental damage and seriously threaten economic development [1]. While climate change and the reduction of the soil's natural water retention capacity due to land use changes (particularly sealing) contribute to increasing the probability of the occurrence of flood events, certain human activities, such as the increase in assets in flood plains (buildings and infrastructure) amplify their adverse impacts [1; 2]. Unlike 15 years ago, it is now considered scientifically proven that the current climate change is man-made [3], as "the scale of recent changes across the climate system as a whole and the present state of many aspects of the climate system are unprecedented over many centuries to many thousands of years" [4]. They are directly related to anthropogenic greenhouse gas emissions, which are causing a global temperature increase and thus an intensification of the hydrological cycle. The effects are already being manifested in an increase in extreme weather events.

From 1970 to 2019, both the number of disasters in Europe and the associated total economic costs attributed to weather-, climate- and water-related disasters on average have increased [5]. Floods were the most common cause of recorded natural disasters (38 %), followed by storms, extreme temperatures, wildfires, landslides and droughts. Likewise, floods caused the highest economic losses (27 %). In comparison, however, extreme temperatures were accountable for the highest number of deaths (93 %) [5]. In the same period, the most destructive flood in Europe was recorded in Germany in 2002 along sections of the Elbe River [5]. It cost the lives of at least 45 people [6; 7]. Devastating damage due to floods can also occur to smaller rivers and streams. This was recently demonstrated by another "flood of the century" in July 2021 in western Germany along some tributaries of the Rhine. According to initial estimates, the insurance costs are about the same as for the 2002 event [8]. Worse is the loss of more than 180 lives [8].

Scientists and politicians around the globe are convinced that flood-causing heavy rainfall will occur more frequently and be more intense in the future [4; 8–11]. In Germany, observations have shown that precipitation has increased by 11 % since 1881, with an increase mainly in the winter months (up to 30 % in some regions) and a decrease in the summer months [12]. Regarding the number of heavy rain days per

year until the end of the 21st century, different climate models come to different results. Some models show an increase, others a decrease compared to the reference period 1961 to 1990. The range of this change spans from 0 days to +5 days for Germany [13].

Unlike climate change, land use changes in watersheds are comparatively rapid and thus can cause abrupt hydrologic and hydraulic changes. Land use change shows different trends in different regions of the Earth [14]. In Europe, increasing urbanisation can be observed at the expense of agricultural land [15; 16]. Urbanisation is understood as an extension of urban areas, including both sealed areas, such as traffic, residential and commercial areas, as well as unsealed areas, such as urban green spaces, sports and leisure facilities. Urbanisation is not only a consequence of population growth, but also of lifestyles that take up more space in a growing economy [17]. Accordingly, urban sprawl has increased even in regions with declining populations [17]. In the context of urbanisation or urban sprawl, the impermeabilisation of the soil plays an important role, as it has a significant impact on the water balance and especially on surface runoff. About 45.1 % of the settlement and traffic areas in Germany are sealed, i.e. permanently covered by impermeable artificial material such as asphalt or concrete [18]. In relation to the total area, this corresponds to a degree of sealing of 5.11 %, which makes Germany one of the most sealed countries in Europe, behind Malta and the Benelux countries [19].

What is certain is that the trends of both processes – climate change and urbanisation – lead to an aggravation of the hydrologic and hydraulic situation in rivers and streams and their catchments. They contribute to a more frequent and more severe occurrence of floods (increase in peak discharges), and an increase in the damage potential. At the same time, there is a long-term tendency for a decrease in base flow due to reduced groundwater recharge.

With regard to climate change, the challenge can only be faced at the global level. With the Paris Climate Agreement, 195 countries have pledged to take joint action to keep global warming well below 2 degrees compared to pre-industrial times [20; 21]. However, there are also critical voices regarding the agreement, as climate targets are binding under international law, but non-compliance does not result in any sanctions, which is why they are considered to be difficult to achieve [22].

Unlike climate change, the adverse effects of urbanisation on the water balance and flood risk can be effectively avoided or mitigated at the level of municipal planning. In

Germany, the development plan (German: Bebauungsplan) regulates the type and extent of building use for parts of the municipality. Here, urban planning concerns (e.g. permissible size, width and depth of the building plots) are specified in a binding manner. The Building Use Ordinance (German: Baunutzungsverordnung, abbreviation: BauNVO) specifies the provisions of the development plan and becomes an integrated part of it. Among other things, it stipulates the permissible degree of sealing per parcel of land (§ 19 BauNVO [23]). In order to avoid unnecessary costs and damage, it is important to harmonise urban planning and architecture with the objectives of rainwater management as early as possible. In this respect, the DWA code of practice 102-1 [24] requires to keep changes to the local, near-natural water balance as low as possible, both quantitatively and qualitatively. To achieve this, restrictions and measures which limit land sealing and promote decentralized water retention, such as the designation of green roofs, swales and infiltration trenches, etc., can be fixed in advance.

However, construction planning requires that the water management conditions for the designated area are available as boundary conditions at the beginning of the planning process [24]. Yet, in the case of smaller, ungauged receiving waters, knowledge about the flow regime (in particular flood characteristics) is often rather sparse. To fill the gaps, (GIS-based) statistical regression methods that relate flood peaks to various watershed characteristics (area and shape of the basin, slope, drainage density, etc.) are preferred for determining flood peak discharges [25]. The application of these conceptual models is associated with certain limitations (cf. chap. 1.2.1.1) and they do not allow a clear causal link between land use change and hydraulic impact. Furthermore, especially rivers and streams in lowlands with their numerous culverts, pipelines, reservoirs, etc. require a hydrodynamic approach to describe backwater effects. Coupled hydrological/hydraulic models can provide a solution here and promote a holistic view of the river or stream and its basin, as demanded by the European Water Framework Directive [26] and the Flood Risk Management Directive [1]. While the input data for hydrological models (DEM, land use, soil types, groundwater information) are often available as geodata, the setup of hydraulic models involves a series of input data that are time-consuming and cost-intensive to acquire. This refers to the watercourse geometries of the open cross-sections, which are typically recorded by terrestrial measurements. In the case of culverts and pipelines, usually only the location is documented; diameter, profile type and elevation data are often completely missing or – especially in the case of older

structures – have not yet been digitally recorded. But procuring geometry data is not the only problem. Typically, every model needs measurement data for calibration and validation – at least flow and at best also water level measurement data. Whereas on superior rivers like the Rhine for example, a gauge is installed on average every 30 km [27], smaller tributaries often have no monitoring station at all. In order to be able to set up and apply reliable models for such unobserved streams, largely physically based models should be used to limit the need for empirical model calibration.

When dealing with hydrological/hydraulic models, special expert knowledge is required. This makes the application in administrations difficult, especially as they often have little time to deal with modelling. Thus, simpler tools are needed to be able to answer crucial water management questions (e.g. approval of discharges) by means of pre-processed algorithms. Since the use of GIS software is nowadays widespread in the environmental sector in public authorities, it appears appropriate to make the modelling results and simplified evaluation routines available via GIS tools. These should be accessible to all concerned authorities and stakeholders in order to have a common basis for discussion.

This thesis is part of the PROSPER-RO research project [28] funded by the German Federal Ministry of Education and Research. The objectives of this project are, among others, to create a hydrologic and hydraulic database for planning processes (e.g. processing of water permits) and to develop and provide a GIS-based expert support system (GIS-DSS) as a shared data and planning platform.

1.2 State of the Art

1.2.1 Flood Flow Characteristics for Ungauged Basins

The determination of flood characteristics for unobserved areas is a complex task that has already been tackled by many scientists. Accordingly, there is a wide range of different regionalization methods that deal with transferring hydrological information from gauged to ungauged watersheds. Hydrologic information can be either the model parameters or the general structure of models that estimate hydrologic responses (e.g. peak flow). Common to all methods is that a certain homogeneity of the sites to be compared is assumed (similar climate, geology, topography, vegetation and soils). [25]

1.2.1.1 Common Regionalisation Methods

In many European countries, statistical regression methods that relate flood peaks to various catchment characteristics are commonly used to determine flood discharges and flows [25]. Linking area-related information with hydrological data from point measurements simultaneously enables the interpolation of point data to the area. Thus, the (peak) runoff per catchment area can be calculated. In Germany, such regionalized flood characteristics are already available for several federal states (cf. Hesse [29], Baden-Württemberg [30]), including Mecklenburg-Western Pomerania [31], where the study area of the present work is located. The advantage of the methods is that they use available geospatial data, making them readily applicable to relatively large areas, but they also come with some limitations (cf. [30]):

- Regionalization methods can only describe average (runoff) behaviour; local and area-specific small-scale factors can usually not be adequately represented. The smaller the catchment area, the greater the impact of the area's characteristics on runoff. According to the data publishers, they are therefore not applicable to catchments with areas smaller than approx. 5 km^2 [30; 31] to 15 km^2 [29].
- The hydraulics of the watercourse, i.e. the propagation of the flood wave in the flow cross-section, is not taken into account but plays a decisive role, since particular structures such as pipelines and culverts can cause backwater when overloaded and thus have a mitigating effect on flood peaks in the lower reaches (often also associated with overflow in the upper reaches).
- Concrete measure planning, such as flood protection planning, requires detailed and comprehensive runoff parameters. For the most part, the regionalised runoff characteristics cannot be used directly as a basis for dimensioning as no information on runoff hydrographs, runoff fill or water levels is provided.
- In urban areas, regression based regionalisation methods are not applicable, as no reliable results can be achieved without knowledge and inclusion of anthropogenic stormwater drainage systems and inflows (including controlled flood retention reservoirs).
- We are dealing with conceptual models, which do not follow a physical cause and effect principle and are therefore not or only conditionally scenario capable.

To circumvent the disadvantages mentioned above, coupled regionalized hydrological/hydraulic models seem to be a good solution, but the challenge of setting up robust models for ungauged basins still persists.

1.2.1.2 Coupled Rainfall-Runoff and Stream Flow Models for Ungauged Basins

Normally, the effort involved in model setup is comparatively high, which is why they are typically only used for individual sites and detailed investigations. The reward, however, is a scenario-capable planning tool which allows a holistic view of the stream system and its basin.

Generally, simulation models can be structurally assigned to one of three categories:

- conceptual models
- semi-deterministic (or conceptual process-based) models
- deterministic (or physically based) models

Conceptual models represent hydrological processes with simplified concepts such as storage cascades. Their empirical relations and their parameters are determined experimentally and capture system states as an interaction of multiple physical factors (black box). They must be calibrated and the parameterisation can only be transferred to other areas to a limited extent [32]. Semi-deterministic models generally explicitly represent the sub-processes of rainfall-runoff and river flow. Yet, they also incorporate simplified conceptual elements. Physically based models aim to represent hydrological processes in space and time as accurately as possible on the basis of physical equations [33]. Their parameters are governed by a cause-and-effect principle and are measurable, which means less effort is required for calibration and a parameter transfer to further areas is possible and reasonable [34]. The type of model used depends on the task or objective, the dominant processes in the catchment, the availability of data, the budget and also on the experience of the researcher. The question now arises about how reliable models can be generated if flow measurement data for calibrating the models are not (or only sporadically) available. Three options coexist (cf. [35]), but they all have their advantages and disadvantages:

1. a-priori model parameter estimation
2. the use of (dynamic) proxy data
3. transfer of model parameters from gauged, (neighbouring) watersheds

Regarding point 1: This is often the common practice when time and budget are tight. In this case, it is strongly recommended to visit the catchment and the stream in question to "read the landscape" and get a good understanding of the dominant processes. The better the process understanding is and the more experience the modeller has with calibrating similar models, the better the results will be. An interesting experiment was reported by Duan et al. [36]. They conducted a study for 12 different basins in the south-eastern United States, asking hydrologists to simulate the daily runoff at a number of different locations using hydrologic models. Within the project, hydrometeorological data as well as basin land surface characteristics data required for model setup and parameter estimation were provided; local runoff data were not supplied for the time being. The results were compared with simulations using the same models where calibration to local runoff data was allowed. Both sets of simulations were then compared to measured discharge data. The Nash-Sutcliffe Efficiency (see 2.2.4, Table 4 and Table 5) was calculated to assess the model fit and consequently the goodness of fit of the model parameters. The median NSE of the daily runoff using a priori parameters (without calibration) was 0.2 – 0.6 for the different catchments and models used [35]. After calibration to local runoff, the median NSE improved to 0.4 – 0.75 [35]. The comparisons allow a quantification of the improvement in model performance through calibration.

Regarding point 2: The use of dynamic proxy data for model calibration refers to the use of surrogate data if flow data is missing, such as regionalized, statistically determined runoff hydrographs or measured physical data, such as groundwater levels, evaporation (indirectly calculated via data from weather stations or remotely sensed), water level (from field measurements or remotely sensed) and inundation patterns (remotely sensed). For example, Sun et al. [37] apply a coupled hydrologic / hydraulic model, which is calibrated using satellite radar altimetry observations of river water level at basin outlet as a substitute of streamflow. They achieved a "fairly reasonable streamflow estimation" with this kind of proxy data. Waseem et al. [38] coupled a physically based hydrologic model (MIKE SHE) with a hydrodynamic streamflow model (MIKE 11) in order to calibrate groundwater levels and river flows for the Tollense river catchment in the north-east German Lowlands in parallel. For the period 2010 – 2017 the water balance error amounts to less than 2 %.

The use of soft data or qualitative information can also be very useful in the context of parameter estimation. For example, citizen reports can be used to identify

inundation areas or a field survey serves to estimate the extent of periodic floodplains. The latter type of information is not dynamic, but still helps to verify model results.

Regarding point 3: The transfer of model parameters from gauged watersheds has already been in the focus of other studies. Johannessen et al. [39] tested the transferability of SWMM model parameters (official SWMM version without UrbanEVA) by calibrating model parameters for identical roof build-ups but different geometries and climates across Norway (Bergen, Oslo, Trondheim and Sandnes), assuming that if model parameters were comparable this would indicate that these were true material constants. Individually calibrated models reproduced the runoff hydrograph more or less well (NSE 0.56 – 0.96) for single rainfall events, while the long-term simulation produced relatively large volume errors due to inadequate representation of evapotranspiration in the official SWMM version. Cross-validations were performed, transferring parameters from calibration sites to validation sites - with unsatisfactory performance (NSE < 0.5). Better results were achieved by "multi-site calibrations" with artificially combined and normalized runoff time series of all comparable roofs (NSE > 0.5). Additionally, material properties such as porosity, field capacity and wilting point were measured in laboratory tests and directly compared with the corresponding calibrated model parameters. Only field capacities were found to be within a comparable range to the calibrated values. Table 1 briefly summarizes the different approaches and results of the study.

Table 1. Different approaches and corresponding NSE in transferring SWMM model parameters between green roofs with similar structure (after [39]).

1)	manual calibration for each individual catchment	NSE 0.56 – 0.96 (satisfactory)
2)	cross-validations (parameter transfer from calibration sites to validation sites)	NSE < 0.5 (not satisfactory)
3)	multi-site calibrations (using artificially combined and normalized time series of all comparable roofs)	NSE > 0.5 (satisfactory)
4)	comparison of calibrated parameters from 1) with laboratory measured material properties (porosity, field capacity and wilting point)	Only field capacities within a comparable range to the calibrated values (not satisfactory)

Due to the “large variability in obtained model parameters, large volume errors and the fact that the calibrated model parameters did not directly correspond to

measured material properties" the authors announce concerns about the general validity of the SWMM LID module for green roofs [39].

Another study was conducted in Belgium with the aim of assessing the transferability of SWAT model parameters for simulating the impact of land use on catchment hydrology [40]. The authors tested the transferability of main controlling parameters within the catchment, a neighbouring catchment and a catchment under a different environmental setting. Transfer within the catchment and to a neighbouring catchment gave a reasonable performance (NSE $\sim$ 0.7), but the transfer between catchments with different environmental conditions was problematic (NSE $\sim$ 0.35 – 0.5) especially for the simulation of base flows.

Andrianaki et al. [41] investigated the application and transferability of SWAT in a partially glaciated alpine catchment in Switzerland characterized by extreme climatic conditions and steep terrain. They used an upscaling approach by calibrating (NSE = 0.84) and validating (NSE = 0.85) an approximately 10 km^2 catchment and then transferring the calibrated parameters to an approximately 100 km^2 basin that includes the smaller one. A comparison of the stream flows measured at the outlet of the larger area with the simulated flows showed an overall deterioration of the model performance with an NSE of 0.49, but the result was still considered acceptable. One of the main reasons identified for the deterioration in model performance was that SWAT does not differentiate between snow and glacier dynamics, as "runoff in spring and early summer (May, June) comes mainly from snowmelt and in July and August from glacier melt".

In practice, less complex conceptual lumped models are preferred to predict streamflow in ungauged basins [25]. These usually only offer simplified flow routing methods (e.g. Manning-Strickler) without the possibility of predicting water levels or incorporating backwater effects. So far, no approaches are known from literature that use model parameter transfer for a coupled hydrological rainfall-runoff model and hydrodynamic stream model to calculate runoff and water level in an unobserved catchment. However, it seems reasonable to assume that this could be successful if at least the decisive processes are represented by the models in a physically well-founded way.

1.2.2 Selection of a Suitable Software Package for Simulating Runoff and Stream Flow

As part of a preliminary study, an evaluation matrix (Table 2) was developed to help select the best suitable software for the defined objectives (cf. chap. 1.3). In order to ensure a broad usability of the models to be set up, especially in the responsible lower water authorities and water and soil associations, the software of choice had to be an open source solution. Ultimately, three software packages were examined in detail: 1) a combination of the rainfall-runoff model HEC-HMS [42] and hydrodynamic flow model HEC-RAS [43] (developed by the US Army Corps of Engineers, Hydrologic Engineering Center), 2) SWAT - the Soil & Water Assessment Tool [44] (developed for the U.S. Department of Agriculture) and 3) SWMM – the Storm Water Management Model (developed by the U. S. Environmental Protection Agency). While the HEC and the SWMM packages were tested for suitability in preparation using a small sample catchment (cf. [45]), the suitability of SWAT was assessed by interviewing an applicant and reviewing literature.

By including a weighting factor into the evaluation, it is possible to incorporate a certain degree of subjectivity. Very important features were therefore multiplied by a factor of 3, moderately important ones by 2 and less important ones were multiplied by 1.

Table 2. Evaluation matrix for the selection of suitable open source software (weighting: 1 = less important, 2 = moderately important, 3 = very important; w. w. = with weighting, w/o w. = without weighting).

	Criteria	Weigh-ting factor	Combination HEC-HMS/ HEC-RAS		SWAT		SWMM	
			w/o w.	w. w.	w/o w.	w. w.	w/o w.	w. w.
1. General criteria								
1.1	Open Source	3	1	3	1	3	1	3
1.2	Graphical user interface	1	1	1	0	0	1	1
1.3	GIS-interface/-Plug-in	1	1	1	1	1	1	1
1.4	Long-term simulation	2	0.5[1]	1	1	2	0.5[2]	1
1.5	Rainfall scenarios	3	1	3	1	3	1	3

[1] reasonable long term results only for basins /streams without groundwater influence

[2] reasonable long term results only for mostly unvegetated areas

	Criteria	Weigh-ting factor	Combination HEC-HMS/ HEC-RAS		SWAT		SWMM	
			w/o w.	w. w.	w/o w.	w. w.	w/o w.	w. w.
1.6	Land use scenarios	3	1	3	1	3	1	3
1.7	Derivability of input data from geodata	3	1	3	1	3	1	3
1.8	External access to input database	1	1	1	1	1	1	1
1.9	External access to output database	1	0	0	1	1	0	0
1.10	Online exchange platform/ user-community available	1	1	1	1	1	1	1
1.11	Reference manual	1	1	1	1	1	1	1
1.12	Possibility of automating model setup	3	1	3	1	3	1	3
1.13	Model stability/ robustness	3	0.5	1.5	1	3	1	3
1.14	Acceptable computing time	3	0.5	1.5	1	3	1	3
2. Rainfall-runoff model								
2.1	Actual land use-dependant evapotrans-piration	3	1	3	1	3	0	0
2.2	Wetting loss	1	1	1	1	1	1	1
2.3	Depression storage	2	1	2	1	2	1	2
2.4	Surface runoff	3	1	3	1	3	1	3
2.5	Urban drainage (sealed surface)	2	1	2	1	2	1	2
2.6	Soil infiltration	2	1	2	1	2	1	2
2.7	Soil water/ stream exchange (intermediate runoff)	1	1	1	1	1	0	0
2.8	Agricultural tile drainage	2	1	2	1	2	1	2
2.9	Groundwater recharge	3	0.5	1.5	1	3	1	3

	Criteria	Weighting factor	Combination HEC-HMS/ HEC-RAS		SWAT		SWMM	
			w/o w.	w. w.	w/o w.	w. w.	w/o w.	w. w.
2.10	Groundwater/ stream exchange (base flow)	3	0.5	1.5	1	3	1	3
3. Hydrodynamic transport model								
3.1	Channel flow (open natural cross sections)	3	1	3			1	3
3.2	Sewer network simulation	1	1	1			1	1
3.3	transient, non-uniform (dynamic wave/ Saint-Venant-equation)	3	1	3			1	3
3.4	Kinematic wave/ Manning-Strickler	1	1	1	1	1	1	1
3.5	Pumping stations	2	1	2			1	2
3.6	Culverts / pipes	2	1	2			1	2
3.7	Weirs	2	1	2			1	2
3.8	Time-varying channel roughness (k_{st})	1	1	1			0	0
4. Results								
4.1	Flow time series	1	1	1	1	1	1	1
4.2	Water level time series	1	1	1	0	0	1	1
4.3	Flow velocity time series	1	1	1	0	0	1	1
4.4	Channel capacity (%)	1	0	0	0	0	1	1
Sum			31.5	61	25	52	31.5	63

Without weighting, the combination of HEC-HMS and HEC-RAS and SWMM seems to be about equally well suited for the task. The SWAT software has its main focus on the simulation of water quantity and quality in agriculture dominated landscapes. It is described as “physically based […] infused with key empirical routines” [46]. The software has the major disadvantage of not offering the possibility to simulate hydrodynamic flow; it only offers simple routing techniques. Although coupling with

an external hydrodynamic flow model would be possible (cf. [47–49]), this was not desired due to deteriorated model stability. One software alone usually runs well, but coupling it with other software packages often results in stability problems or the computation time step has to be screwed down so far that the processing time increases drastically. This is the experience of coupling physics-based models MIKE SHE with MIKE 11 (by DHI) in the frame of a former research project (named KOGGE [50]). The reason we still considered the HEC combination was the assumption that the two software packages are well compatible with each other. However, within the scope of a preliminary study, we found out that the stability of the coupled HEC model decreased just as significantly. Subject of the study was the automated setup and application of a geodata-based coupled HEC-HMS and HEC-RAS model using the example of a subcatchment of the Schmarler Bach [45]. In contrast to the original idea, the stream system had to be greatly simplified in order to obtain a stable model. External sources also confirm that numerical instabilities, numerical errors or mass balance errors can occur when linking different systems (cf. [51]). This difficulty is particularly detrimental to the repetitive process of manual model calibration and slows progress considerably.

Nevertheless, the HEC software has advantages in calculating actual land use dependent evapotranspiration (ET), while SWMM incorporates a better algorithm for computing groundwater and drainage flow to the stream. The latter is of particular importance, as the investigation area is located in the lowlands and therefore groundwater recharge plays a significant role in the water balance and stream flow regime. Especially for long-term simulations, it is important that the water balance components are correctly represented. The reason why the HEC combination was given only 0.5 points in this regard (Table 2, No. 1.4) is that long term modelling, although technically possible, does not provide meaningful results for cross seasonal simulations as groundwater recharge and storage are not calculated correctly. In this context, evaporation calculation in SWMM should also be criticized, as the software is not capable of calculating the actual evapotranspiration depending on the land use (e.g. arable land, grassland, forest, residential area etc.). For predominantly agricultural catchments, this approach is insufficient, since different stands evaporate significantly differently and thus allow different amounts of groundwater recharge.

Great importance is also attached to the application of the dynamic wave method (Saint-Venant-equation) for the calculation of hydrodynamic stream flow, since we

are dealing with rather low bed gradients and therefore backwater effects often have to be considered. Here, both packages (HEC and SWMM) are on an equal level. A plus point goes to HEC-RAS though, because of the ability to take into account a yearly variation of the river bed roughness (manning value). This is especially relevant for streams that are heavily weedy in summer, as also observed in our study area. Since we are not focussing on calibrating the water levels as accurately as possible throughout the year, but only want to reproduce the particularly high water levels as well as possible, we can accept this shortcoming.

In the end, the decision was made in favour of SWMM because the software fully meets all of the priority criteria (weighting factor = 3) – with only one exception: the calculation of actual land-use-dependent evapotranspiration. And this is where the new extension developed by the University of Applied Sciences Münster, SWMM-UrbanEVA, sets in (chap. 2.2.2.2). It was developed especially for blue-green infrastructures in urban areas and aims to more accurately simulate urban vegetation evapotranspiration [52].

1.3 Objectives and Structure

This cumulative dissertation consists of three scientific articles (Figure 1). The first article (chapter 2) investigates whether SWMM-UrbanEVA is suitable to represent the water balance variables for an agricultural influenced catchment in the northeast German lowlands through the more detailed evapotranspiration calculation. Previously, the tool was applied only on small scales (e.g. green roofs) [53].

The objectives can be stated as follows:

- model parameterization on the basis of available geodata
- accurate simulation of water balance variables
- good agreement of simulated and measured flows
- development of a scenario and long-term capable model

Following the successful application of SWMM-UrbanEVA in an example area, article ll (chapter 3) is dedicated to the development of an approach to compute high-resolution flood characteristics (maximum flow, maximum head, maximum capacity, degree of filling, etc.) for ungauged watersheds on the basis of a scenario-capable model. Objectives in this context are:

- derivation of physical model parameters from available geodata and transfer of their dependencies to unobserved sites
- automation of model setup and transfer procedure

The flood characteristics for the actual state form the basis for article lll (chapter 4), which aims to develop an interactive GIS-based algorithm capable of calculating flood characteristics for planned small-scale land use changes associated with soil sealing. The forecasting tool shall

- be embedded in a web-based decision support system (DSS),
- be applicable by practitioners who do not have modelling skills,
- generate reliable results,
- deliver and illustrate results in a matter of seconds and
- provide the ability to compare variants.

Subsequently, a detailed discussion of errors and a comparison of the implemented methods with external work follows. The work completes with an outlook.

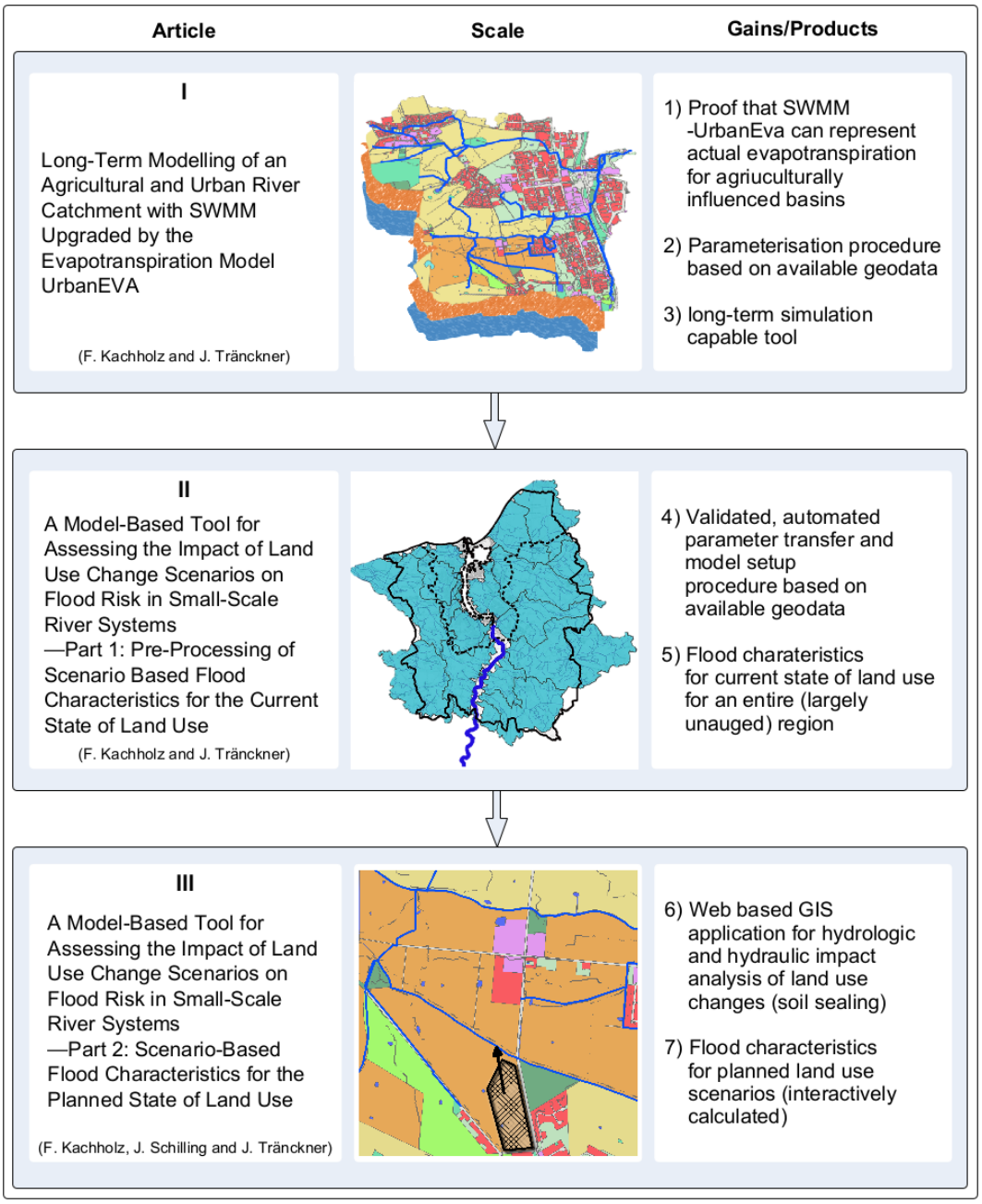

Figure 1. Overview of publications and related products (from catchment to region to land use planning scale).

Chapter 2 is based on:

F. Kachholz and J. Tränckner (2020) Long-Term Modelling of an Agricultural and Urban River Catchment with SWMM Upgraded by the Evapotranspiration Model UrbanEVA. Water, 12(11), 3089; Available from DOI: https://doi.org/10.3390/w12113089

Author Contributions: Conceptualization, F.K.; methodology, F.K. and J.T.; validation, F.K.; formal analysis, F.K.; investigation, F.K.; resources, F.K.; data curation, F.K.; writing—original draft preparation, F.K.; writing—review and editing, J.T.; visualization, F.K.; supervision, J.T.; project administration, J.T.; funding acquisition, J.T.

Chapter 3 is based on:

F. Kachholz and J. Tränckner (2021) A Model-Based Tool for Assessing the Impact of Land Use Change Scenarios on Flood Risk in Small-Scale River Systems—Part 1: Pre-Processing of Scenario Based Flood Characteristics for the Current State of Land Use. Hydrology, *8*(3), 102; Available from DOI: https://doi.org/10.3390/hydrology8030102

Author Contributions: Conceptualization, F.K. and J.T; methodology, F.K.; software, F.K.; validation, F.K.; formal analysis, F.K.; investigation, F.K.; resources, F.K.; data curation, F.K.; writing—original draft preparation, F.K.; writing—review and editing, J.T. and F.K.; visualization, F.K.; supervision, J.T.; project administration, J.T.; funding acquisition, J.T.

Chapter 4 is based on:

F. Kachholz, J. Schilling and J. Tränckner (2021) A Model-Based Tool for Assessing the Impact of Land Use Change Scenarios on Flood Risk in Small-Scale River Systems—Part 2: Scenario-Based Flood Characteristics for the Planned State of Land Use. *Hydrology*, *8*(3), 130; Available from DOI: https://doi.org/10.3390/hydrology8030130

Author Contributions: Conceptualization, F.K. and J.T.; Methodology, F.K. and J.S.; Software, F.K. and J.S.; Validation, F.K.; Formal analysis, F.K.; Investigation, F.K.; Resources, F.K.; Data curation, F.K.; Writing—original draft preparation, F.K.; Writing—review and editing, J.T.; Visualization, F.K.; Supervision, J.T.; Project administration, J.T.; Funding acquisition, J.T.

In order to improve readability, the articles are presented in a harmonized typeface. I.e. equation, figure and table designations are numbered consecutively. Likewise, citations or sources are numbered consecutively and listed at the end of this work.

2 Long-Term Modelling of an Agricultural and Urban River Catchment with SWMM Upgraded by the Evapotranspiration Model UrbanEVA

2.1 Introduction

The storm water management model (SWMM) was originally developed for the simulation and evaluation of storm runoff and sewer hydraulics in urban areas [54]. Since the introduction of SWMM in 1971, it has been continuously improved and thus opens up more and more fields of application. One of the biggest advantages of SWMM is that it combines both a hydrological rainfall-runoff model with a hydrodynamic drainage model in one software. This makes the numerical calculation very effective and stable, as no external coupling is necessary. Besides the modelling of urban infrastructure, like pipes, pumps, flow dividers and storage units, etc., it also allows the modelling of open streams with natural cross sections. Furthermore, the rainfall runoff model enables reliable groundwater simulation, as it uses physical parameters to calculate storage and discharge. Comparable models, e.g., HEC-HMS, only represent the aquifer in a simplified way [55]. As versatile as SWMM is, it has one drawback. This consists in the fact that SWMM calculates purely physical actual evaporation from different environmental compartments but does not account for the biological transpiration of plants. When simulating a single rain event, this is not relevant, since ET practically does not take place and therefore has no significant impact on discharges. Considering a long-term simulation in a region, where the transpiration of plants accounts for a large part of the total ET, the components of the water balance, like soil infiltration and percolation to the GW zone, cannot be modelled accurately. In cross-season simulations, this leads to incorrect feed of storage systems and hence to systematic volume errors in the river flow.

Despite the simplified ET calculation, SWMM has been used more often in rural areas in recent years [56–60]. Due to its broad application, the desire for continuous improvement of SWMM is growing not only among the developers of the software but also among its users. For some research questions or applications, it is possible to use SWMM's existing components to improve model performance [61]. For the ET calculation of plants, the internal software tools are no longer sufficient, so that the source code must be adjusted. Regarding the implementation of a vegetation-specific ET this has been done successfully at the University of Utah, USA [62] and the

University of Applied Sciences Münster, Germany [63]. The two use different approaches:

The authors of [62] allow the input of multiple time series of potential ET and additionally implement a water stress coefficient for the calculation of actual ET, which serves to reduce ET rates at low soil water contents. The comparison between simulated and measured actual ET rates showed that the updated ET routine works well for a bioretention site (R = 0.75) and green roof (R = 0.88). According to [62], the input of a "mismatched" (crop non-specific) potential ET time series can lead to an overestimation of 12–19 % of annual actual ET and an underestimation of 14–19 % of annual runoff.

The second approach [63–65] integrates a vegetation layer into SWMM's low impact development (LID) module and calculates actual interception and transpiration on the basis of one input time series for potential grass reference ET. In the process, a crop factor is implemented, which reflects the water demand of a plant and reduces or increases the ET rates depending on the vegetation type [66]. The upgraded SWMM version is called SWMM-UrbanEVA and has been developed in order to cope with the ET of vegetation at the micro- (green roof) to mesoscale (city district) [64]. By applying SWMM-UrbanEVA, the volume error of the runoff from a green roof could be improved from almost 17 % to about 4 % [65].

The present work tests the applicability of SWMM-UrbanEVA in the macroscale of a river catchment at the example of the Schmarler Bach system in the north German lowlands. Results are compared with the results of the conventional SWMM software.

2.2 Materials and Methods

2.2.1 Study Area and Monitoring Station

The study area is the catchment of the Schmarler Bach system, located in the north-eastern German lowlands. It is part of the city of Rostock and its rural surroundings (see Figure 2). The stream network altogether is 35 km long, consisting of open segments, pipes, and culverts. The main stream discharges into the river Warnow, which drains into the Baltic Sea. In total, 65 % of the 23-km² catchment area is occupied by vegetation, while approximately 34 % of the area is partial impervious, which is due to urban use (residential area, traffic area, and industry/trade; see Table 3). The annual average precipitation is 600–700 mm, of which 350–575 mm evapotranspirates depending on the type of land use and water availability [67]. The

topography is relatively flat, ranging from 29 to 0 m above mean sea level. In most parts of the area, the depth to GW is relatively low (< 5 m), which causes a significant seasonal component of base flow in the river system.

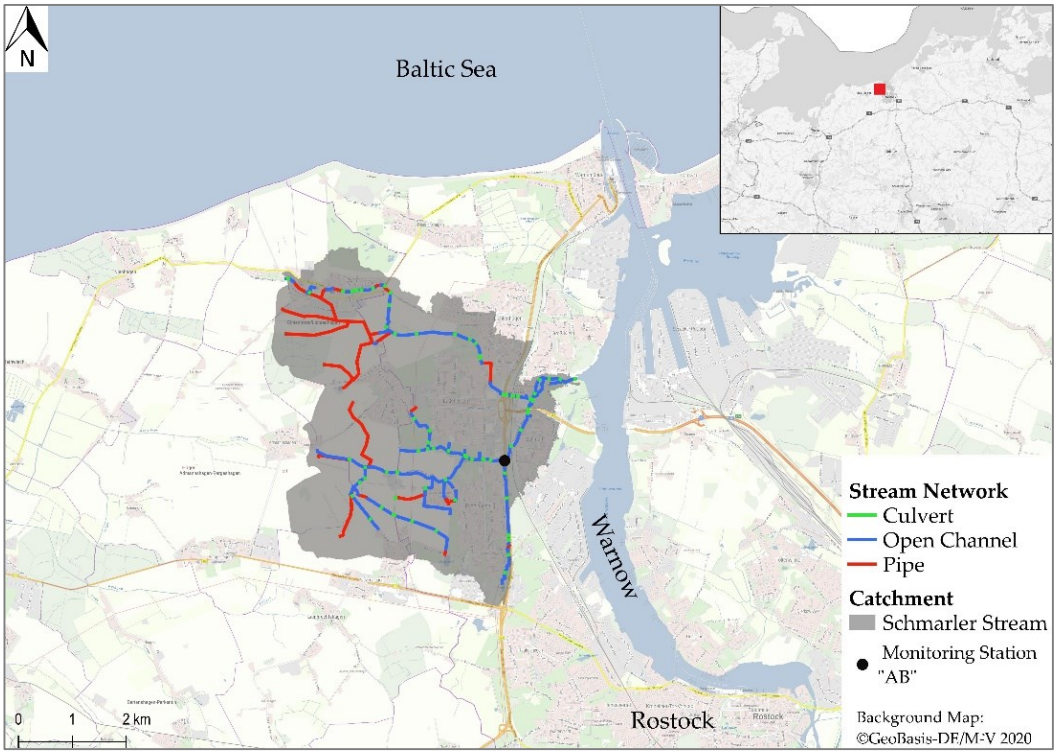

Figure 2. Schmarler Bach system and catchment.

Table 3. Different types of land use and their area percentage in the Schmarler Bach catchment.

Land Use Class	Abbreviation	Area Fraction (%)	Thereof Sealed (%)
agriculture	AC	29.2	0
wetland	WL	0.1	0
grassland	GL	1.3	0
industry/trade	IT	5.0	62.5
deciduous forest	DF	0.3	0
mixed forest	MF	6.0	0
coniferous forest	CF	1.3	0
orchard	OR	11.5	0
residential area	RA	17.8	49.4
parks	PA	15.3	26.7
traffic area	TA	11.0	51.0
water surface	WA	1.2	0

In the area of the Schmarler Bach station 2 + 400, a monitoring station for continuous measurement of water level and flow velocity was installed (see Figure 2) in order to

calculate flow rates from the two parameters. To accomplish this, an ultrasonic doppler flow meter was used. Since the device only measures flow velocity in the central lamella, a calibration function based on regular comparative manual multi-point measurements was set-up to obtain the mean flow velocity of the complete cross section. Figure 3 shows the corrected data at the monitoring station "Autobahn" (AB). Due to random errors, the noise of the data is quite high. Therefore, the time series was smoothed using the 3-h moving median. The latter was processed to separate the base flows, based on the sliding interval method [68] by forming the minimum of 3-day periods, respectively (Figure 4).

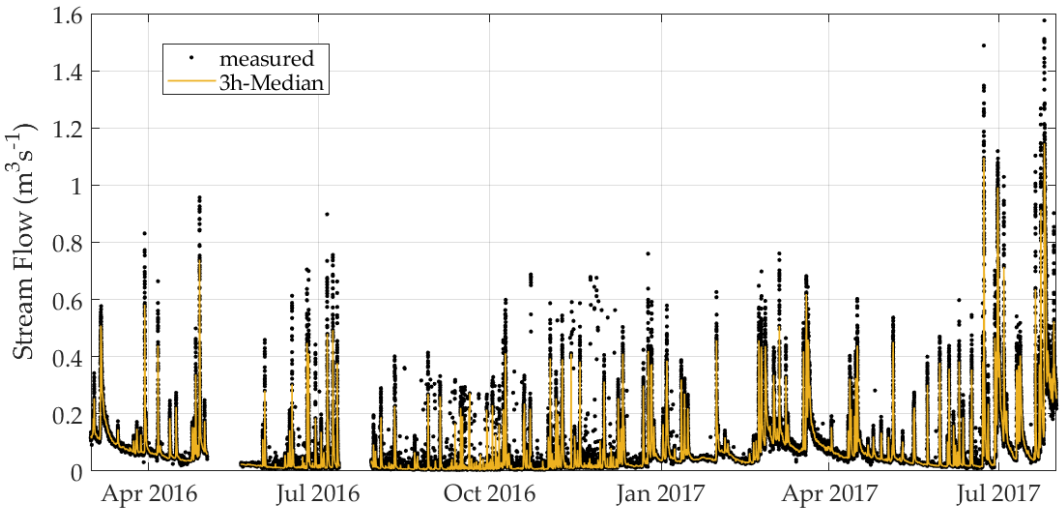

Figure 3. Measured stream flow and corresponding smoothed curve (3-h-median sliding interval) at the monitoring station "Autobahn" (AB).

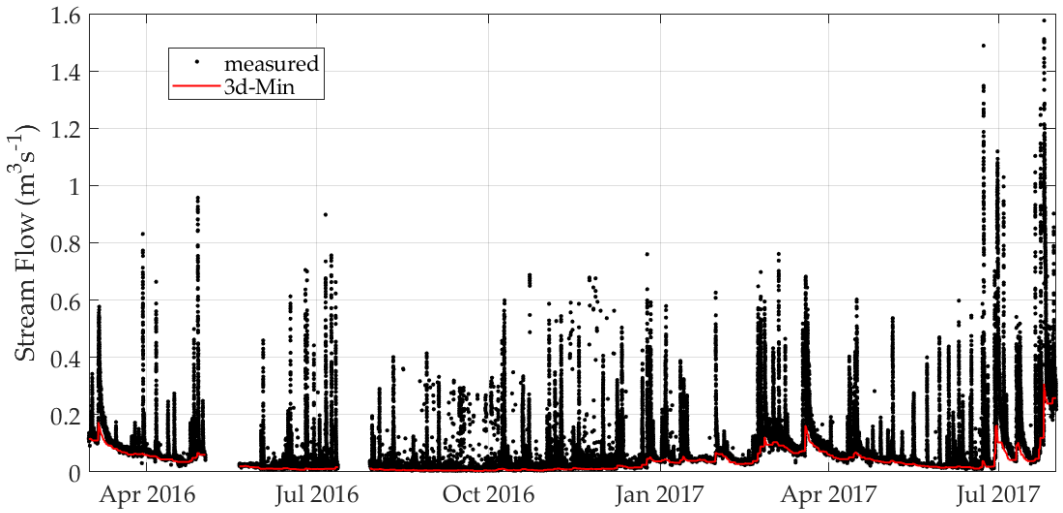

Figure 4. Measured stream flow and 3-day-minimum (sliding interval) to represent base flow at the monitoring station "Autobahn" (AB).

2.2.2 Software Description

2.2.2.1 SWMM

The Storm Water Management Model SWMM is an open source software used for the simulation of the surface/subsurface runoff from primarily urban areas. It was developed by the United States Environmental Protection Agency (EPA) and combines a hydrological rainfall-runoff model with a hydrodynamic drainage model. The former traditionally consists of four compartments: (1) the atmosphere, (2) the land surface, (3) the sub-surface, and (4) the GW compartment. The rainfall-runoff model is semi-distributed and operates on a number of subcatchments consisting of permeable and impermeable sub-areas. Furthermore, SWMM's version 5 introduces the low-impact development controls (LIDs), such as a bioretention cell or a green roof, used to calculate runoff, storage, and infiltration in a more detailed way [54; 69]. Different calculation algorithms are available for the different compartments of the rainfall-runoff model; the ones used in this study are described below.

The atmosphere module contains time series for precipitation and ET_0. The latter can only be set globally for the entire model area while distinct precipitation time series can be defined for every subcatchment. Originally, evaporation can occur for standing water on subcatchment surfaces, for subsurface water in aquifers, for water held in storage units, and for open channel flow [54]. The land surface receives precipitation and generates surface runoff using the nonlinear reservoir routing method. For infiltration calculation in the sub-surface zone of the subcatchments, SWMM offers five optional methods. For this study, the Horton method was chosen. It assumes that the infiltration capacity is high at the beginning of a rain event (maximum infiltration rate) and then decreases exponentially with increasing water content in the soil until a state of equilibrium is reached (minimum infiltration rate). However, for infiltration within the LID, SWMM only offers the Green & Ampt Scheme. In SWMM, the aquifer can lose or transfer water respectively through deep percolation, ET, and lateral GW flow to the drainage network. The height of the water table varies with time depending on the rates of inflow and outflow. Lateral GW flow is represented through a user-defined power function of the changing water table of the aquifer and depth of water in the receiving node of the conveyance system [54]:

$$Q_{GW} = A1(H_{GW} - H_{CB})^{B1} - A2(H_{SW} - H_{CB})^{B2} + A3(H_{GW}H_{SW}) \quad (1)$$

Q_{GW} = lateral groundwater flow ($m^3s^{-1}ha^{-1}$);

H_{GW} = GW level above aquifer bottom (m);

$H_{CB} =$ height of channel bottom above aquifer bottom (m);

$H_{SW} =$ height of surface water at receiving node above aquifer bottom (m);

$A1 =$ groundwater flow coefficient ($\mathrm{m}^{(1-B1)}\mathrm{s}^{-1}$);

$B1 =$ groundwater flow exponent (-);

$A2 =$ surface water flow coefficient ($\mathrm{m}^{(1-B2)}\mathrm{s}^{-1}$);

$B2 =$ surface water flow exponent (-); and

$A3 =$ surface $-$ groundwater interaction coefficient ($(\mathrm{m}-\mathrm{s})^{-1}$).

A threshold set by the user makes it possible to determine from which water level lateral GW flow to the stream network will occur [69; 70]. This also enables the simulation of tile drainage.

The hydrodynamic drainage model is subdivided into nodes and conduits and receives its water from the subcatchments (runoff from surface and GW interflow) at defined nodes. The drainage network may consist of open sections, pipes, culverts, and other control structures like pumps and weirs. Gravity flow within the conduit link is calculated using the one-dimensional Saint–Venant equation, allowing different options (kinematic/diffuse/dynamic wave). Here, the dynamic wave option was applied, which enables the simulation of channel storage, backwater effects, and entrance/exit losses [70; 71].

2.2.2.2 SWMM-UrbanEVA

As an upgrade of the original SWMM version, SWMM-UrbanEVA was developed at the University of Applied Sciences Münster (Germany) to calculate ET more precisely. It was designed as part of the well-known LID module (Figure 5) and contains an approach for calculating the actual ET of vegetated areas based on the potential grass reference ET (ET_0). The existing three-layer system of the traditional LID module (surface-soil-storage) serves to model the infiltration and percolation processes depending on soil parameters. It is supplemented by a new vegetation layer in which vegetation-specific properties, like the crop factor (Kc) [66] and the leaf area index (LAI), can be parameterized (Figure 5).

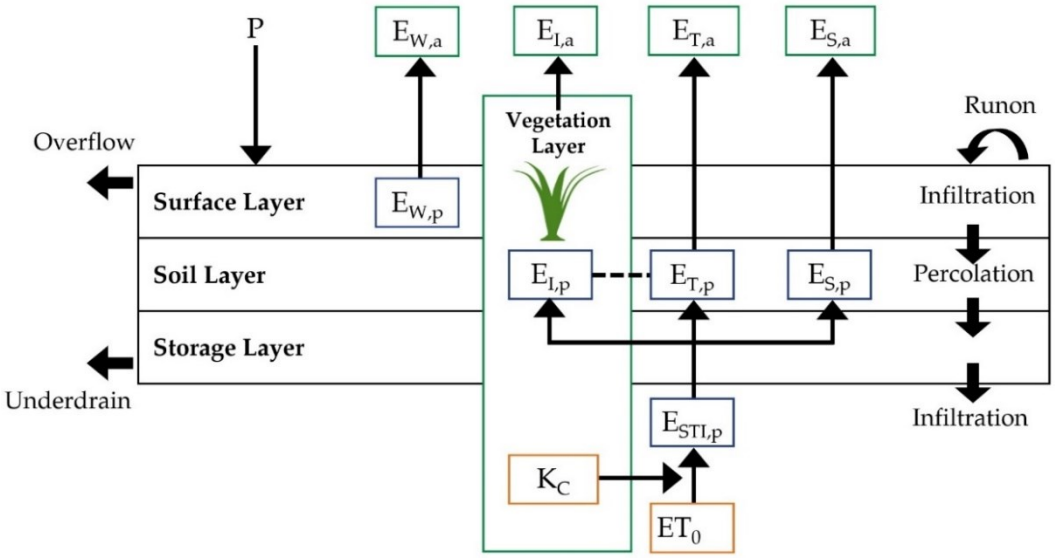

Figure 5. Components of evapotranspiration as part of the enhanced LID module of SWMM-UrbanEVA. (P = Precipitation, Kc = crop factor, ET_0 = potential grass reference ET, $E_{STI,p}$ = plant specific potential ET, $E_{I,p}$ = pot. interception, $E_{T,p}$ = pot. transpiration, $E_{S,p}$ = pot. soil evaporation, $E_{W,p}$ = pot. evaporation of free water surface, $E_{W,a}$ = actual evaporation of free water surface, $E_{I,a}$ = actual interception, $E_{T,a}$ = actual transpiration, $E_{S,a}$ = actual soil evaporation) —modified after [52].

The actual vegetation-specific ET ($E_{STI,a}$) is computed for every time step and comprises the sub processes of interception, transpiration, soil evaporation and evaporation of free water surfaces:

$$E_{STI,a} = E_{I,a} + E_{T,a} + E_{S,a} + E_{W,a} \quad (2)$$

$E_{I,a}$ = actual rate of interception (mmh^{-1});

$E_{T,a}$ = actual rate of transpiration (mmh^{-1});

$E_{S,a}$ = actual rate of soil evaporation (mmh^{-1}); and

$E_{W,a}$ = actual rate of free water surface (mmh^{-1}).

The calculation of each component is based on the potential vegetation-specific ET ($E_{STI,p}$). The latter is obtained by multiplying Kc with the input ET_0:

$$E_{STI,p} = ET_0 \times K_C, \quad (3)$$

$E_{STI,p}$ = vegetation − specific potential ET (mmh^{-1}); and

ET_0 = grass reference evapotranspiration (mmh^{-1}).

Interception and transpiration are energetically decoupled from soil evaporation via the vegetation-covered fraction (*SCF*) of the surface [72; 73].

The interception height (I) is derived depending on the leaf area index according to the approach of [74]. The LAI reflects the ET-active surface in the annual cycle and determines the maximum storage capacity of the leaf canopy:

$$I = \mathrm{S}_{max} \times \left(1 - \frac{1}{1+\frac{SCF \cdot P}{S_{max}}}\right), \tag{4}$$

$$SCF = 1 - 0.7^{LAI_{doy}}, \tag{5}$$

$$S_{max} = S_L \times LAI_{doy}, \tag{6}$$

$I =$ potetial interception height (mm);

$S_{max} =$ max. interception height (mm);

$S_L =$ leaf storage coefficient (mm), Hörnschemeyer et al. [64] recommend $\mathrm{S_L}$=0.29 (mm)

$LAI_{doy} =$ LAI corresponding to day of year (-) (here monthly resolution);

$SCF =$ vegetation covered fraction (-); and

$P =$ precipitation (mm).

Interception occurs only from the wetted part of the leaf and is determined on the one hand by the precipitation height at low precipitation rates and on the other hand by the maximum interception capacity (S_{max}) at high precipitation rates [74]. The potential interception height of the current time step i (S_I) depends on the previous time step i−1 ($S_{I,i-1}$):

$$S_I = S_{I,i-1} + I. \tag{7}$$

The actual intercept height $S_{I,a}$ is then derived depending on the interception capacity and the interception height of the current time step:

$$S_{I,a} = \begin{cases} S_I & for\ S_I \leq S_{max} \\ S_{max} & for\ S_I > S_{max} \end{cases}. \tag{8}$$

To calculate the potential interception rate $E_{I,p}$, the potential evapotranspiration $E_{STI,p}$ is reduced using the vegetation-covered fraction and the wetted part of the leaf A_b [75; 76]:

$$E_{I,p} = SCF \times A_b \times E_{STI,p}, \tag{9}$$

in which:

$$A_b = \left(\frac{S_{I,a}}{S_{max}}\right)^{\frac{2}{3}}. \tag{10}$$

The actual interception rate $E_{I,a}$ finally results from the minimum fill level of the interception height and the potential evaporation rate:

$$E_{I,a} = \min\left(S_{I,a}, E_{I,p}\right). \tag{11}$$

The part of the precipitation that does not intercept is returned to the input precipitation, which enters the following infiltration and drainage processes:

$$P_{net} = P \times (1 - SCF) + (P - E_{I,a}) \times SCF \tag{12}$$

P_{net} = Precipitation subtracted by interception losses (mmh^{-1}); and

P = input precipitation (mmh^{-1}).

Equivalent to the potential interception rate, the potential transpiration rate $E_{T,p}$ is projected onto the vegetation-covered area. In contrast to interception, transpiration takes place from the dry portion of the leaf ($1–A_b$). Furthermore, the actual interception evaporation rate $E_{I,a}$ is subtracted as an upstream process:

$$E_{T,p} = SCF \times (1 - A_b) \times E_{STI,p} - E_{I,a}. \tag{13}$$

Since the process of transpiration is fed from the soil reservoir, the calculation of the actual transpiration rate $E_{T,a}$ is done in dependence of the available soil water:

$$E_{T,a} = \min\left(\frac{(\theta - \theta_{WP}) \times D}{\Delta t}, E_{T,p}\right), \tag{14}$$

θ = actual moisture content (-);

θ_{WP} = moisture content at wilting point (-);

D = thickness of soil layer (mm); and

Δt = simulation time step.

Soil evaporation is computed for the uncovered area share ($1–SCF$), as it is assumed that evaporation underneath vegetation is negligible [77].

$$E_{S,p} = (1 - SCF) \times E_{STI,p} \tag{15}$$

$E_{S,p}$ = potential soil evaporation (mmh^{-1}).

The actual soil evaporation depends on the water content of the soil and is expressed by the relative soil moisture W_{rel}. The latter describes the proportion of available soil water within the range of the usable field capacity:

$$W_{rel} = \frac{\theta - \theta_{WP}}{\theta_{FK} - \theta_{WP}}, \tag{16}$$

W_{rel} = relative soil moisture (-); and

θ_{FK} = moisture content at field capacity (-).

According to [78], the potential evaporation rate is already met before the water content in the soil reaches field capacity. For this reason, the potential evaporation rate is increased by the coefficient e_s if the relative soil moisture falls below a certain threshold (see Equations (17) and (18)). According to the recommendations of [73; 78], this threshold is set to 0.6:

$$e_s = \begin{cases} \left(\frac{W_{rel}}{0.6}\right)^{0,5} & for\ W_{rel} < 0.6 \\ 1 & for\ W_{rel} \geq 0.6 \end{cases}, \tag{17}$$

$$E_{S,p} = e_s \times E_{S,p}. \tag{18}$$

The actual soil evaporation $E_{S,a}$ is finally calculated from the minimum of the available soil water per time step and the potential soil evaporation rate:

$$E_{S,a} = \min\left(\frac{(\theta - \theta_{WP}) \times D}{\Delta t}, E_{S,p}\right). \tag{19}$$

If ponding occurs, two options can be chosen: In the case that vegetation height is short and completely covered by ponding water, only evaporation from the free water surface occurs while the other ET processes are suspended:

$$E_{I,a} = 0, \tag{20}$$

$$E_{T,a} = 0, \tag{21}$$

$$E_{S,a} = 0, \tag{22}$$

$$E_{W,p} = E_{STI,p}, \tag{23}$$

$$E_{W,a} = \min\left(\frac{h_{pond}}{\Delta t}, E_{W,p}\right), \tag{24}$$

h_{pond} = height of ponding surface water (mm).

In the case of a high stand, such as a forest, only soil evaporation stops while interception, transpiration and evaporation of the free water surface will continue.

2.2.3 Model Setup

Both the setup of the rainfall-runoff model and the setup of the stream model was realized on the basis of GIS data. VBA scripts were used to convert them to the text format used by SWMM. Water courses were provided as lines and marked with a hierarchical stream segment index, which enables the assignment of a stream segment to a subcatchment and vice versa. Stream cross sections were derived from a high-resolution digital elevation model (DEM) with a grid size of 0.2 m. Each subcatchment was shaped by intersecting the superficial subcatchments based on DEM analysis and land use polygons (Figure 6). Soil type maps were used to derive average soil attributes for each subcatchment and LID control while the aquifer was treated as homogeneous sand across the model area but with different fill levels depending on the average ground elevation of the subcatchments. GW flow to the river only occurs if a defined threshold is exceeded by the water table. Here, it is 1.2 m below the average ground height, as in the case of a drainage pipe, which comes on stream when the surrounding soil is saturated. The unsealed area of a subcatchment was simulated using the LID controls, more precisely a bioretention cell with the upgraded ET calculation. Furthermore, an equal model was set up for comparison with the same LID controls but with the conventional evaporation calculation.

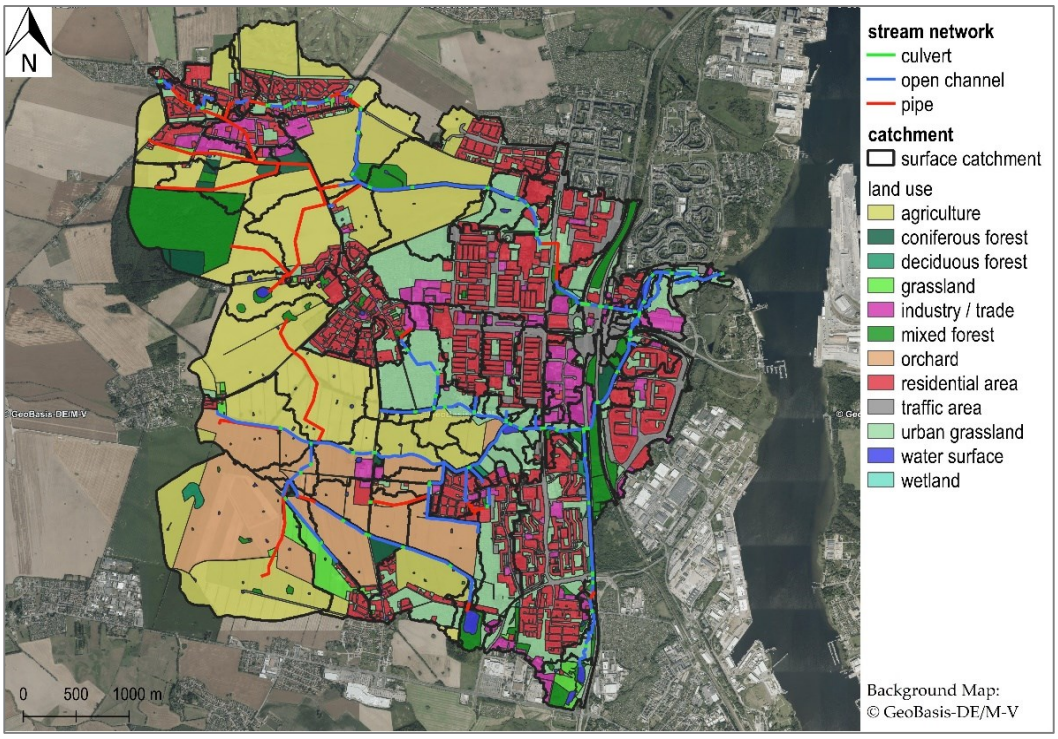

Figure 6. Model subcatchments as intersection of the surface catchments and land use polygons.

Important additional input parameters for SWMM-UrbanEVA are the crop factor and the leaf area index with its annual cycle (Figure 7). In general, the largest leaf area indices are recorded in July and June and the smallest in December and January. The coniferous forest shows the smallest decrease in winter.

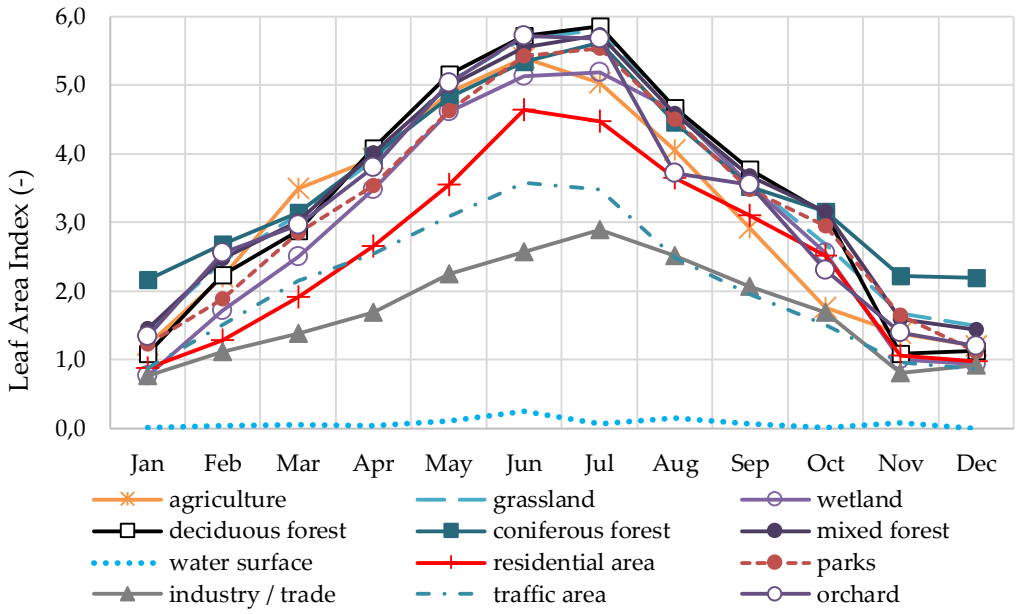

Figure 7. Average leaf area index per month derived from satellite data for different land use classes (based on one cloudless satellite image per month from November 2013 till October 2015).

2.2.4 Calibration and Error Measures

The goal of a model calibration is to determine unknown parameters by adapting the calculation result to observed conditions by varying these parameters. Basically, there are two options: an automated (e.g., Latin Hypercube Sampling) and a manual calibration procedure. In automatic calibration, parameters are adjusted automatically according to a predefined search scheme and numerical measures of the goodness of fit [79]. Within this framework, a large number of parameter combinations must be generated and tested; depending on the number of parameters to be calibrated, several hundred to thousands of simulation runs are necessary. The procedure is often used for either single events or comparatively less complex models with a short runtime (see [79; 80]). With long simulation durations (in this study, ~3 h for 20 months) and a large number of model parameters, automatic calibration is only of limited use. Especially for physically based models, a specific manual calibration can ensure that physically reasonable parameter combinations and value ranges are maintained. This is especially important if the detected parameter combinations are to be transferred to further similar but unobserved areas. Therefore, the manual calibration approach was chosen. In a first step, the sensitivities of all model parameters were tested with regard to their effect on stream flow. This was done by a graphical evaluation of the flow hydrographs. In a next step, the detected sensitive parameters were modified so that the difference between the calculated values from the measured values became minimal. In the process, only one model parameter per simulation run was varied within its plausible limits. The goodness of fit of the model was assessed using the error measures and performance criteria in Table 4.

Table 4. Error measures and performance criteria (Q_{calc} = calculated flow, Q_{obs} = observed flow; Obs = measured value (observed); Calc = calculated value; Indices: i = location, t = time, n = number of measurement data).

Designation	Abbre-viation	Formula	No.
Volume Error	E_{Vol}	$E_{Vol} = 1 - \frac{\int Q_{calc}\, dt}{\int Q_{obs}\, dt}$	(25)
Mean absolute Error	MAE	$MAE = \lvert\bar{E}\rvert = \frac{\sum_t \lvert Obs_{i,t} - Calc_{i,t}\rvert}{n}$	(26)
Correlation Coefficient	R	$R = \frac{\sum_t (Calc_{i,t} - \overline{Calc_{i,t}}) \times (Obs_{i,t} - \overline{Obs_{i,t}})}{\sqrt{\sum_t (Calc_{i,t} - \overline{Calc_{i,t}})^2 \times \sum_t (Obs_{i,t} - \overline{Obs_{i,t}})^2}}$	(27)

Designation	Abbre-viation	Formula	No.
Nash-Sutcliffe Efficiency	NSE	$NSE = 1 - \frac{\sum_t \left(Obs_{i,t} - Calc_{i,t}\right)^2}{\sum_t \left(Obs_{i,t} - \overline{Obs_{i,t}}\right)^2}$	(28)

The volume error quantifies the total deviation in the period under consideration. The MAE indicates to what extent the simulated values deviate on average from the measured values while having the same units as the model output. R and NSE allow statements to be made about the adaption of the dynamics of the simulated flows, whereby the former tests the linear correlation and the latter allows an assessment of how well the simulated values agree with the measured ones. The disadvantage of the NSE is that it is very sensitive to outliers due to the squared differences between measured and simulated values [81]. The following table (Table 5) provides a classification to assess the goodness of fit for R and NSE.

Table 5. Assessment of the evaluation criteria R and NSE.

	Very Good	Good	Satisfactory	Not Satisfactory	Source
R	R ≥ 0.93	0.8 ≤ R < 0.93	0.6 ≤ R < 0.8	R < 0.6	[82]
NSE	>0.80	0.60 ≤ NSE ≤ 0.80	0.50 < NSE < 0.60	≤0.50	[83]

2.3 Results and Discussion

2.3.1 Sensitivity Analyses

The following table shows the parameters with the highest sensitivity to stream flow and the effects of parameter changes. Parameters not listed in Table 6, such as soil properties or the degree of sealing, have a sensitive effect on stream flow, too. However, since they were derived from soil maps or satellite data, respectively, they vary widely in space and were considered to be fixed in the process of calibration.

Table 6. Parameter sensitivities and effects of parameter changes regarding stream flow (* only SWMM-UrbanEVA).

Parameter	Unit	Calibrated Value, Range, or Calculation Formula	Sensitivity to Stream Flow	Effects of Parameter Changes/Comment
Subcatchment Characteristics				
Width	m	$\frac{\sqrt{Area}}{6}$	medium	The greater the width of the subcatchments, the shorter the flow path, the earlier and larger the direct peak runoff
Manning value impervious	s $(m^{1/3})^{-1}$	0.05	medium	large values slow down surface runoff and reduce peak flow
Detention storage impervious	mm	0.5	medium	Cuts peak runoff; small rain events are “swallowed” if value is too high
LID Control				
Average LAI *	m m^{-1}	1.7–3.6	medium	The higher the value, the more ET, the less GW base flow in the stream
LAI monthly coefficients * (pattern)	-	0.2–1.7	medium	increases seasonal dynamics of actual ET throughout the year; Increased ET in summer leads to lower GW levels and therefore less GW inflow to stream
Crop factor * (Kc)	-	0.7–1.5	high	The higher the value, the more ET, the lower the GW level, the less GW base flow in the stream
Groundwater (Physical Parameters)				
Porosity	-	0.43	high	Increasing the value causes delay of GW peak discharge; more extreme course of the base flows in the stream (high flows higher, lower flows lower)
Conductivity Slope	-	18	medium	the higher the value, the later the lateral GW discharges react (delay of GW peak flows)
Upper Evaporation Fraction	-	0.1	high	the lower the value, the higher the base flow in average;

Parameter	Unit	Calibrated Value, Range, or Calculation Formula	Sensitivity to Stream Flow	Effects of Parameter Changes/Comment
				positive correlation with lower GW loss rate
Lower GW Loss Rate (Seep)	mm hr^{-1}	5.0 × 10−6	high	the lower the value, the higher the base flow in average
Groundwater Flow Editor				
A1	-	0.04 (0.0003 for sealed areas)	high	The smaller the value, the flatter/slower the flows decrease, making base flows higher
B1	-	2	high	The smaller the value, the larger the peaks, less base runoff
A2 and A3 B2	-	0 1	high	Level of surface water does not significantly affect GW flow; by setting the coefficients to zero and B2 to 1, it is excluded from the power function
Threshold Water Table Elevation	m	1.2 m below surface height	high	the lower the threshold, the higher the lateral GW discharges to the stream

Initial values for the vegetation coefficients were determined according to [66]. Since they depend on local climate conditions [84], they were slightly varied and adjusted in the calibration process to achieve the best simulation results (Table 7).

Table 7. Final vegetation coefficients of the different land use classes.

Land Use Class	Crop Factor KC (-)
agriculture	1.5
wetland	1.3
grassland	1.3
industry/trade	0.7
deciduous forest	0.8
mixed forest	0.8
coniferous forest	0.8
orchard	1.0
residential area	0.7
parks	1.3
traffic area	0.7

Land Use Class	Crop Factor KC (-)
water surface	0.7

The parameters under the heading "subcatchment characteristics" influence the peak height of the direct runoff while the other parameters have a direct or indirect effect on the GW level and thus on the GW inflows to the stream. Here, the role of ET under the heading "LID Controls" in Table 6 should be emphasized, as it affects the amount of deep percolating water. In particular, the LAI monthly coefficients together with the average LAI enable an intensified ET in summer (June + July, see Figure 7) controlled by the LAI and a reduced ET in winter as well as a transition phase in spring and autumn, respectively. The crop factor Kc is highly sensitive. Kc > 1 increases and Kc < 1 decreases ET compared to the input grass reference ET. LAI and Kc form the key parameters for influencing the annual cycle of base flows in the stream.

2.3.2 Calibration Results

Figure 8 shows the simulated hydrographs with SWMM and SWMM-UrbanEVA and the observed stream flows at the monitoring station. Accordingly, Table 8 expresses the model fit in numbers by error measures and performance criteria.

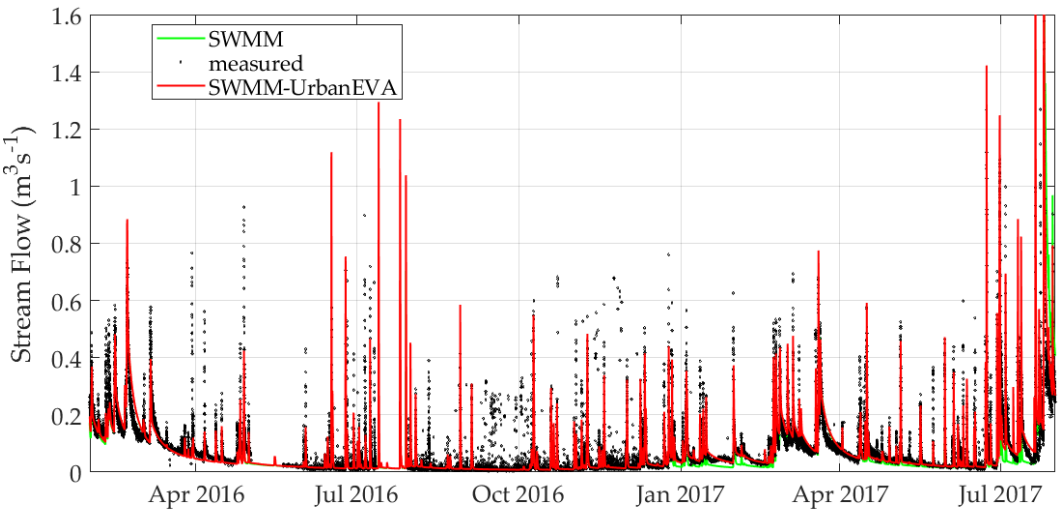

Figure 8. Simulated stream flow with SWMM and SWMM-UrbanEVA and observed flow at the measurement station AB.

Table 8. Model performance based on error measures and performance criteria related to the total flow rate in the period 21 January 2016 to 31 July 2017.

	E_{Vol} (%)	MAE (m^3s^{-1})	R (-)	NSE (-)
SWMM	10.4	0.032	0.80	0.44
SWMM-UrbanEVA	3.6	0.026	0.82	0.68

The measured and as well the simulated graphs show that the stream flow is composed of direct runoff peak flows and a base flow component. The direct runoff peak discharges strongly depend on the intensity of the input precipitation, which can vary locally, especially during heavy rainfall events. Therefore, it is important to mention that the input precipitation was not measured directly in the model area but about 8 km south of it. However, in contrast to individual rain events, it is assumed that the long-time sums of precipitation in the model area are the same as at the measuring station.

The volume error of the total stream flow calculated with SWMM is quite low but decreases even more with SWMM-UrbanEVA. The same applies to the MAE. The R and NSE of the SWMM-UrbanEVA results indicate a good fit; in contrast to this, the total results obtained from the original SWMM version are worse, which is mainly reflected in the volume error and NSE. It should again be noted that the performance criteria are sensitive to non-matching peak flows, for example, if it has rained over the precipitation measurement station but not in the model area itself or vice versa. Since direct runoff peak flows are not significantly influenced by ET, they will not be considered further in this study. However, a model comparison based on error measures and performance criteria does not go far enough. Since evaporation has different effects in different seasons, a process-oriented consideration is necessary.

2.3.3 Water Balance

The following table (Table 9) lists important parameters of the water balance in the period from 1 December 2015 to 31 July 2017 (20 months). Continuity errors are smaller than 1 %. The initial conditions and storage levels at the beginning of the simulation are the same for the SWMM and the SWMM-UrbanEVA model. The water balance variables of the subcatchments are summarized under the heading “Runoff Quantity”. It includes both the runoff of sealed areas of the subcatchments and those of the permeable areas. The latter are modelled as LID modules (bioretention cells). The direct surface runoff (95 mm in both cases) primarily comes from paved areas, since hardly any surface runoff is formed within the LID modules (<1 mm in both cases). It can be seen that the ET in SWMM-UrbanEVA is smaller than that calculated with SWMM in the period of time selected, hence the proportion of water that is passed on to the GW zone (“Infiltration Loss”) is larger. Therefore, more water is available to the GW flow, which is ultimately reflected in the GW inflow to the stream (“GW Inflow”). The latter makes up the largest volume share in the stream overall.

Table 9. Extract from the SWMM status report for the simulation period 1 December 2015 – 31 July 2017 (entire model area).

	SWMM-UrbanEVA	SWMM
Runoff Quantity	Depth (mm)	Depth (mm)
Total Precipitation	1162	1162
Evaporation Loss	666	715
Infiltration Loss	373	324
Surface Runoff	95	95
Groundwater	Depth (mm)	Depth (mm)
Infiltration	373	324
GW Flow (tile drainage)	388	368
Flow Routing	Volume (10^6 L)	Volume (10^6 L)
Wet Weather Inflow	2144	2144
GW Inflow	8771	8302

Looking at the distribution of evaporation and infiltration loss within the LID modules, important differences between the two models and their different land use classes become apparent (Figure 9).

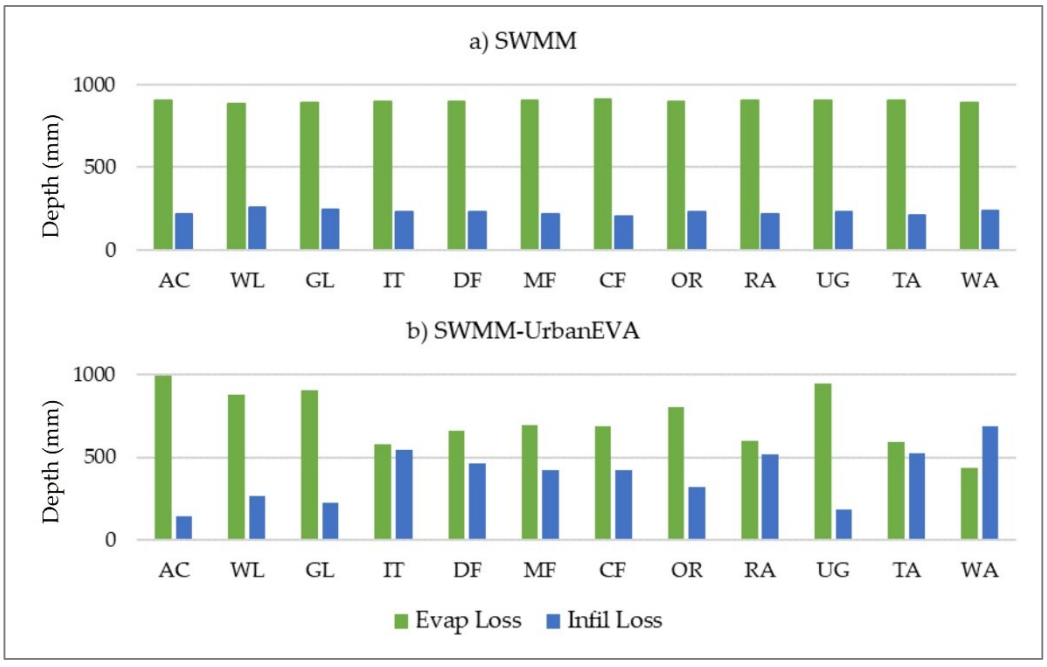

Figure 9. Evapotranspiration and infiltration loss in (a) the SWMM and (b) the SWMM-UrbanEVA LIDs (pervious area of a subcatchment).

With the official SWMM version, there are hardly any differences between the land use classes; the slight differences are only due to different soil types and different water availability depending on the placement in the terrain. The evaporation loss is about 900 mm while the infiltration loss is slightly more than 200 mm. In contrast, ET

in SWMM-UrbanEVA varies from around 440 (water surfaces) to 990 (agricultural areas) and infiltration from 140 to 690 depending on the land use class. In addition, a strong linear relationship between ET and percolation to the GW zone can be determined in the model area, which is suggested by the correlation coefficient of 0.99. This again underlines the influence of ET on the percolation to GW and the resulting base flow component in the river.

2.3.4 Groundwater Table and Groundwater Flows to Stream

In the considered model area, GW inflow plays a decisive role with respect to the stream flow. These in turn depend on the GW level, more precisely on the difference between the GW level and the bottom of the receiving node of the hydraulic system, and on the values for A1 (constant) and B1 (exponent) used in the GW power function. The GW hydrographs (Figure 10) are now to be examined more closely using the example of an agricultural area and a mixed forest area.

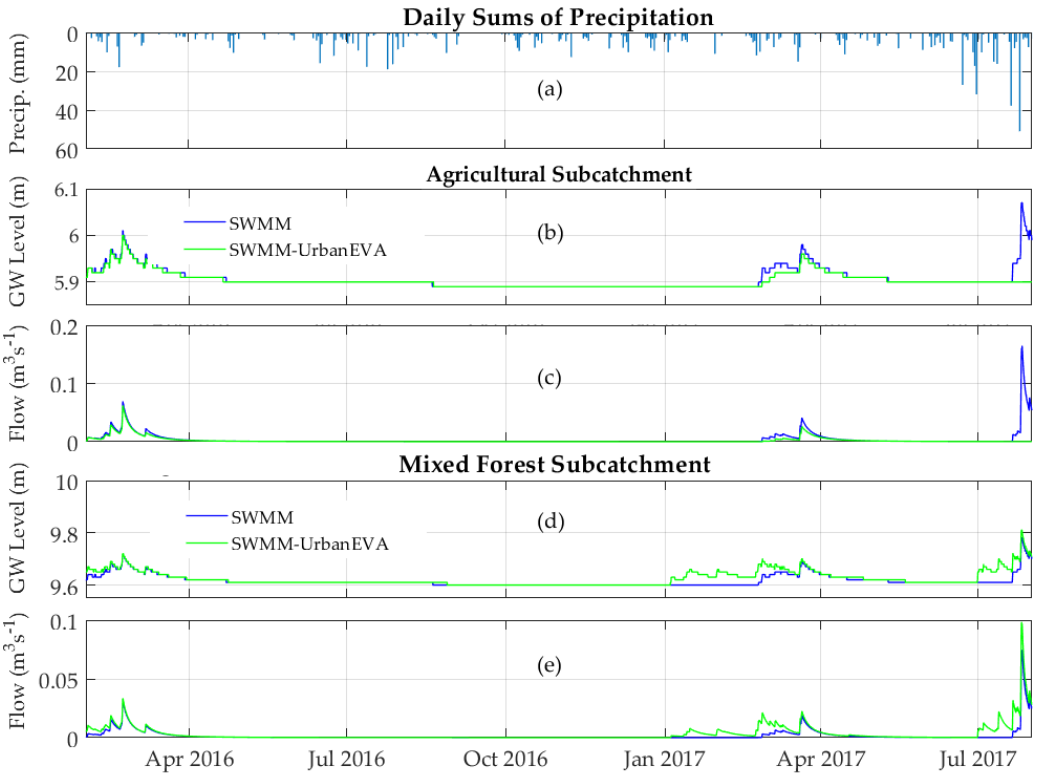

Figure 10. Daily sums of precipitation (a), GW flow and GW level for an agricultural subcatchment (b), (c) and for a mixed forest subcatchment (d), (e) simulated with SWMM and SWMM-UrbanEVA.

Figure 10b,c refer to an agricultural subcatchment with a crop factor of 1.5 (highest value) and a drainage threshold height of 5.89 m. In this case, the crop factor in SWMM-UrbanEVA increases the evaporation rates fundamentally and the leaf area

index in turn decreases ET in winter and increases it in summer (especially in June/July). The effect under the arable land is that the GW level simulated with SWMM-UrbanEVA is slightly lower in winter and is at the threshold in a "normal" summer, such as 2016, so that no GW flow occurs. However, a significant difference between the two software versions is noticeable in wet July 2017. Due to the abundant rainfall, the GW level and flow simulated by SWMM is higher than even in winter. In SWMM-UrbanEVA, on the other hand, the precipitation is simply "swallowed" by ET so that it is not reflected in the GW level or flow.

The situation is different under a mixed forest with a crop factor of 0.8 (Figure 10d,e). Here, the GW levels and flows generated by SWMM-UrbanEVA are higher in January and February and almost identical in spring and summer—except for July 2017. In July 2017, the GW level and flow in SWMM-UrbanEVA rises already at the beginning of July and not only from the middle of the month as it is the case in the SWMM model. For the land use "forest", the same A1 and B1 parameters were applied as under an agricultural area. It was assumed that the forest is not crossed by drainage pipes but crossed by drainage ditches. However, the very high GW peak flows suggest that a more differentiated land-use-oriented approach to the parameters A1 and B1 would have been useful to reduce the GW flow dynamics under this forest land use class.

2.3.5 Base Flow Separation

The more water evapotranspirates, the less is available for deep seepage and GW inflow to the stream. To show the differences in base flows, a hydrograph separation was performed based on a 3-day sliding interval. Figure 11 illustrates the separated base flow hydrographs of the measured, the SWMM, and the SWMM-UrbanEVA stream flow at the observation point AB.

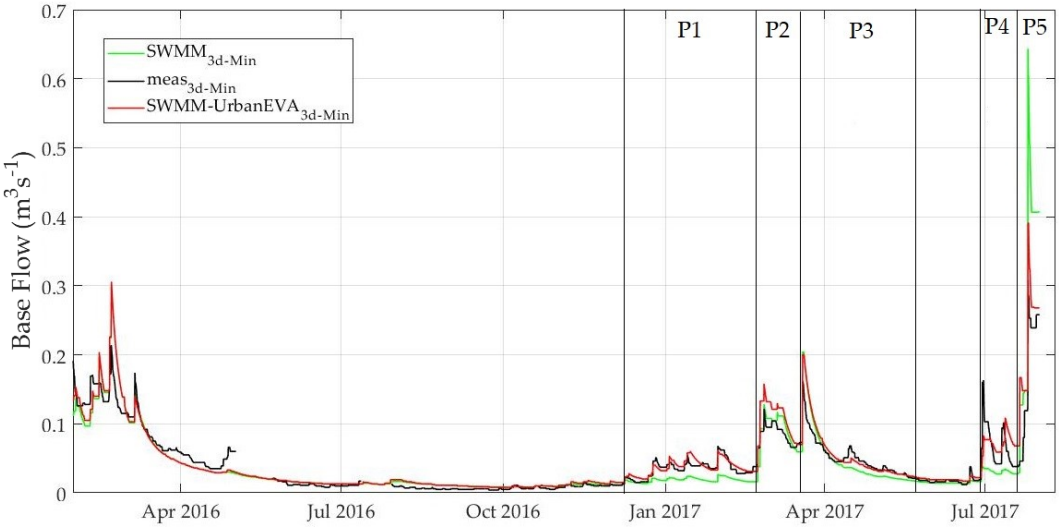

Figure 11. Minimum flows of a 3-day sliding interval of measured data (abbreviation "meas"), flows generated with the official SWMM version and SWMM-UrbanEVA.

In principle, the dynamics from January 2016 to mid-December 2016 in both models correspond very well with reality. The months of June to October 2016 are normally dry summer months with typically little base flow. It can be assumed that only the low-lying wetlands still contribute to base flow. At this point, it must be emphasized once again that in the model, GW only drains to the river if a fixed threshold value is exceeded. As the figure shows, the simulated base flows differ mainly from mid-December 2016 to the end of May 2017 and in July 2017. Five phases can be distinguished more precisely:

P1: 1 December 2016–20 February 2017

Transition phase from low to high base flows; SWMM-UrbanEVA base flows adapt very good to the measured ones, while those produced with SWMM are basically too low. Here, the evaporation in SWMM is too high since leaf fall cannot be incorporated in SWMM.

P2: 20 February 2017–19 March 2017

Phase of high base flows; SWMM-UrbanEVA base flows are higher than the observed ones while those generated with SWMM fit well. Here, the discrepancy can be explained by two possible reasons: According to [66], the crop factor is not constant but changes in dependence of three developmental stages with specific water demands: an initial start-up phase, an intermediate phase in which the highest crop factors (or crop coefficients) are recorded, and a final phase in which the factor decreases again. If this could be taken into account in SWMM-UrbanEVA, it would be

possible to calibrate the model, especially the aquifer, differently to achieve an even better adaptation. Another reason could be incorrect leaf area indices, as these were derived from satellite data and this indirect measuring method can lead to underestimation; only spectral data are evaluated and leaves lying on top of each other might not be considered. Besides, the spatial resolution is rather low.

P3: 19 March 2017–31 May 2017

Very high base flows at the beginning of the period caused by voluminous precipitation and exhausted storage capacities in the soil layer. The subsequent emptying of the storage systems is basically reproduced well by both models, but the SWMM-UrbanEVA base flows react more dynamically and therefore adapt a little better.

P4: 1 July 2017–20 July 2017

In this summer month, base flows are above average, due to the relatively humid previous month of June and the subsequent heavy rainfall events in July. At the same time, July is the month with the highest recorded leaf area indices.

In the SWMM-UrbanEVA model, GW drainage systems start to operate as early as 1 July, in contrast to the SWMM model, which starts later. This results in a better adapted course of the SWMM-UrbanEVA base flow compared to the measured data.

P5: 20 July 2017–31 July 2017

In the last third of the month, in addition to the high pre-humidity, very strong rainfall occurs, which causes the GW level to rise and restart all drainage systems. In this phase, the largest deviations between SWMM-UrbanEVA and SWMM are registered. The SWMM base flows are extraordinarily high and therefore do not offer a realistic curve. The SWMM-UrbanEVA hydrograph adapts much better, but the peak value of the base flow is still too high during this period. This is probably due to wooded areas, which provide too high peak flows (see Figure 10).

Table 10. Model performance based on error measures and performance criteria related to the base flow rate in the period 21 January 2016 to 31 July 2017.

	MAE (m^3s^{-1})	R (-)	NSE (-)
SWMM	0.014	0.88	0.81
SWMM-UrbanEVA	0.011	0.93	0.85

If the basic flows are considered without the direct runoff peak flows, the valuation criteria improve considerably. Table 10 shows that the base flows are very well represented by the SWMM-UrbanEVA model both on average and in their dynamics. The results produced with SWMM are nevertheless in the “good” range.

2.4 Conclusions

The present study was carried out to show the importance of ET and its influence on the base flows of a stream system in the north German lowlands. It was shown that for near natural landscapes, such as agricultural areas, the inclusion of land-use-dependent ET is indispensable for the calculation of water balances over a cross-seasonal period. However, this only applies to areas where the inflow of GW or drainage water to the stream or river plays an important role. Especially in relatively wet summer months, SWMM extremely overestimates the GW inflow because the stocks do not evapotranspirate enough rainwater.

In contrast to the original SWMM version, SWMM-UrbanEVA makes it possible to distinguish between different land use classes and their specific water demands, which is particularly important in small catchments, where the respective characteristics are more pronounced.

A suggestion for improvement can still be made here: Since the water demands of a plant behave differently in different growth stages, it would be useful to allow the input of a dynamic crop factor to achieve an even better adaptation. Nevertheless, single precipitation events (scenarios) can be calculated with SWMM as well as with SWMM-UrbanEVA since ET does not affect direct runoff peaks.

Summarizing, SWMM-UrbanEVA introduces a significant improvement towards process-oriented water balance modelling. However, the introduced additional processes (transpiration, interception, and evaporation) account for computation time. For the presented model area with its 626 subcatchments, 590 junction nodes, and 580 conduit links (including Rainfall-Runoff, Horton Infiltration, GW Flow, and dynamic wave flow routing), SWMM-UrbanEVA requires 2 h 50 min for 20 months, while SWMM requires only 20 min. The ratio is 1:8.5. The computing time of SWMM-UrbanEVA is approximately the same as that of comparable software (e.g., MIKE-SHE).

However, the ability to integrate urban drainage systems and near natural river basins in one single model puts the increased computing time in a different

perspective. In other model environments, integrated modelling would require numeric coupling of different modules, often connected with serious numeric stability problems.

3 Scenario Based Flood Characteristics for the Current State of Land Use

3.1 Introduction

3.1.1 Background

Flooding is a natural and recurring phenomenon. It ensures fertile floodplains and therefore favours agriculture in river valleys. Besides, the use of rivers as transport routes for trade promoted human settlement along the waterways. However, for both reasons, land cultivation and water transport, rivers and streams have often been straightened [85]. In parallel, population growth is inevitably accompanied by increasing land sealing, which in turn accelerates surface runoff [86–88] at the expense of evaporation and infiltration. In Italy, for example, an average increment of 8.4 % in soil sealing induced an average increase in surface runoff equal to 3.5 % and 2.7 % respectively for 20- and 200-year return periods [89]. Increased surface runoff, flow course shortening, or deformation and loss of retention space are drivers for raising peak flows and increased flood probabilities. These factors are superimposed by changing hydro-meteorological conditions due to climate [90–92]. Accordingly, responsible development of land use should also take the resulting impact on river runoff and flood probability into account. This requires a sound understanding of the hydrological and hydrodynamic processes in the regarded catchment and the affected river basin.

The term flood risk is always related to the probability or recurrence interval of a certain runoff or water table. Generally, these values can be derived via three ways:

1. Statistical analysis of historic time series
2. Statistical regionalization of flood characteristics
3. Hydrologic modelling (if a water table is required, supplemented by hydrodynamic models)

Time series analysis requires the availability of monitoring data of flow and/or water table over a sufficient long observation period (10 a minimum, 30 a or more is better [93]). Since monitoring stations are maintenance-intensive and costly, those data are only available for a very limited number of rivers or river sections. Smaller streams and tributaries tend not to be surveyed at all.

To close this data gap, various procedures for regionalizing flood parameters are in use. Most of them are based on observed discharges in similar regions. Simple

methods are related solely on the size of the catchment and assume the same discharge per area at the location with measurement and at the location without measurement. Further development of this is the multiple regression, which links several relevant basin parameters (e.g., basin size, slope, flow length, basin shape, soil, and geology parameters) to peak discharge. There are a number of other procedures, yet these will not be considered further here. Statistical regionalization methods are relatively simple to apply and require comparatively little time, which is why they are justifiably utilized in practice for certain questions.

The third option is to employ (regionalized) hydrologic models to predict runoff from ungauged watersheds, with the objective of relating various model parameters to the physical characteristics of the watershed [94; 95]. Models used in this context are usually conceptual, lumped models, describing the runoff process in a simplified way, based on comparatively few model parameters. Influencing factors and thus significant model parameters differ from region to region and depend on the dominant hydrological processes in the respective catchment region and on the desired result (e.g., peak flows vs. average monthly or annual flow values). A study conducted in the Ivory Coast marked that land use and rainfall distribution over the year are important model parameters in the context of regionalization [96]. The role of precipitation was also highlighted by a study from Australia using a monthly water balance model, where the mean annual precipitation at different locations ranged from 600 mm to 2400 mm [97]. However, this shows that model results are also sensitive to the precipitation characteristics, which is actually an input variable.

Astonishingly, deterministic models with a clear conceptual link between physical conditions in the catchment and the resulting hydrologic processes have been rarely applied in ungauged systems, probably mainly due parametrization questions. However, namely process-oriented semi or fully distributed models should be well suitable for those situations provided that the physical data can be derived from geodata or remote sensing. This would allow for physically funded parameter transfer from modelling studies with calibration data. A corresponding study dedicated to flash floods achieved only a small decrease of performance of 10 % by transferring calibrated model parameters to a new validation site [98].

None of the studies mentioned above consider river or stream hydraulics, which is of particular importance in the formation of flood flows. In particular, small rivers in cultivated or urbanized areas are modified by man-made structures such as culverts

and pipelines, which have a significant influence on flow dynamics and water level. Leading back to the initial problem of analysing future land use changes on stream hydraulics, deterministic models should also provide a hydrodynamic functionality, requiring additional physical data, i.e., river profiles and infrastructural data.

Meanwhile, in many parts of the world, the availability and quality of hydrologically and hydrodynamically relevant geodata (soil type, land use, DEM, groundwater levels, etc.) is very good. Setup and parametrization of physically based models directly based on these data should therefore be more and more possible.

However, this concept has a clear constraint: The application of those models, even if well parametrized, is hardly applicable by regional planners who are typically not modelling experts. When providing those models for regional planning purposes, they must be tailored for the envisaged group of end-users. A promising way to do so is the combination of model setup, parametrization and pre-processing for the status quo with a simplified GIS-based analysis for land-use change scenarios.

3.1.2 Objectives and Structure of the Study

Summing up the arguments above, the overall objective of this study is twofold:

1. To develop a concept to setup and parametrize a deterministic distributed model based on available geodata.
2. To develop a simplified algorithm for analysing land-use change scenarios that is based on the models developed but can be used by regional planning practitioners.

Following these targets, the study is separated into two papers. Part 1 (here chap. 3) is dedicated to model setup and parametrization and the determination of flood characteristics for the current state and thus forms the basis for the second part. The innovative approach of the method presented lies in the automated transfer of physical model parameters based on geodata for the use of spatially and temporally highly resolved deterministic rainfall runoff and stream models. The desired results can be generated comparatively fast but are, at the same time, physically validated.

Part 2 will describe the developed simplified procedure for the rapid calculation of land use change effects on flood characteristics and its embedding in a GIS-based decision support system (here chap. 4).

3.2 Materials and Methods

3.2.1 Study Area and Data Used

The study area is located in the northeast of Germany and covers approximately 530 km². It comprises the city of Rostock and its neighbouring municipalities (see Figure 12) and contains more than 1500 km of small tributaries that drain into the Warnow or directly into the Baltic Sea. In order to achieve a high spatial resolution in the model setup and to maintain an overview in the process, the study area was divided into several smaller catchments.

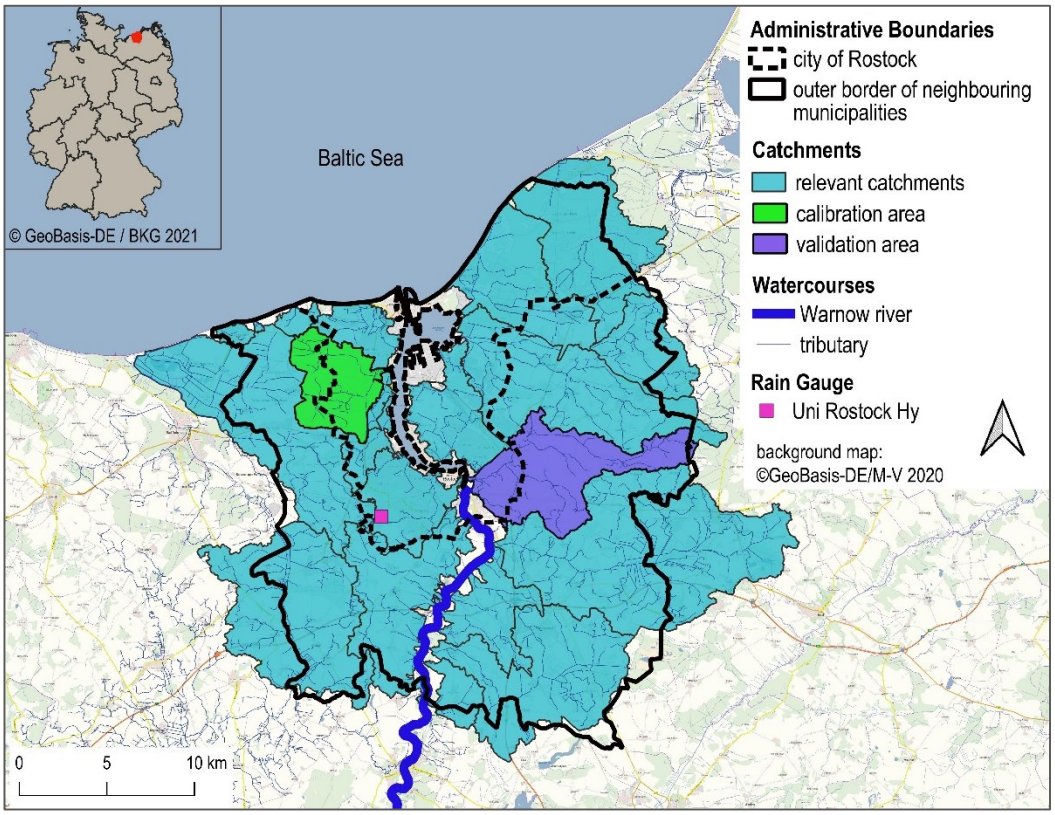

Figure 12. Relevant surface catchments of the study area, administrative boundaries, and rain gauge used for simulations.

Although the catchments are located close to each other and are subject to very similar climatic conditions, they differ in some characteristics. For example, the landscape in the south-east is relatively hilly, while the catchments near the Baltic Sea are rather flat. The catchments within the city have a high proportion of sealed surfaces, while agricultural land use dominates in the surrounding municipalities.

For model calibration, the Schmarler Bach catchment was used (Figure 13) as continuous flow and water level measurement data had already been collected here [50]. The 23 km² area has little gradient and is therefore one of the flat

representatives (-1 m – 30 m above sea level). A pumping station keeps the water level in the lower reaches below the level of the Baltic Sea. Approximately 34 % of the area is partially impervious, which is due to urban use (residential area, traffic area, and industry/trade) [99]. The second largest share is arable land with 29 %. With intensive urban use, the number of storm water disposals increases. At Schmarler Bach, there are a total of 91 points, which is the largest number compared to the other model sites.

The monitoring station is located in the southern branch of the stream network. Its catchment is about 12 km² in size and is already significantly influenced by urban use.

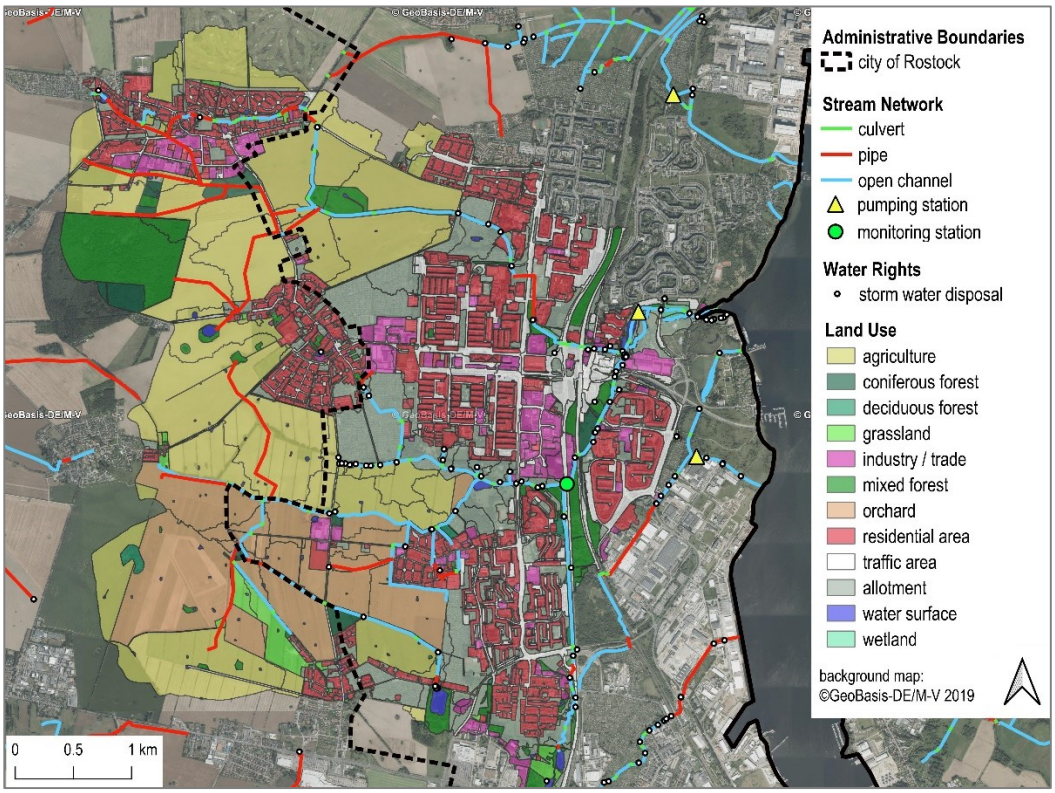

Figure 13. Schmarler Bach catchment used for model calibration.

The catchment of the Carbäk stream was used for testing the concept of parameter transfer based on geodata without additional calibration (Figure 14). With its 42 km², it is about twice as large as the Schmarler Bach catchment. Due to the large east–west extension, the surface elevations span between 0 m to 65 m above sea level and thus show a comparatively larger range. Differences can be noted in land use patterns: While arable land takes up more than 50 % of the area, partial sealed uses are only represented by 18 %. Accordingly, there are fewer storm water disposals to count (44

in total). The catchment of the monitoring station is 33 km² in size and thus almost 3 times larger than the catchment of the monitoring station in the Schmarler Bach.

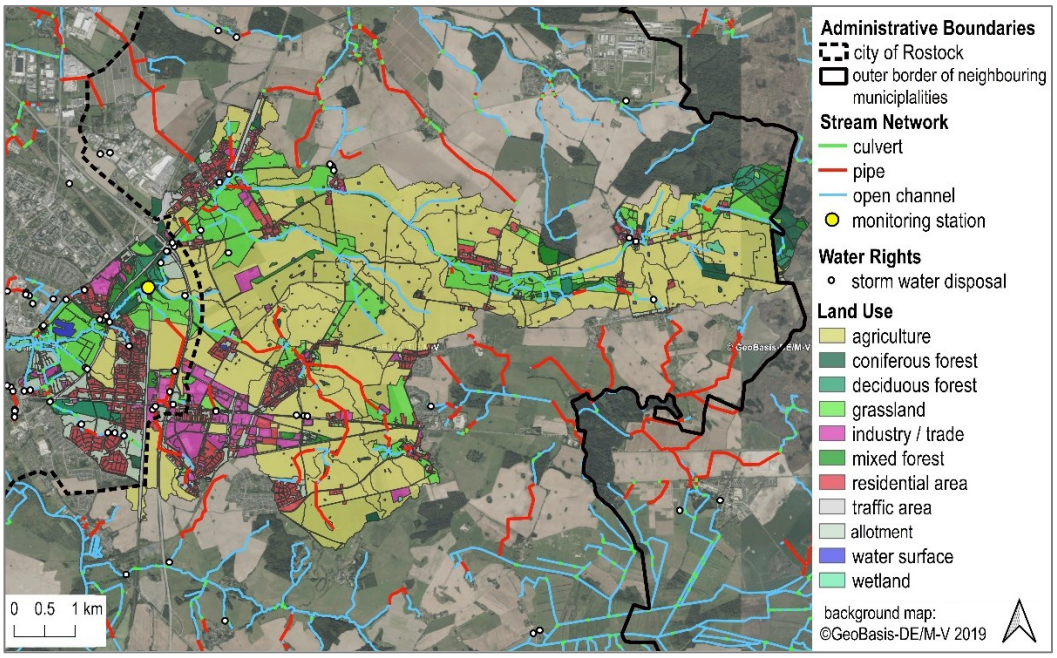

Figure 14. Carbäk stream catchment used for model validation.

Figure 15 compares the measured flows of the two monitoring stations and illustrates the daily sums of rainfall of the rain gauge “Uni Rostock Hy” (the University of Rostock, department of hydrology and applied meteorology). Schmarler Bach flows show high peaks in the summer months, especially in wet June and July 2017, which is due to intensive rainfall and the large proportion of sealed areas that provoke a high amount of direct (and fast) runoff. In contrast, the Carbäk shows the highest flows generally in winter and spring and also in the extraordinary wet month June/July 2017. This suggests that the source of high flows in the Carbäk catchment are different from those in the Schmarler Bach. Since the Carbäk catchment is intensively farmed and drained, the high flows can be attributed to agricultural tile drainage interflows. These occur in the stream when the surrounding soil is saturated, which is usually the case when more rain falls than evapotranspirates. As these interflows have to pass through the soil to enter the drainage network, they require more time compared to surface runoff, which results in a stretched, flattened course of discharges.

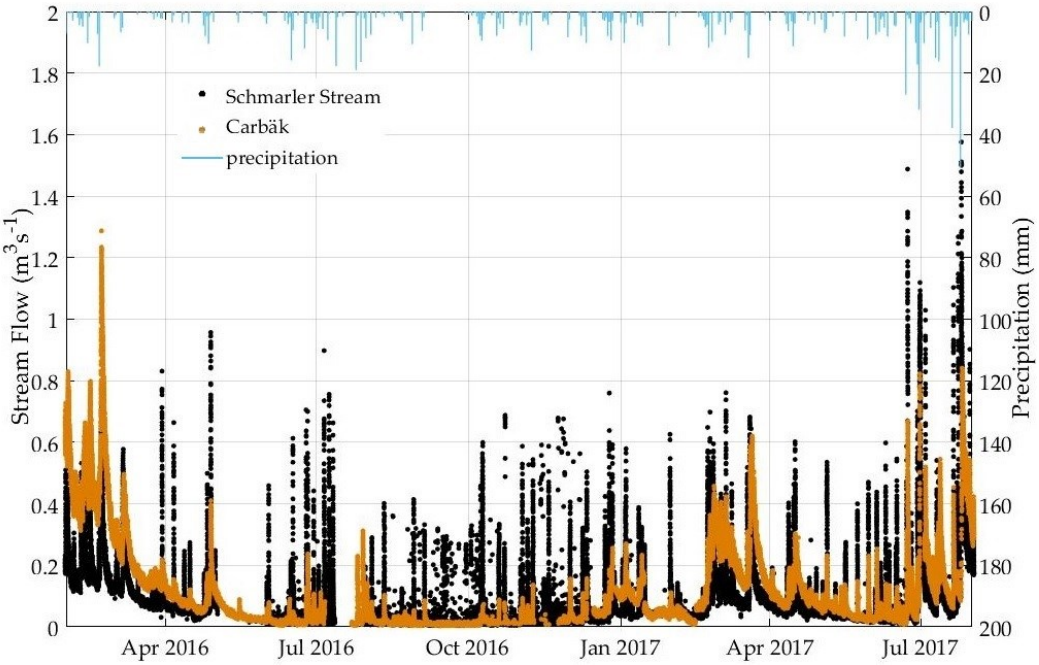

Figure 15. Measured flow at the two monitoring stations in the Schmarler Bach and in the Carbäk; measured precipitation approximately 7 km south of the Schmarler Bach catchment and 9 km west of the Carbäk, respectively.

3.2.2 Data Processing and Modelling Software

The basis for further work is the homogenization of geodata, which was carried out using QGIS (version 3.10.2) [100; 101]. The attributes of the homogenized geodata are further processed with the help of a spreadsheet program. Here, Microsoft (MS) Excel was used together with its Visual Basic for Applications (VBA) interface [102]. VBA contributes to automation and enables faster processing of repetitive tasks. A free alternative to MS Excel is LibreOffice Calc [103], which also provides a VBA interface, but with limited macro support.

Prior to actual model development, a thorough review of available modelling software tools was performed. There is a wide range of hydrologic models with different pros and cons (cf. [104]). For the purposes of this study, the software should fulfil the following criteria:

- Freeware for wide transferability and applicability
- Combined representation of rainfall-runoff and hydrodynamic streamflow processes to avoid external coupling of different models
- Physically based, parameters widely derivable from geodata
- Sufficient spatial distribution, capable to allocate distinct land use changes in the regarded river basin

- Easy and automatable setup and parametrization of the model

Namely, the required hydrodynamic functionality is rarely available. After a first screening, the combination of HEC-HMS [42] with HEC-RAS [43] and SWMM-UrbanEVA [52], an extension of the widely used software SWMM, were the most promising candidates. The UrbanEVA upgrade involves the implementation of vegetation-specific evapotranspiration and its reduction by a shading factor in the case of urban shading. A detailed description can be found in [52; 99]. In a following detailed comparison, the decision was made in favour of SWMM-UrbanEVA.

SWMM (storm water management model [105]) was originally developed for the simulation and evaluation of storm runoff and sewer hydraulics in urban areas [106]. However, with the extension for evapotranspiration calculation, SWMM is very well suited for the simulation of near-natural catchments outside urban areas [99]. The calculation of water balance variables and streamflow is largely physically based. The SWMM input file is a simple text file that can be opened, read, and modified in any text editor, which facilitates an automated model generation. One of the biggest advantages of SWMM is that it combines both a hydrological rainfall-runoff model and a hydrodynamic drainage model in one software, which makes the numerical calculation very effective and stable, since no external coupling is needed.

3.2.3 The General Concept

In order to obtain flood characteristics for the actual state of land use, a method was developed that consists of several steps, each involving the use of different software tools (Figure 16). The individual steps are described in detail in the following subsections.

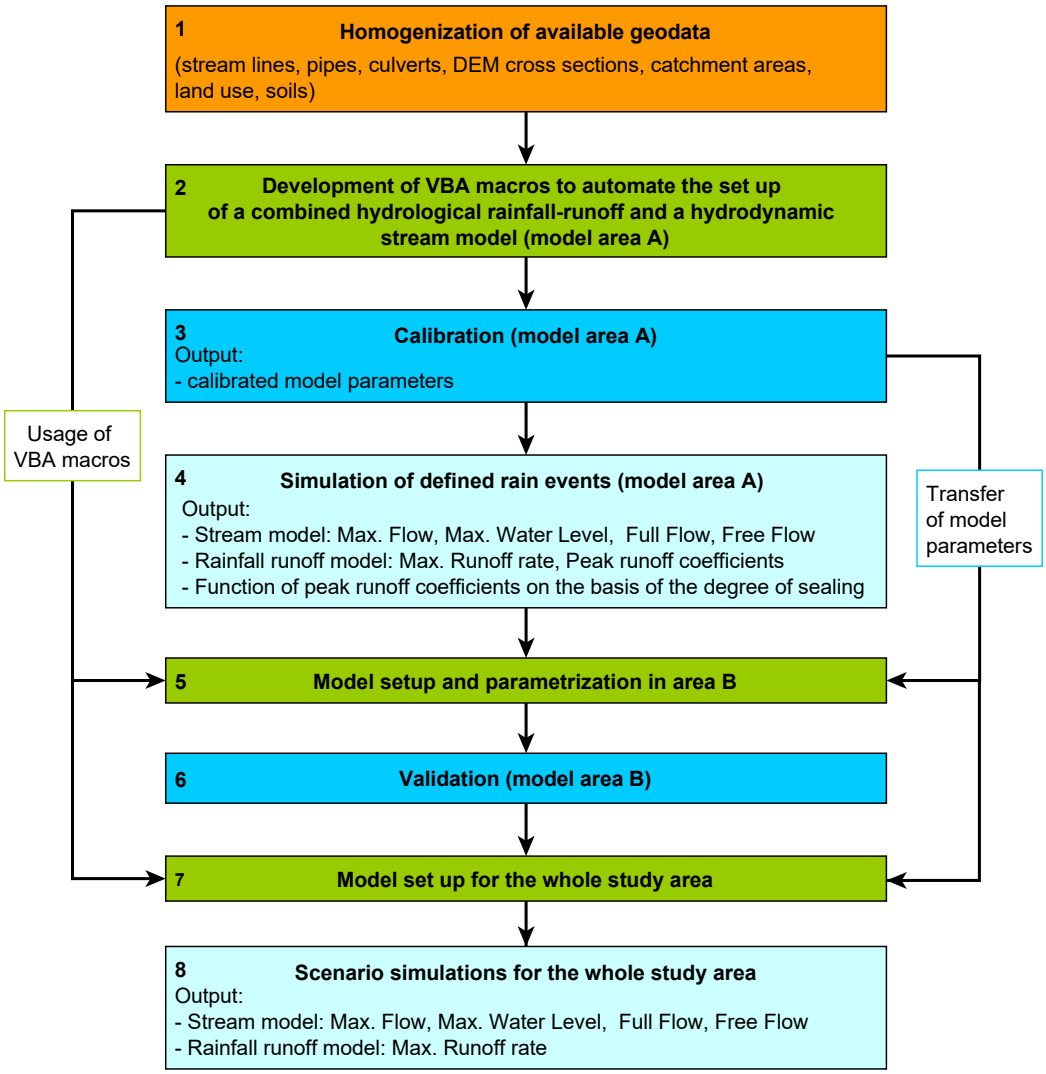

Figure 16. Pre-processing of flood characteristics for the current state of land use (orange: QGIS tools, green: VBA and MS Excel tools, blue: SWMM-UrbanEVA, light blue: SWMM).

3.2.4 Derivation of Model Parameters from Geodata

In the first step, geodata are homogenized so that uniform datasets without gaps are available for the entire study area. The necessary sub-steps for this were carried out with QGIS. Table 11 provides an overview of the data used and the attributes and model parameters derived from it.

Table 11. Geodata used for the setup of the SWMM-UrbanEVA model (WIN = hierarchical watercourse identification number).

Available geodata	Format	Parameters/attributes derived for SWMM
hydrodynamic stream model		
open channel segments	vector (line)	WIN, chainage, positioning

Available geodata	Format	Parameters/attributes derived for SWMM
watercourse routes	vector (line) with measures	WIN, chainage, positioning
Pipes, culverts	vector (line)	chainage, diameter, material (roughness)
storm water disposals (water rights)	vector (points)	diameter, material (roughness)
DEM_0.2	raster (0.2 m resolution)	stream cross sections / transects
DEM_5	raster (5 m resolution)	ground elevation above pipes, culverts and storm water disposals
rainfall-runoff model		
surface catchments for 50m-stream segments	vector (polygon)	area size, flow length, outlet (computation node of hydrodynamic model)
land use maps	vector (polygon)	generalized land use types, leaf area index, crop factor, detention storage, roughness
groundwater isohypses	vector (lines)	average groundwater level for each subcatchment
soil maps	vector (polygon)	conductivity, porosity, field capacity, wilting point
DEM_5	raster (5 m resolution)	average terrain slope
soil sealing maps	raster (10 m resolution)	degree of sealing

For the construction of the hydrodynamic stream model, mainly vector data in the form of lines are used. These include open channels, pipelines, and culverts (Figure 17). Points are generated at certain positions on these lines, which later become the calculation nodes (or junctions) in SWMM. Cross sections (also called transects in SWMM) of the open channels were generated every 50 m on the basis of the DEM with a cell size of 20 cm. The high spatial resolution thus enables the recording of smaller streams with a width of less than 2 m. When deriving cross profiles using the DEM, it should be noted that the lowest point represents the water level and not the actual bed, if water is present. Since we are interested in flood forecast and thus in high water levels, and the deviation of the absolute water levels in the upper layer of the trapezoidal or parabolic cross-sections is small (< 10 cm), this inaccuracy is negligible here.

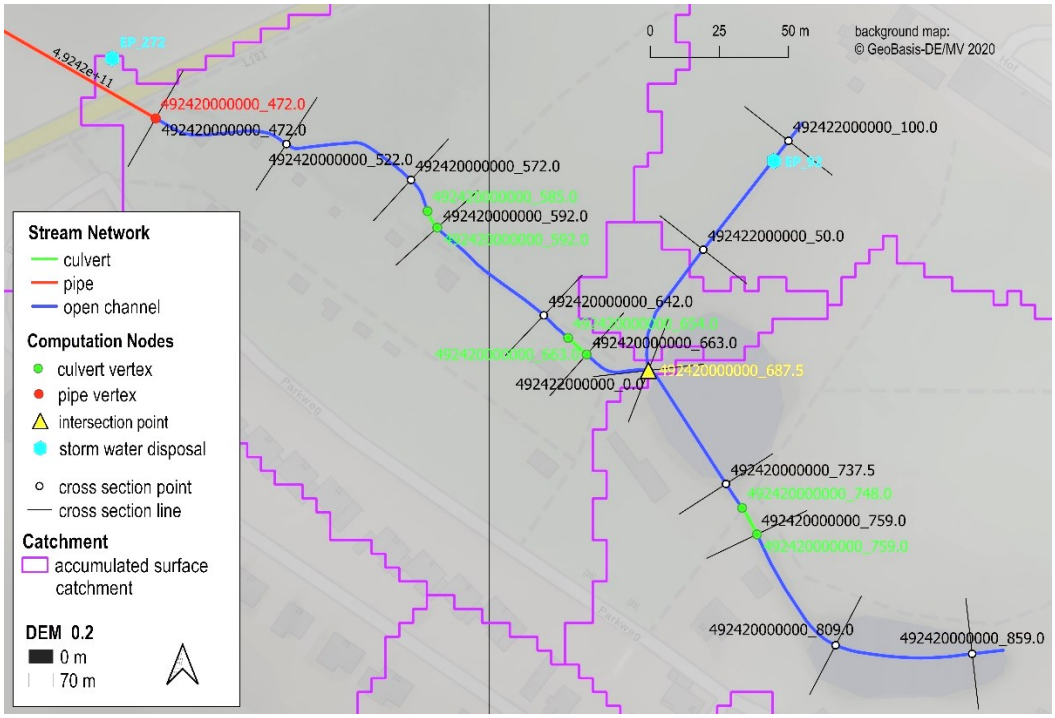

Figure 17. Calculation nodes of the stream network composed of pipe and culvert vertices, cross sections points, intersection points, and storm water disposals (DEM_0.2 = digital elevation model with a cell size of 0.2m).

In addition to the points of the watercourse network, the storm water disposal points are added, which represent the last point of the storm sewer network before the rainwater enters the stream. With the information on the diameter and/or the maximum permissible discharge, the direct runoff from the linked areas can be throttled during the simulation. In this way, the storm sewer network does not have to be included in detail. In the end, five categories of points are produced from which the hydrodynamic model is built: Cross section (open channel), pipe and culvert points, intersection points, and storm water disposal points. They are all assigned a unique ID composed of the hierarchical 12-digit watercourse identification number (WIN) in conjunction with the chainage (e.g., 492000000000_4847.0).

For the rainfall-runoff model, the subcatchments are generated on the basis of the surface subcatchments of the 50m-stream segments. Since the spatial resolution is quite high, they have to be generalized to save computing time during the simulation. Therefore, the subcatchments of the 50m-stream segments are accumulated in such a way that new subcatchments start whenever two streams meet or rainwater is discharged from the storm sewer network. Each generated subcatchment is assigned an outlet, which serves to exchange the simulated water volumes between the rainfall-runoff model and the stream. Information on the mean groundwater level is

also required for the model construction, which is derived from the groundwater isohypses or from the corresponding interpolated raster map, respectively. The subcatchments are then subdivided according to 13 land use classes (Table 12).

Table 12. Types of land use in the study area.

Category	Land use classes
water	water surface
near natural/ cultivated land	agriculture; wetland; grassland; deciduous forest; mixed forest; coniferous forest; parks; orchard; beach
urban	industry / trade; residential area; traffic area

For the intersected subcatchments, mean values of ground height, slope, soil attributes and degree of sealing are calculated. The point data for the hydrodynamic flow model and the area-based data for the rainfall-runoff model are processed further using Excel and VBA.

3.2.5 Automating the Model Setup

The computation points of the hydrodynamic stream system are loaded into an Excel table and sorted according to their WIN and chainage. After assigning the node properties (Figure 18, attributes = white boxes), the cross sections of the open channels (transects) receive special treatment to a certain extent, as their processing is relatively complex. Once the transect corrections are completed, all categories of calculation points including their attributes can be listed together and sorted in order to create the list of junctions. Now the invert elevations at the culvert and intersection nodes can be interpolated using the open cross-sections upstream and downstream. From the list of junctions, the list of conduits is created. Each conduit is assigned an inlet and outlet node and a unique ID. A flow restriction may only be applied to the conduits connecting the storm water disposals with the stream. If the permitting authorities have specified a diameter for the lower end of the storm sewer channel, then the diameter limits the flow. Otherwise, the flow limitation is realized via the approved peak discharge.

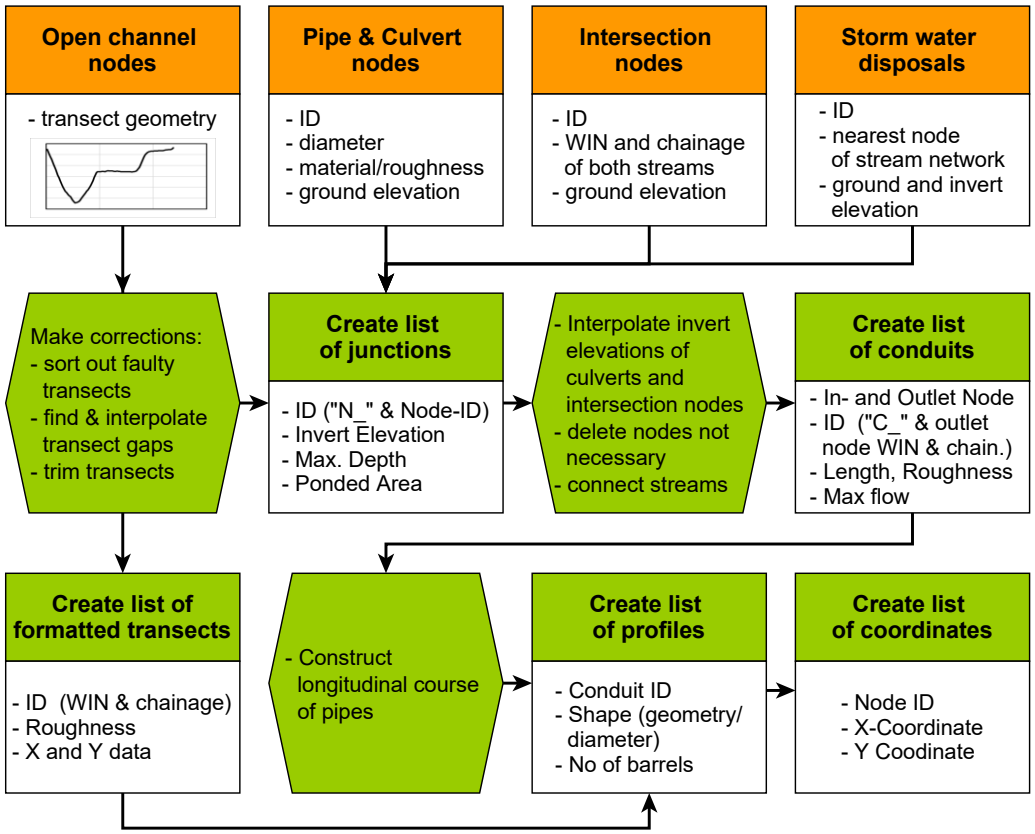

Figure 18. Hydraulic flow model build-up—steps to create the SWMM-input file (orange: QGIS output; green: VBA/Excel steps; white boxes contain respective attributes).

Pipeline routes are designed depending on a specified minimum gradient and a minimum cover with soil, beginning with a depth of 2 m below ground.

For the hydrological rainfall-runoff model, a large part of the work has already been done in QGIS. The output is a large attribute table in which the properties of each subcatchment (surface, land use, soil, and aquifer properties, inlet node of hydraulic network) are stored. The necessary VBA steps now consist of copying the values under the appropriate SWMM headings and formatting them in a software-readable format.

3.2.6 Model setup, Calibration, Parameter Transfer and Validation

The catchment and stream model setup was developed and tested in a case study using the Schmarler Bach site. The combined model was consistently built up on the basis of homogenized geodata using VBA macros (VBA – Visual Basic for Applications) to automate the process. By splitting the river course in fairly short sections of about 50 to 100 m, spatially high-resolution flood characteristics (maximum flow, maximum head, maximum capacity, etc.) can be provided for a relatively large area.

After setup, a detailed calibration was performed on the basis of continuous monitoring data of flow and water level. Calibration methods and their fields of application are presented and discussed in [99]. Table 13 presents performance criteria applied to check the model accuracy with regard to the stream flow. It has been supplemented by the peak error E_{peak}, which represents the relative deviation of the simulated from the observed maximum value of a specific peak flow event.

Table 13. Error measures and performance criteria. (taken from [99], supplemented).

Designation	Abbre-viation	Formula	No.
Volume error	E_{Vol}	$1 - \frac{\int Q_{calc}\, dt}{\int Q_{obs}\, dt}$	(29)
Mean absolute error	MAE	$\frac{\sum_t \lvert Obs_{i,t} - Calc_{i,t} \rvert}{n}$	(30)
Correlation coefficient	R	$\frac{\sum_t (Calc_{i,t} - \overline{Calc_{i,t}}) \times (Obs_{i,t} - \overline{Obs_{i,t}})}{\sqrt{\sum_t (Calc_{i,t} - \overline{Calc_{i,t}})^2 \times \sum_t (Obs_{i,t} - \overline{Obs_{i,t}})^2}}$	(31)
Nash-Sutcliffe efficiency	NSE	$1 - \frac{\sum_t (Obs_{i,t} - Calc_{i,t})^2}{\sum_t (Obs_{i,t} - \overline{Obs_{i,t}})^2}$	(32)
Peak error	E_{peak}	$\frac{Q_{calc}}{Q_{obs}} \cdot 100$	(33)

Q_{calc} = calculated flow, Q_{obs} = observed flow; Obs = measured value (observed); Calc = calculated value; Indices: i = location, t = time, n = number of measurement data.

In the process, physical model parameters were derived from geodata and adjusted to obtain the best model fit regarding stream flow. In a subsequent step, the resulting correlations between geodata and model parameters were transferred to another monitored river basin, the Carbäk catchment, and validated with measured flow data. This way the general validity of the calibrated model parameters is checked, and it is simultaneously tested whether the transfer of largely physically based model parameters is fundamentally satisfactory – despite the different territorial characteristics. After assessing the applicability of this modelling concept, the method was transferred to other river basins in the area without monitoring data.

The parametrized models are finally applied to simulate precipitation scenarios of defined duration and return period in order to generate flood characteristics for the current state of land use. The flood-relevant return period is related to the predominant land uses in the study area and corresponds to the demanded protection

level. For heterogeneous land use, this requires defining different return periods and running the model with the appropriate precipitation data.

3.2.7 Scenario Simulation on the Basis of Defined Rain Events

3.2.7.1 Selection of Statistical Rainfall Events

When choosing statistical rainfall events, it is first necessary to consider which risk classes are present in the study area. The risk class in turn depends on the predominant land use. For the area of the Hanseatic City of Rostock, assignments of protection levels (return period) to land use classes have already been made (Table 14). Within the framework of this study, these were as well transferred to the surrounding rural district.

Table 14. Assignment of land use classes to risk classes (protection level/return period) (excerpt taken from [107], modified).

Protection level / return period	Land use class	
0 a	– Beach – Dune – Moorland – Ruderal land – Wooded area	– Watercourse > 3 m – Ditch < 3 m – Standing water body – Coastal waters
2 a	– Military green space	– Agricultural grassland
10 a	– Arable land – Football pitch – Tennis court	– Sports and recreation – Other sports facilities
25 a	– Single housing – Town square – Carpark – Allotment	– Orchard plantation – Rainwater retention basin – Campsite
100 a	– Row housing – Large block housing – Sewage treatment plant – Railway and railway track	– Industry and commerce – Motorway – Landfill – Cemetery

To determine hydraulic parameters such as statistical flows and water levels as well as profile capacities, simulations were carried out on the basis of statistical precipitation events. Their return periods were selected according to Table 14,

whereby a return period of 50 a was additionally taken into account. The duration of the decisive (worst) precipitation event depends primarily on the size of the subcatchment and the corresponding flow length, i.e., the smaller the catchment, the shorter (and at the same time more intense) the decisive rainfall event. Here, the duration categories 1h, 3h, 6h, 9h, and 12h were applied and combined with the return periods to generate 18 precipitation scenarios (Table 15).

Table 15. Selected statistical precipitation events and applied intensity course.

duration	return period	intensity course
1 h	2 a, 100 a	statistical calculation according to [108] as described in [109]
3 h	10 a, 25 a, 50 a, 100 a	assumption of a block rain
6 h	10 a, 25 a, 50 a, 100 a	assumption of a block rain
9 h	10 a, 25 a, 50 a, 100 a	assumption of a block rain
12 h	10 a, 25 a, 50 a, 100 a	assumption of a block rain

The precipitation amounts were retrieved from the heavy rainfall regionalization (German abbreviation: KOSTRA atlas) of the German Weather Service [110]. The KOSTRA atlas provides raster data on precipitation amounts and intensities per area for Germany as a function of duration D and annuality T (return period). The data are available in an 8.5 km x 8.5 km grid. Each model site is uniformly over-rained, i.e., one representative cell is assigned to each catchment. If a catchment is covered by two or more cells in equal proportions, the cell with the highest precipitation amounts is used.

Since there is usually a clear intensity variation for short durations, the intensity course was statistically determined using the long-term rain data of the monitoring station in Warnemünde (central north of the study area). The data have a temporal resolution of 5 minutes and were recorded by the German Weather Service. The characteristic precipitation pattern for the respective rainfall duration is obtained by normalising the measured natural rain events of the same duration, which is achieved by temporal centring of the 5 min peak intervals [109].

The application of design rain events in scenario simulation, selected based on stipulated flood reoccurrence intervals, is a pragmatic choice, typically applied in urban hydrology. There is a tendency where the return period of the flood or peak flow is smaller than that of the initializing rainfall event. This way, the choice is “on the safe side”.

3.2.7.2 Initial Condition

Before the scenario simulations of the different rainfall events can be started, some preliminary work is necessary. Here, the generation of a start condition on which the model rainfall is based is of particular importance. This refers to all reservoir levels in the catchment, i.e., the water level above the terrain, the proportion of the soil pores filled with water, the groundwater level, and the water level in the stream network. For this purpose, the model is run with monthly average evaporation and precipitation data in order to generate a so-called hot start file at the end of the simulation. The final condition of this pre-simulation then forms the start condition for the scenario simulation. In this case, a condition was chosen that leads to average flows in the watercourse.

3.3 Results and Discussion

3.3.1 Parameterization

Table 16 presents important model parameters for the dominant processes in the study area. It was the intention to reduce the number of individually calibrated parameters to a minimum and to assign as much parameters as possible directly based on geodata information. In particular, the parameters derived from high spatial resolution geodata, such as the soil maps, were taken as given. For example, infiltration-relevant physical soil properties, such as conductivities, porosity, wilting point, and field capacity, were determined based on the soil type. The most important hydrological processes affecting streamflow are surface runoff, which is responsible for peak flows, and groundwater inflow, which is the base or starting point for peak flows. Therefore, the most effort was put into the calibration of these processes.

Groundwater flow is designed to simulate near-surface agricultural tile drainage. Strictly speaking, it imitates interflow. The threshold water table elevation controls the extent to which water-level groundwater inflow to the stream occurs. It was assumed (or calibrated) that the drainage pipes are on average 1.2 m below ground level. In dealing with the material properties, borehole profiles were surveyed. Many of these contained a near-surface aquifer with an underlying impounding boulder clay layer, which is typical for the north-eastern German lowlands. As part of a generalization, the material properties were assumed to be uniform for the entire study area and checked against literature values.

When calibrating surface runoff, the roughness, detention storage, and flow length (= area size / width) play a role. The latter was derived as a function of the area size to ensure parameter transfer. For the former, a distinction was made between sealed and pervious surface portions. The proportion of sealed surfaces was derived from satellite data (Copernicus Sentinel-2) with a resolution of 10m and was therefore taken as given.

Soil infiltration and evapotranspiration have an indirect influence on groundwater flow, since they control how much water reaches the groundwater and thus fill the reservoir. Further details can be found in [99].

Table 16. Excerpt of important model parameters of the study area (* only SWMM-UrbanEVA).

Parameter	Unit	Value, range, or calculation formula	Subject to calibration	Spatial distribution [1,2]	Source / derived from
Surface Runoff					
Width	m	$\frac{\sqrt{Area}}{6}$	yes	individual	function of area size
percent of impervious area	%	0 - 94	no	individual	satellite data
average slope	%	0 - 37	no	individual	DEM
roughness pervious	s $(m^{1/3})^{-1}$	0.3	yes	pervious area share	in accordance with literature values
roughness impervious	s $(m^{1/3})^{-1}$	0.025	yes	impervious area share	in accordance with literature values
detention storage pervious	mm	12	yes	pervious area share	in accordance with literature values
detention storage impervious	mm	0.5	yes	impervious area share	in accordance with literature values
Soil infiltration / percolation					
max. Infiltration Rate	mm hr^{-1}	19 - 281	no	individual	soil maps
min. Infiltration Rate	mm hr^{-1}	2 -171	no	individual	soil maps
soil porosity	-	0.23 - 0.79	no	individual	soil maps
field capacity	-	0.1 - 0.75	no	individual	soil maps
wilting point	-	0.04 - 0.36	no	individual	soil maps
seepage rate	mm hr^{-1}	2 -171	no	individual	soil maps
Plant parameters *					

Parameter	Unit	Value, range, or calculation formula	Subject to calibration	Spatial distribution [1,2]	Source / derived from
vegetation factor vf	-	0.7 - 1.5	yes	land use class dependent	in accordance with literature values
average leaf area index (LAI)	m m^{-1}	1.7 - 3.6	no	land use class dependent	satellite data
LAI monthly coefficients	-	0.2 - 1.7	no	land use class dependent	satellite data
Groundwater flow					
conductivity	mm hr^{-1}	150	yes	global	in accordance with borehole data and literature values
porosity	-	0.43	yes	global	in accordance with borehole data and literature values
wilting point	-	0.05	yes	global	in accordance with borehole data and literature values
field capacity	-	0.12	yes	global	in accordance with borehole data and literature values
threshold water table elevation	m	1.2 m below ground elevation	yes	individual	DEM
lower groundwater loss rate	mm hr^{-1}	5.0E-06	yes	global	in accordance with borehole data and literature values

[1] individual → each subcatchment has its own individual value

[2] global → one value for the entire study area

3.3.2 Calibration Results

Figure 19 shows the simulated hydrographs with SWMM-UrbanEVA and the corresponding observed stream flows at the monitoring station of the calibration site "Schmarler Bach". The upper diagram (a) shows the entire observation period (21 January 2016 to 31 July 2017), while the lower diagram (b) focuses on the section from May to July 2017. Table 17 presents the corresponding error measures and performance criteria. The visual impression shows a good to very good match between the measured and simulated values. The volume error (E_{vol}) of 2.4 % is very small, as is the mean absolute error (MAE) of 0.03 m^3s^{-1}. The dynamics are well reproduced (correlation coefficient R = 0.84) and the coverage of simulated and

measured flows (Nash–Sutcliffe efficiency NSE = 0.84) is overall in the very good range. However, since the focus of this work is primarily on flood characteristics, high flows are of particular interest here. These occur in the catchment area of the Schmarler Bach mainly in the summer months. In particular, the months of June and July 2017 exhibited the highest flows in the observation period. The events of mid/late July even led to local flooding of streets and cellars in the inner city of Rostock [111; 112].

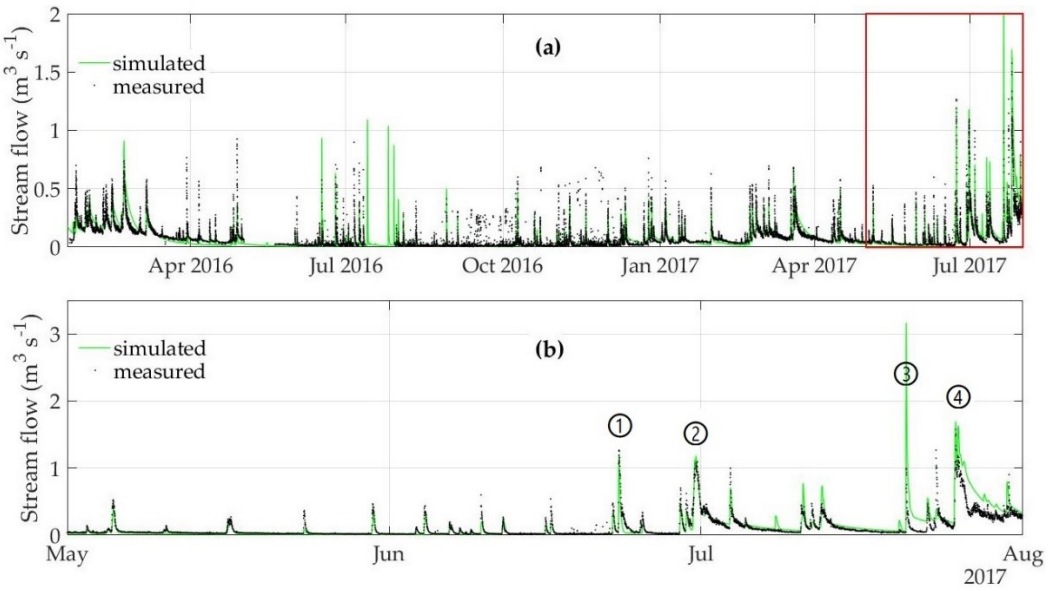

Figure 19. Comparison of simulated and measured flows at the monitoring station (chainage 2+417) of the Schmarler Bach (calibration site); the red box in the upper (a) diagram marks the time span of the lower (b) diagram.

Table 17. Model performance based on error measures and performance criteria related to the measured flow rate at the monitoring station in the Schmarler Bach in the period 21 January 2016 to 31 July 2017.

E_{Vol} (%)	MAE (m^3s^{-1})	R (-)	NSE (-)
2.4	0.032	0.84	0.84

While the model apparently reproduces the more frequent, smaller rainfall events very well, there are nevertheless differences between the observed and simulated peak flows for the larger events (Figure 19, diagram b and Table 18). Events 1, 2, and 4 only deviate by a maximum of 10 % from those measured, but event 3 (20.07.2017) shows a significant difference as it is more than three times as large as the observed maximum value. Here, it can be assumed that the precipitation centre was directly above the rain gauge (7 km south of the Schmarler Bach) and the catchment itself was located rather on the edge of the rain field at that time. In fact, heavy rainfall events

are often short and very localised, especially in urban areas, which was also reflected in the data of different rain gauges in the city of Rostock (cf. Figure 21). The duration of the rain event is considered relatively short (Table 19) and reinforces the thesis. For this reason, the event of 20.07.2017 is classified as less relevant for the Schmarler Bach.

Table 18. Peak error of the four largest flows in the observation period at the monitoring station in the Schmarler Bach.

	①	②	③	④
Date	23.06.2017	30.06.2017	20.07.2017	25.07.2017
Peak error (%)	95	110	318	108

Table 19. Duration and total amount of corresponding rain events measured at the gauge Uni Rostock Hy.

	①	②	③	④
Date	23.06.2017	30.06.2017	20.07.2017	25.07.2017
Duration of rain event (h)	2.3	17.5	1.3	4.8
Total amount of rain event (mm)	18	41	38	28

3.3.3 Validation Results

Figure 20 shows the simulated hydrographs with SWMM-UrbanEVA and the observed stream flows at the monitoring station of the validation site "Carbäk". Table 20 lists the corresponding error measures and performance criteria. While the cumulative flows in the Schmarler Bach are only slightly too low (E_{vol} = 2.4 %), they are 9.6 % too high in the Carbäk. The MAE is also higher by 0.013 m^3s^{-1}. However, the dynamics of the flows are reproduced well by the model (R = 0.88). Nevertheless, the individual observed values are less well-met overall compared to the Schmarler Bach. Thus, the Nash–Sutcliffe efficiency coefficient is at the upper (good) edge of the satisfactory range (NSE = 0.59).

Table 20. Model performance based on error measures and performance criteria related to the observed flow rate at the monitoring station in the Carbäk stream in the period 27 January 2016 to 17 Aug 2017.

E_{Vol} (%)	MAE (m^3s^{-1})	R (-)	NSE (-)
-9.6	0.045	0.88	0.59

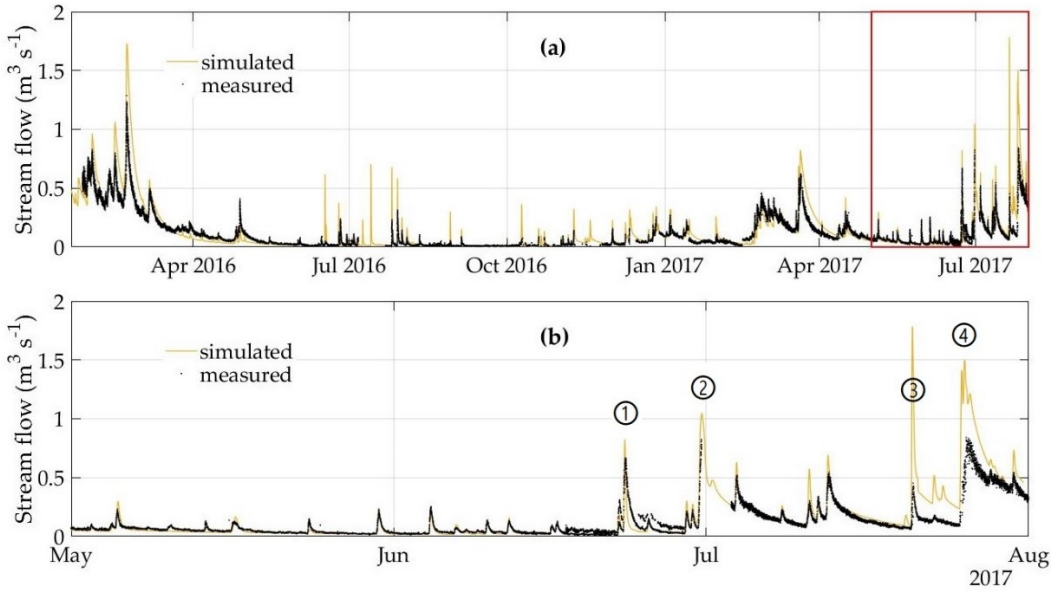

Figure 20. Comparison of simulated and measured flows at the monitoring station (chainage 3+413) of the Carbäk stream (validation site); the red box in the upper diagram marks the time span of the lower diagram.

Looking more closely at the events of June/July 2017 (Figure 20b; Table 21), an overestimation of flows is noticeable here for the extreme events. Events 1 and 2 were overestimated by 26 % and 27 % respectively, whereby a data gap is to be found for event 2 during the increase in flow. The observed flows therefore probably do not represent the maximum value. As for the Schmarler Bach site, the rainfall event of 20.07.2017 (no. 3) is also classified as not relevant for the Carbäk site. Here, however, it leads to a significant increase in the base flow and thus influences the subsequent event of 25.07.2017 (no. 4).

Table 21. Peak error of the four largest flows in the observation period at the monitoring station in the Carbäk stream.

	①	②	③	④
Date	23.06.2017	30.06.2017	20.07.2017	25.07.2017
Peak error (%)	126	127	394	178

3.3.4 Error Discussion

The quality of the results depends to a large extent on the input data. Therefore, important input variables and other possible sources of error are discussed here:

Input precipitation

The input precipitation is the crucial input variable and has a decisive influence on the model result. In both cases, Schmarler Bach and Carbäk, the input precipitation

was measured outside the model sites, i.e., approximately 7 km south of the Schmarler Bach and 9 km west in the case of the Carbäk, respectively. As mentioned above, there are several precipitation gauges in the study area – but not all of them are set up professionally or they are at least positioned very differently (e.g., on top of a building, underneath a tree, next to a building). Due to the therefore very different systematic measurement error (especially wind error), the measured data are not directly comparable. The only measurement series that is available without gaps in a high temporal resolution (5 minutes) and could be corrected for the systematic measurement error is the rain gauge "Uni Rostock Hy" of the Department of Hydrology and Applied Meteorology. Therefore, the rain gauge series was applied to the entire study area. However, this does not mean that the measurement series is equally representative for every location in the study area. In particular, heavy rain cells appear in a very localized manner and intensify or weaken significantly along their path. This is exemplified by Figure 21, which illustrates the event on 20 July 2017 (event no. 3) for the different gauges.

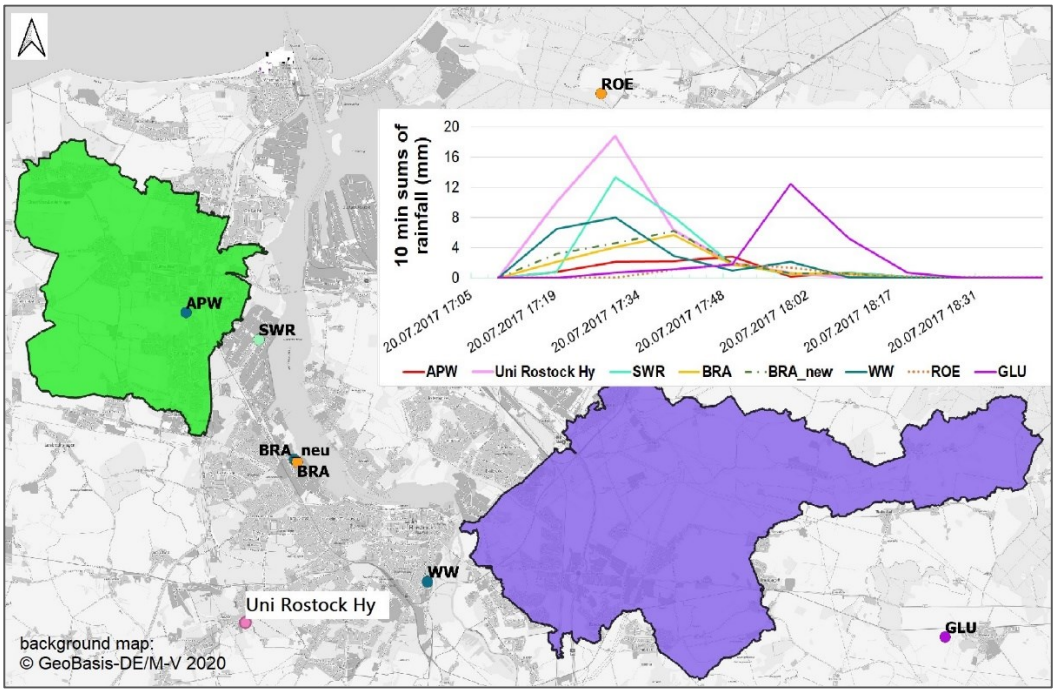

Figure 21. Different rain gauges of the study area and measured rainfall on 20 July 2017 (green catchment: Schmarler Bach, purple catchment: Carbäk).

The gauge "Uni Rostock Hy", which was used for both model sites, shows the highest measured rainfall intensities, while others closer to the model sites measured less precipitation. Whether this is a consequence of the measurement error cannot be

clarified. However, especially against the background of the observed flows, it is very likely that less precipitation actually fell in the two model domains on 20 July.

Storm water disposals

With regard to the maximum flows, the throttling via the discharge points plays a significant role. It is possible that not all existing storm water disposals were included in the model setup, but only the officially documented ones. In addition, the diameters of the discharge pipes within the city limits are less well known, so that the throttling was carried out almost exclusively via the approved maximum permissible discharge. In the case that the approved discharge is greater than the actual possible discharge due to existing diameters, it comes to an overestimation of peak flows.

Size of subcatchments

Furthermore, the size of the generated subcatchments might affect the resulting maximum flows. A comparison of the two model sites shows that the subcatchments of the Schmarler Bach are, on average, 0.036 km^2 in size, while the subcatchments of the Carbäk are a little larger (0.051 km^2 on average). In the case of the Carbäk, the overestimation of runoff peaks of the individual drainage units could be explained by the retention function of small-scale hydrological structures (runoff barriers, small inner basins), which cannot be sufficiently taken into account by the model in large subcatchments.

Measured flows

The measured flows themselves can also be subject to errors. According to literature, measurement errors of flow measurements using the multipoint method (also called velocity area method) are in the range of ± 10 % for carefully conducted measurement campaigns [113]. Particularly high flows often have to be extrapolated and are usually not verified by comparative multipoint measurements. In the case of the Carbäk monitoring gauge, an ultrasonic doppler flow meter was used to continuously measure the water level and flow velocity in order to calculate the flow rates from the two parameters. Since the device only measures the flow velocity in the central lamella, a calibration function was set up based on regular comparative manual multi-point measurements to obtain the average flow velocity of the complete cross-section. This way, flow rates of up to 0.6 m^3s^{-1} are confirmed by manual measurements. The highest flows recorded by the continuously measuring device in the timespan June/July 2017 are 0.8 m^3s^{-1} and thus lie in the extrapolated range of flows. However,

since the velocity recorded in the central lamella by the measuring device and the mean profile velocity manually measured have a very strong linear correlation (R = 0.99) [114], the potential error caused by extrapolation is classified as rather small.

3.3.5 Scenario Simulations Based on Defined Rain Events

3.3.5.1 Initial Condition

As a starting condition, a state was chosen that leads to average flows in the watercourse. Under the given climatic conditions (highest mean flows in January/February, lowest mean flows in June), such a state arises in March/April, which is why 31 March was chosen as starting point. In order to ensure that a particularly wet or dry month is not picked at random, monthly mean values for the period 2007 to 2017 were calculated for the climate data evaporation and precipitation. The model was initialized with these average data (Figure 22) until the annual course of the flows did not change anymore, which was the case after 2 years. In this way, a hot start file was created for the (average) 31 March, in which the status of all subcatchments, junctions, and conduits is stored. With the hot start file and the introduced model rain, the scenario simulation can now be started.

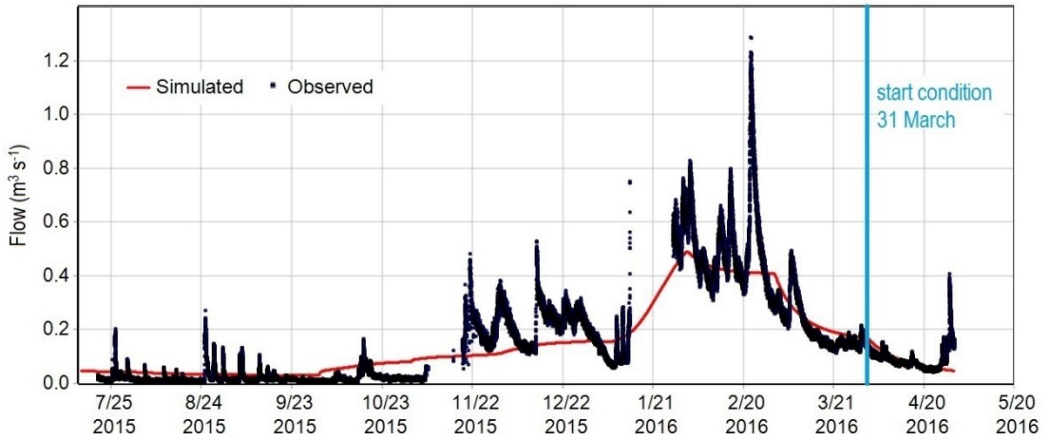

Figure 22. Comparison of the simulated flows (m^3s^{-1}) based on monthly average evaporation and precipitation data and the observed flows using the example of the Carbäk stream.

3.3.5.2 Intensity Course of Model Rainfall

Figure 23 shows the applied intensity course for the 1-hour event. The centring of the maximum volume intervals results in a clear intensity course with the highest value during the 35 min interval, in which almost a quarter of the total rain falls. By multiplying the percentages with the total rainfall volume from the KOSTRA atlas, the amount for each interval will be attained.

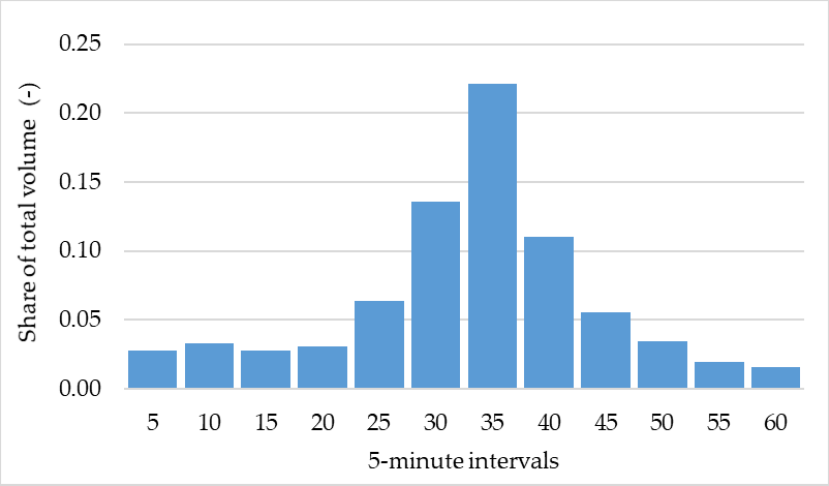

Figure 23. Statistically derived intensity course of the 1h-rain event.

Since the intensity variability is less prominent for longer durations, a block rain was assumed for the durations ≥ 3 h, i.e., the total amount of precipitation is distributed evenly over the 5-minute intervals.

3.3.5.3 Flood Characteristics for the Current State of Land Use

Once the models are set up, they can be used to generate a wide range of results. Some of these are listed in Table 22. In the context of this work, the focus was primarily on determining the extent to which the watercourses are already at load during defined statistical rainfall events, or how much capacity is still available before flooding sets in. If flooding occurs, it is important to know how much volume will flow out (Table 22 max_Volume_stored_ponded), so that (decentralized) retention measures can be planned if necessary. For the planning of the development of new sites and the associated storm water discharges, these data and information must be available.

Table 22. Results from the scenario simulation with defined rainfall events.

		Designation	Unit	Declaration
Watercourses	Conduits	Full_Flow	$m^3 s^{-1}$	Maximum flow at normal flow (water level gradient = bottom gradient)
		max_Flow_rate	$m^3 s^{-1}$	Maximum flow
		max_Flow_velocity	$m s^{-1}$	Maximum flow velocity
		max_Capacity	-	Proportion of the cross profile filled with water at the time of the maximum water level
		Q_free	$m^3 s^{-1}$	Flow rate that would additionally fit into the cross profile at maximum flow rate; value calculated from model results: Q_free= Full_Flow - max_Flow_rate

		Designation	Unit	Declaration
	Nodes	max_Hydraulic_head	m above sea level	Maximum absolute Water level
		max_Volume_stored _ponded	m^3	Max. stored volume above banks in case of flooding
		max_Lateral_inflow	$m^3\ s^{-1}$	Lateral inflow from the subcatchments
		max_Total_inflow	$m^3\ s^{-1}$	Inflow from upstream + lateral inflow from the subcatchments
		max_Flow_lost_ flooding	$m^3\ s^{-1}$	Excess flow with fully exhausted cross profile; flood volume per unit of time
Subcatch-ments		max_Runoff_rate	$m^3\ s^{-1}$	Maximum direct runoff (surface runoff)
		sum_Runoff_rate	m^3	Sum of direct runoff (surface runoff)

Figure 24 illustrates the free capacities in m^3s^{-1} of the 50m segments at the example of the Schmarler Bach system for the 1h rain event with a 100a return period. Values smaller than zero (dark red) indicate that the segment is already overloaded and overflowing. This is particularly critical when it affects vulnerable land uses and their infrastructural facilities that should not be flooded during a 100-year event, as is the case for example in the northwest of the area. Measures should be introduced here to reduce peak flows. As well, redensification should only be approved if the proportions of the water balance variables are not shifted towards intensification of surface runoff at the expense of infiltration and evaporation.

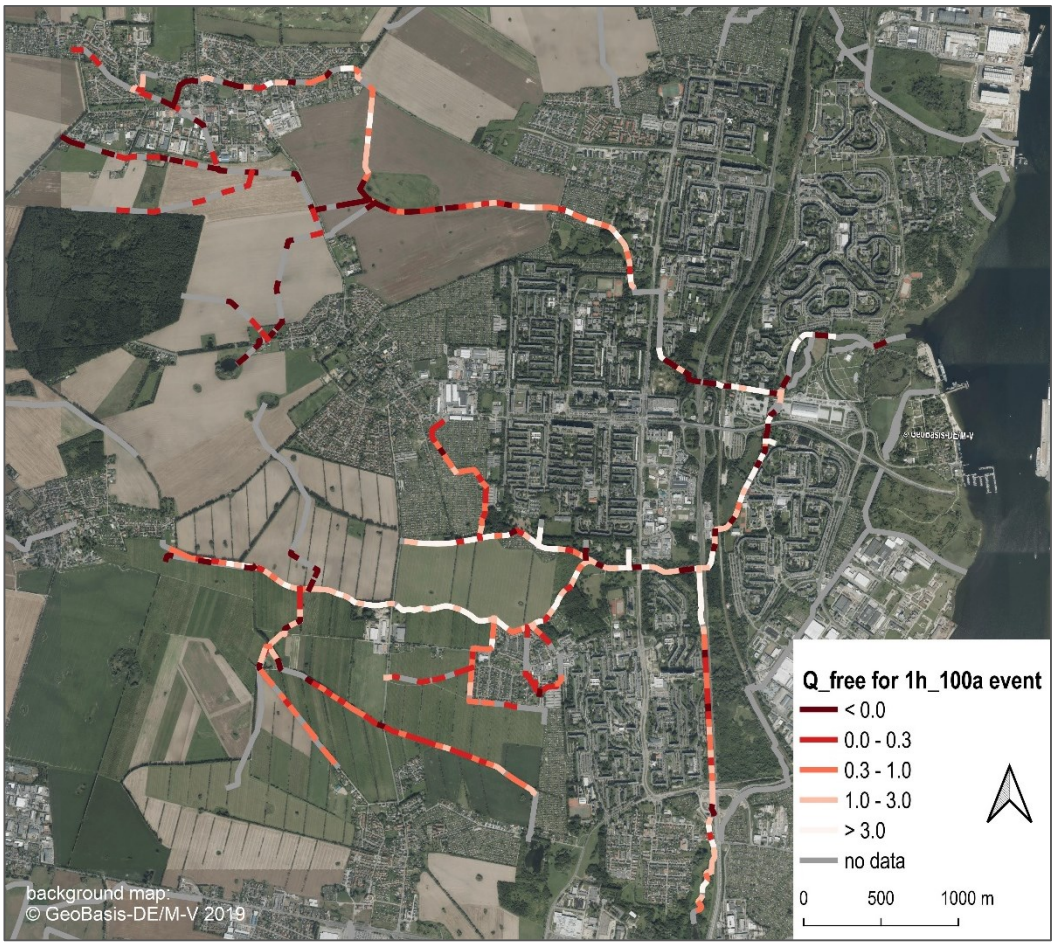

Figure 24. Q_free - Flow rate (m^3 s^{-1}) that would additionally fit into the cross profile at maximum flow rate regarding a rainfall event of 1h duration and 100a return period.

3.4 Conclusions and Outlook

The present study shows how robust hydrological/hydraulic models can be set up for small rivers relatively quickly on the basis of geodata and parameter transfer. These can be used to generate spatially highly resolved information of flow and water level for flood risk analysis based on statistical rainfall scenarios.

In the course of parameterization and calibration, the surface runoff and the groundwater interflow turned out to be the most influential processes regarding stream flow. Groundwater parameters, such as conductivities, porosities, etc., were adjusted in the process of calibration and then globally applied to the entire area. A spatially higher resolution would be conceivable, but this would require a very good knowledge of the subsurface layers or involve a complex spatial interpolation. With respect to surface runoff, flow length, roughness, and detention storage in particular were subject to calibration. If the methods were transferred to differing areas, these

parameters as well as groundwater parameters would have to be recalibrated. With respect to detention storage, it would also be possible to specify it individually for each subcatchment based on a DEM analysis. This way it would not have been necessary to calibrate the parameter. The average slope, the degree of sealing, and the soil parameters were also derived directly from geodata without calibration. In general, the higher the spatial resolution of the model parameters, the less sense it makes to calibrate individual values of them, since individual small subcatchments sometimes have hardly any visible effect on the results at the observation point. A spatially high model resolution is therefore only recommended with qualitatively good data.

In the study area, the parameter transfer to the validation site only led to a slight loss of model accuracy. Even better model results could have been expected regarding the impact of the suboptimal position of the rain gauge. Provided there is a comparably good geodata situation, the approach offers a good chance to set up fairly reliable models, including hydrodynamic processes, namely for the numerous small rivers without any monitoring.

The construction of river section profiles from laser scanning data introduces a certain error, since only the profile above the water level can be sampled. Still, for small rivers with small water depth, the method seems to be sufficiently exact, since the investigated statistical events create a multiple times higher flow than the flow filling the profile at the scanning date. For larger streams and significant water depth, error compensation strategies could be advisable, like assuming mean flow conditions at the scanning date and subtracting it from the simulated flows to achieve even better results regarding water levels.

For the purpose of flood risk analyses, the main advantages compared to a simple GIS-based flood regionalization are i) the physically integrated and highly distributed land use and ii) the inclusion of stream hydrodynamics. This way, even small-scale land-use changes can be directly incorporated and analysed. The hydrodynamic functionality not only provides water level but can also be used in targeted development of the river system and its infrastructures.

With its extension UrbanEVA, SWMM also provides the functionality of a full water balance model. Accordingly, the model can be used as well to quantify alterations in the water balance for planned land use changes, particularly the surface runoff that potentially triggers flooding. Recently, the new mandatory German standard DWA-A

102-1 [24] requires that spatial planning must not fundamentally change the quantitative proportions of water balance variables. This will lead to a significant boost for low-impact design (LID) in urban areas. Initially, SWMM-UrbanEVA was exactly developed for the purpose of better describing LID structures in urban hydrology. In our study, detailed urban drainage infrastructure is purposely not included, but the model environment would allow for such refining.

4 Scenario-Based Flood Characteristics for the Planned State of Land Use

4.1 Introduction

Since the beginning of human settlement history, humans have preferred to settle near rivers and streams. Small settlements became large settlements and these became today's cities. As settlements progress, areas formerly close to nature are rezoned as building land and cities are redensified. This inevitably leads to increased soil sealing. Soil sealing strongly modifies the water cycle by reducing infiltration, evapotranspiration, and groundwater recharge, thus intensifying (rapid) surface runoff. As a result, the risk of flooding is increased [86; 88] especially where no retention areas exist. For a region in China it has been shown that over the last 20 years urbanisation has led to an increase in the runoff coefficient of 13.4 %, resulting in an increase in the maximum flood discharge of 12.9 % on average [115]. In [116] a methodology is described which relates urban growth studies based on the analyzation of satellite data to distributed hydrological runoff modelling using the soil conservation service (SCS) method. The results of the corresponding case study indicate that annual runoff depth had increased by 8.10 mm between 1989 and 1997 due to urban sprawl.

The social and economic 'costs' of flooding are expected to rise in the future, not only due to land use changes, but also due to climate change [92; 117; 118]. In order to minimize flood risk by a proper communal planning, the impact of land use changes on runoff and river surcharge must be considered at an early stage. In this context, the cooperation and exchange of information between all relevant authorities, organisations, associations, and companies is of particular importance [119]. Typically, process models are applied for those questions. However, their application requires expert knowledge and detailed data, which are not available in this phase of planning.

The aim was therefore to develop a tool that enables a rapid, but still reliable assessment of flood risk due to land use change, which is applicable by regional planners or authorities without specific knowledge in hydrologic/hydraulic process modelling. The results shall be made available in a coherent way to all relevant actors across administrative boundaries. Due to the spatial nature of this issue, the use of a geo-information system (GIS) is appropriate. For a wide applicability, the tool shall be based on freely accessible software. Meanwhile, open source free software (namely

QGIS) has achieved a technically mature level, "giving the researcher the ability to create their own tools, according to their needs" [120]. To provide an ideal solution for sharing basic data and calculation results, the tool shall be embedded in a GIS-based decision support system, accessible via a conventional web browser. Decision support systems have been developed since the 1970s [121] but the progressing digitalization and especially the free availability of geodata facilitates and improves the development enormously. In addition, powerful computers ensure faster real-time processing of geodata, which minimizes computing times. Many GIS-DSS were specifically designed for flood risk analysis and assessment [122–126]. However, to ensure that the DSS will be used by stakeholders once it has been developed, the following three key challenges must be met according to [127]:

- The DSS has to address the actual goals of the decision-makers and stakeholder wishes
- The DSS should provide a user-friendly interface and good visualization capabilities for a real participatory use by the stakeholders and decision-makers
- The stakeholder and decision-makers should have a clear understanding of the model concept and should ideally be able to edit it by themselves e.g., for scenario analysis purposes

There is a wide variety of approaches to address these, depending on the regarded topics, end-users and scientific background of the model developers. They reach from statistical and/or conceptual models processing meta information [128] to high resolute and well-considered 2D/3D flood risk mapping [129–131]. Partly, they are collaboratively developed with the end-users [132] or even use virtual reality environment to increase information depth and awareness. In tendency, the participatory character of the model decreases with increasing model accuracy. The concept of [128] is highly participative but does not provide physically exact information. Particularly, 3D maps are mainly prepared for citizens.

Our concept is ranging between these two edges: it is highly cooperative and based on deterministic physical modelling. More precisely, a tool was developed that allows an interactive calculation of the runoff from a particular planned land use and the subsequent propagation of the flow in the river system. The so called 'storm water routine' (SWR) was developed, as part of a larger GIS-DSS for regional and municipal

planning activities [133]. The development is primarily based on open-source tools to enable barrier-free use by relevant stakeholders. It combines:

- a physically based process model of the catchment hydrology and river hydraulics, set up for the current state of land use [134] and
- a GIS-routine calculating the additional runoff for land use change scenarios and its routing through the stream system.

The objectives of this tool have been defined in a participatory process with regional water authorities, water associations, and wastewater operators. They identified the lack of information on land use change induced changed runoff and missing information on specific hydraulic capacity at the point of discharge as major deficiencies in the approval of new storm water discharge permits. In distinct cases with expected larger impacts, individual studies are commissioned to consultancies, but a consistent and continuous assessment for a total river basin is missing. While most of the partners do not have their own modelling expertise, the application of GIS is meanwhile daily practice. GIS also provides the required visualization capabilities and interface for editing scenarios in the area of interest. Accordingly, it was agreed to develop a tool to holistically assess the hydrologic and hydraulic impacts of land use changes for the total river system. In contrast to commissioned studies, the tool should be operable by the decision-makers and stakeholders themselves by using the well-known GIS environment. Since the tool is based on the pre-processed results of hydrologic/hydraulic models, but is not directly linked to the models, the end user does not necessarily need to have modelling experience.

While part 1 (chap. 3) of this paper has described the set-up and parametrization of the process model and the definition of rainfall scenarios, this article focuses on the GIS-based calculation of additional runoff and the routing. The reliability of the approach has been reviewed by a comparative calculation of river flow with the detailed process model and the simplified GIS-based approach, revealing its strengths and weaknesses.

4.2 Materials and Methods

4.2.1 Study Area

The study area, approximately 530 km^2 in size, is located in the north-eastern German lowlands and includes the Hanseatic City of Rostock and its 18 surrounding municipalities (Figure 25). The latter are part of the Rostock rural district. While the

core of the city is dominated by uses such as housing, industry, and commerce as well as transport areas, the surrounding rural district is mainly characterised by arable land and grassland. The study area overlaps 19 largely independent surface catchments, with the headwaters of the streams mostly in the rural district and the mouths in the urban area of Rostock or the Baltic Sea.

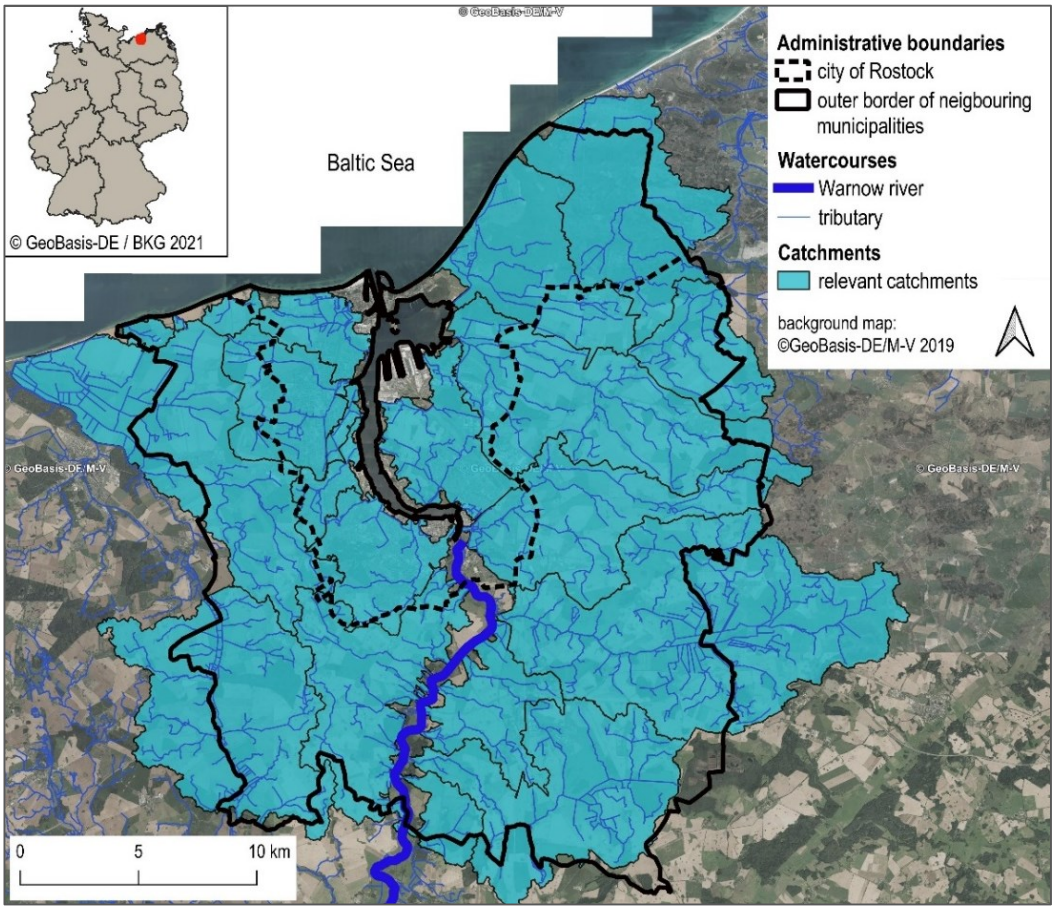

Figure 25. Relevant surface catchments of the study area and administrative boundaries.

The history of the city of Rostock goes back to the 13th century. Since then, the city has grown not only in its territorial area but also in its population, reaching nearly 210.000 inhabitants today [135]. For Rostock, an increase of nearly 15.000 inhabitants is expected by 2035 [136]. In contrast, projections indicate that the rural district will experience a population decline of 1.8 % by 2030 [137]. However, as in many developed countries, population and sealing do not develop in parallel, but the demand for building ground is increasing, even in areas with shrinking population. Main drivers are the demand for residential units, the development of logistic centres and industrial parks.

4.2.2 Basic Data

In the course of the study, spatial data from different sources were used and integrated into a homogeneous and consistent data set. The data relevant for the application of the storm water routine are presented in the following.

Land Use Map

The Hanseatic City of Rostock provides a spatially high-resolution geodata set that was created on the basis of aerial photographs and supplemented by existing geodata. Since such a dataset did not exist for the rural district, it was generated from the data of the Official Real Estate Cadastre Information System (German abbreviation: ALKIS) in combination with satellite data. The result is a polygon shape file that depicts the land use in its actual state on the basis of 48 classes. In the GIS-DSS, this land use map represents the reference state for all future changes of land use. In addition, different levels of protection (risk classes) were defined for each land use class according to their vulnerability (see [134]). The level of protection is expressed by the return period which describes the probability of recurrence of a natural event, in this case a statistical model rainfall of a certain duration. For hydrologic/hydraulic modelling [134], the 48 classes were generalized to 13 land use classes (Figure 26a).

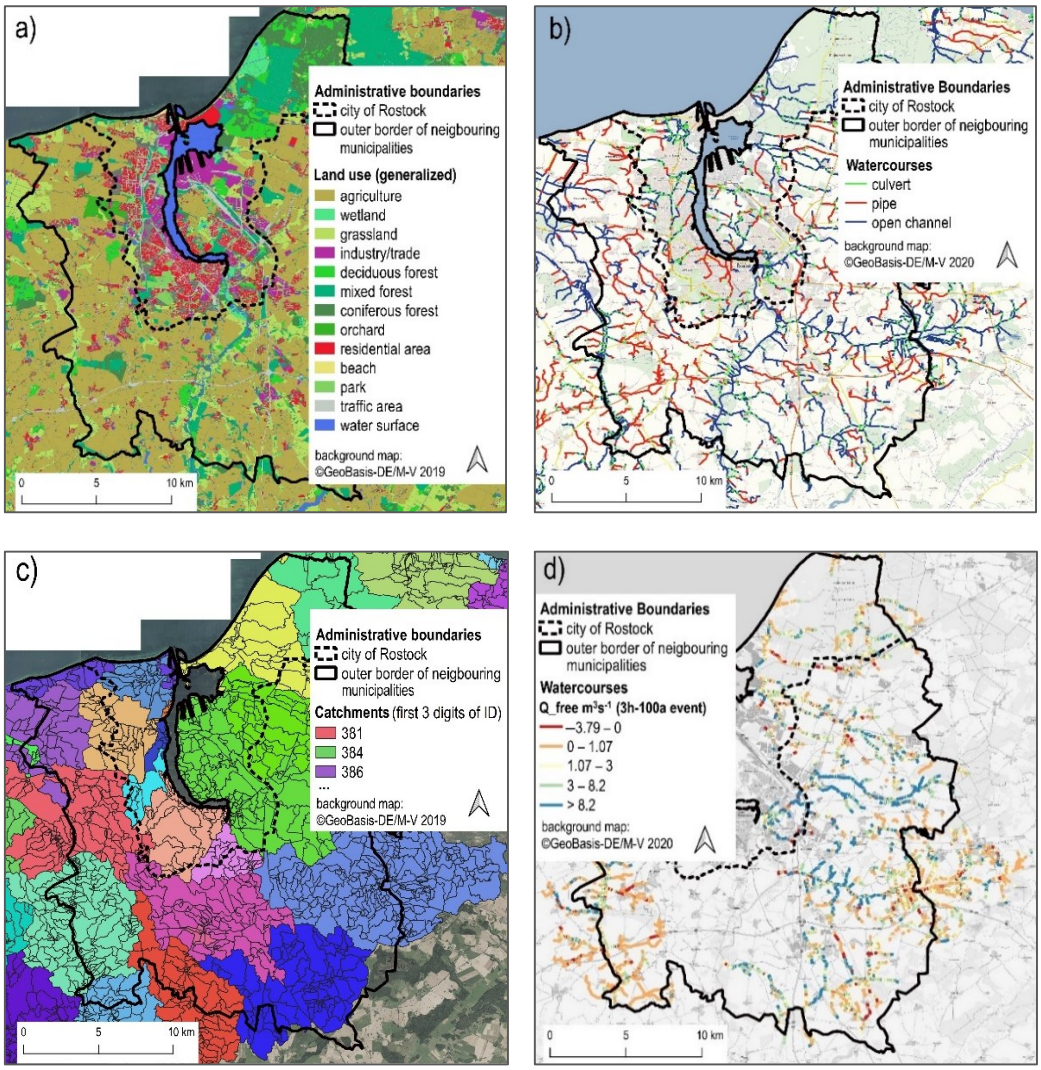

Figure 26. (a) Land use (generalized); (b) watercourses consisting of open channels, pipes and culverts; (c) catchments with first three digits of hierarchical ID (colours are chosen at random); and (d) free profile capacities (m^3s^{-1}) at the example of the rain event 3h-100a.

Watercourse Cadastre

The watercourse cadastre contains stream networks (Figure 26b) and their catchments (Figure 26c). The watercourse lines were brought together from several different sources and corrected in order to create a tree structure. Thus, each tributary flows to a receiving stream and is connected to it at a certain point. These hierarchical routes were divided into 50 m sections and equipped with an individual and hierarchical identification number (12-digit watercourse identification number: WIN) and chainage.

Each watercourse was assigned a surface catchment. These were calculated on the basis of a digital elevation model (DEM) with a cell size of 5 m. The stream catchments were also further subdivided so that each 50 m section is assigned its own subcatchment. Due to the strict hierarchy of both watercourses and catchments, which is maintained by means of the WIN, sections or subcatchments located upstream or downstream can be quickly identified and aggregated if necessary [138].

Flood Characteristics

For the watercourses and catchments of the study area, spatially high-resolution flood characteristics for the current state were pre-processed using combined rainfall-runoff and hydrodynamic stream models [134]. The flood characteristics are available for 18 precipitation events of different durations and return periods (see Table 23).

Table 23. Selected statistical precipitation events according to protection level of land use classes ([134], modified).

Duration	Return Period
1 h	2 a, 100 a
3 h	10 a, 25 a, 50 a, 100 a
6 h	10 a, 25 a, 50 a, 100 a
9 h	10 a, 25 a, 50 a, 100 a
12 h	10 a, 25 a, 50 a, 100 a

The return period expresses the level of protection that has been defined for a particular land use class [139]. For example, if a return period of 100 a has been defined for a residential area, the area should not be flooded by a rainfall event that statistically occurs every 100 a. However, for reasons of economic efficiency, the area is allowed to be flooded by an even rarer and thus larger event. In order to detect the worst case, different durations were taken into account, as long rainfall durations are usually critical for large areas and shorter durations are relevant for smaller areas with shorter flow paths. Table 24 shows the pre-processed flood characteristics used in the storm water routine of the DSS.

Table 24. Flood characteristics for the actual state applied in the SWR based on scenario simulations with defined rain events.

	Designation	Unit	Declaration
Watercourses	Q_{full}	$m^3\ s^{-1}$	Maximum possible flow at normal flow (water level gradient = bottom gradient)
	$Q_{max,act}$	$m^3\ s^{-1}$	Maximum flow
	$Q_{free,act}$	$m^3\ s^{-1}$	Flow rate that would additionally fit into the cross profile at maximum flow; value calculated from model results (Figure 26d): $Q_{free,act} = Q_{full} - Q_{max,act}$
Subcatch-ments	$R_{max,act}$	$m^3\ s^{-1}$	Maximum direct runoff (surface runoff)

Maximum Rainfall Intensities

Within the framework of the heavy rainfall regionalisation, the KOSTRA Atlas of the German Weather Service provides precipitation amounts as a function of duration D and annuality T (return period) [110]. While a block rain was assumed for the duration stages greater than or equal to 3 h, the intensity course for the duration stage 1 h was determined statistically based on DWA-A 118 [109] and includes a clear rain peak after about half of the time. The resulting maximum rainfall intensities (ri_{max}) were listed in tabular form and linked to the geodata of the hydrologic catchments.

4.2.3 Detection of Flood Characteristics for Planned Land Use Changes

4.2.3.1 Pre-Processing of Functions to Calculate Peak Runoff Coefficients

For the development of the storm water routine, functions were derived beforehand on the basis of the existing model results (see Table 24), which enable the calculation of the peak runoff coefficient for new land use polygons on the basis of a specified degree of sealing. In the first step, the peak runoff coefficients are determined for each subcatchment of a reference model site (Schmarler Bach site, see [134]) for the 18 simulated model rainfall events. The coefficient describes the ratio of the maximum runoff rate per area to the corresponding maximum rainfall rate per area (Equation 34) and depends primarily on the proportion of paved areas (degree of sealing), the slope of the terrain and the rainfall intensity [109]. As the study area is located in the lowlands, the gradient plays a minor role here. This was supported by the model results, as the dependence of the coefficient on the gradient was tested and evaluated as not significant.

$$\Psi_p = \frac{r_{max}}{ri_{max}} \tag{34}$$

$\Psi_p = peak\ runoff\ coefficient\ (-)$

$r_{max} = maximum\ runoff\ rate\ per\ area\ (l\ s^{-1}\ m^{-2})$

$ri_{max} = maximum\ rainfall\ intensity\ per\ area\ (l\ s^{-1}\ m^{-2})$

Subsequently, a comparison of the peak runoff coefficients and the degrees of sealing was performed in a correlation diagram. Thereby polynomial functions were derived, which describe the correlation between the two parameters. The functions are used to calculate the peak runoff coefficient for a new land use polygon on the basis of the defined degree of sealing and the selected rainfall scenario.

4.2.3.2 The Storm Water Routine

The storm water routine aims to provide potential future runoff and flood risk associated with planned land use changes. For this purpose, a method was developed that enables the calculation of the direct runoff and resulting potential flows for planned land uses on the basis of pre-processed flood characteristics. The procedure takes place in the Web GIS-DSS and is divided into eight basic steps (Figure 27). These were automated using Python programming language.

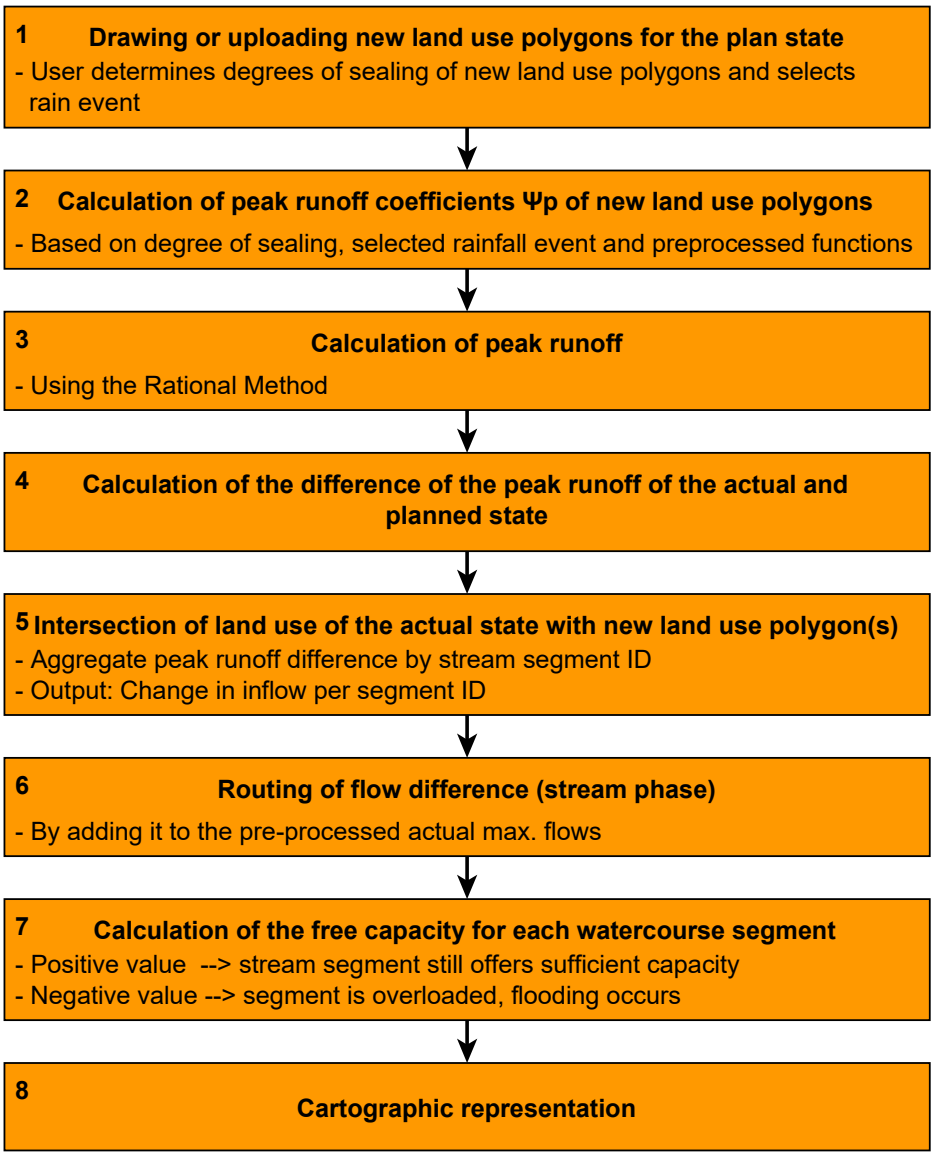

Figure 27. Determination of flood characteristics for the planned state of land use using GIS-DSS tools.

In the first step, a new land use polygon is either directly drawn into the map of the graphical user interface or uploaded as a shape file. In this process, the user specifies the planned degree of sealing and selects the precipitation scenario with the corresponding maximum rainfall intensity per area. For the determination of the peak runoff coefficient, pre-processed polynomial functions were used that allow a calculation based on the degree of sealing. The peak runoff $R_{max,plan}$ for the new land use polygon can thus be determined with the equation

$$R_{max,plan} = \Psi_p \times ri_{max} \times A_{new} \quad (35)$$

$R_{max,plan} = maximum\ runoff\ rate\ in\ plan\ state(l\ s^{-1})$

$A_{new} = area\ of\ new\ polygon\ (m^2)$

The change in the peak runoff of the affected areas is computed by intersecting the maximum runoff of the actual land use (results from scenario simulations, see Table 22) with the maximum runoff of the new polygon both in raster format. For this purpose, the runoff rates are converted into runoff rates per raster cell (with a size of 100 m²).

$$r_{diff} = r_{max,plan} - r_{max,act} \tag{36}$$

$r_{diff} = runoff\ rate\ difference\ per\ pixel\ (l\ s^{-1}100m^{-2})$

in which:

$$r_{max,plan} = \frac{R_{max,plan}}{A_{SC}} \times 100 \tag{37}$$

$$r_{max,act} = \frac{R_{max,act}}{A_{SC}} \times 100 \tag{38}$$

$r_{max,plan} = maximum\ runoff\ rate\ per\ pixel\ in\ plan\ state\ (l\ s^{-1}100m^{-2})$

$r_{max,act} = maximum\ runoff\ rate\ per\ pixel\ in\ actual\ state\ (l\ s^{-1}100m^{-2})$

$A_{SC} = area\ of\ corresponding\ subcatchment\ (m^2)$

After intersecting the new polygon with the 50 m subcatchments, the change of peak runoff can finally be aggregated by segment ID and thus assigned to each receiving stream segment. There are two possibilities for the allocation of the runoff: a) If no receiving segment is specified, the discharge is automatically distributed to the segments according to its area share in the subcatchment (Figure 28 a). b) It is also possible to assign the discharge change to a defined segment and to throttle it via a maximum permissible discharge (Figure 28b).

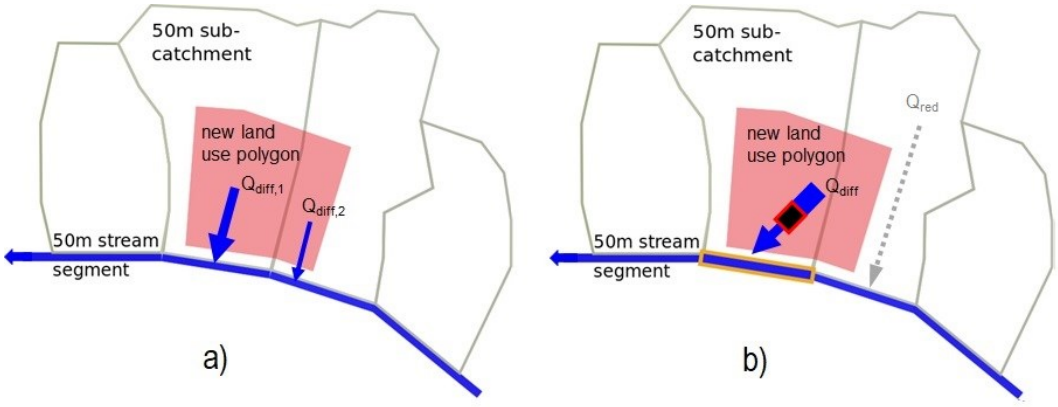

Figure 28. Allocation of the runoff difference to the 50 m-stream segments without (a) or with (b) definition of a receiving segment (black box with red outline = throttle).

In the case of Figure 28b, the corresponding stream segment receives the peak runoff difference and the neighbouring upstream segment loses runoff compared to the actual state (Q_{red}) due to the reduced drained area. The new inflow (Q_{diff}) is added to the maximum stream flow of the actual state ($Q_{max,act}$) and routed downstream according to the WIN

$$Q_{max,plan} = Q_{max,act} + Q_{diff} \quad (39)$$

$Q_{max,plan} = maximum\ flow\ in\ plan\ state\ (l\ s^{-1})$

$Q_{max,act} = maximum\ flow\ in\ actual\ state\ (l\ s^{-1})$

$Q_{diff} = aggregated\ runoff\ difference\ (l\ s^{-1})$

From the full flow (Q_{full}, Table 22), which represents the maximum possible flow for a specific cross profile, and the new flow of the planned state ($Q_{max,plan}$), the flow that would still fit into the profile ($Q_{free,plan}$) is determined. If the value is positive, the profile still offers enough capacity for the additional flow. If it is negative, the segment is overloaded and flooding occurs.

$$Q_{free,plan} = Q_{full} - Q_{max,plan} \quad (40)$$

$Q_{free,plan} = flow, that\ would\ still\ fit\ in\ profile\ in\ plan\ state\ (l\ s^{-1})$

$Q_{max,act} = maximum\ flow\ in\ actual\ state\ (l\ s^{-1})$

Both the stream flows for the 50 m segments as well as the capacities of the planned state are mapped in the GIS-DSS. For the visualisation, the line width is adjusted according to the total flow. As well, six colour levels have been assigned for the capacity to indicate how much space the profile still offers or whether it is already overloaded.

4.2.4 Validation of the Storm Water Routine

The validation of the storm water routine was performed by comparing its results for an exemplary land use change with the corresponding results from the combined hydrological/hydraulic model in SWMM. SWMM was considered to be a suitable benchmark, as it takes water body shapes at individual points into account and is able to calculate precisely dynamics of the flow, including effects of throttling and retention [134].

The exemplary land use change is the conversion of almost 70.000 m² of an orchard into a virtually planned residential area ('planned area') with a degree of sealing of 70 %. The site is located in the catchment of the Schmarler Bach in the north-west of

the investigation area (Figure 29a). Within the catchment area, the site is located in the southern-central part, just beyond the city boundary in the administrative area of the rural district (Figure 29b).

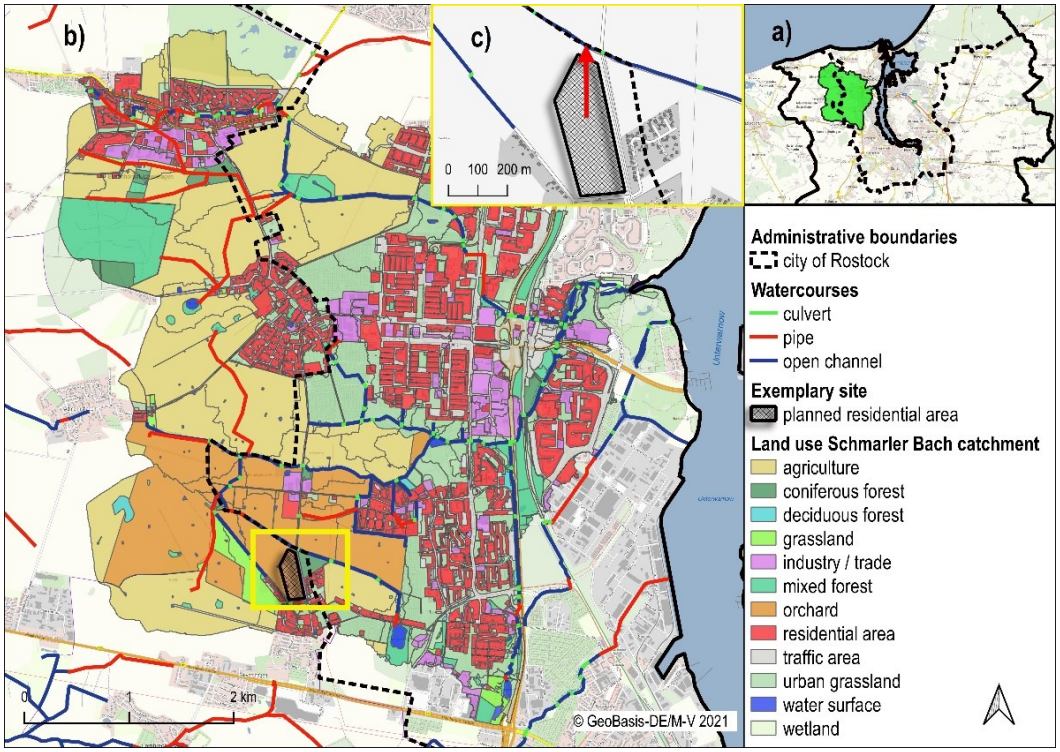

Figure 29. Schmarler Bach area with land use of the actual state. a) Outline map, b) complete Schmarler Bach catchment with the exemplary planned residential area in the central south (yellow box), c) detail section of the planned residential area.

The discharge point into the river is set to a user-defined stream segment (red arrow in Figure 29c) as described in Figure 28b. Hence, the new residential area will drain in northern direction towards the open ditch just below the culvert (Figure 29b,c). On the flow path towards the mouth into the Warnow River, numerous structures such as culverts and pipes act as throttling elements in particular at high flows.

For the validation, representative precipitation scenarios were tested (cf. Table 23). The comparison between SWR and hydrological/hydraulic model was conducted for peak runoff from the development site and peak flows in the affected river sections.

4.3 Results

4.3.1 Derived Functions for the Determination of Peak Runoff Coefficients

Using the simulation results for the maximum surface runoff and the maximum rainfall intensity, the peak runoff coefficients for the current state were calculated according to Equation 34. Figure 30 shows the correlation of the peak runoff

coefficient and the degree of sealing. Functions for the determination of the peak runoff coefficients on the basis of the degree of sealing are displayed in Table 25. These are used in the storm water routine to determine peak discharges for planned land use changes.

Table 25. Functions relevant for the study area for the determination of the peak runoff coefficient Ψ_p (y) on the basis of the degree of sealing (x)

		Return period				
		2a	10a	25a	50a	100a
Duration	1h	$y = 10^{-7}x^3 + 10^{-5}x^2 + 2.1\times10^{-3}x$				$y = 10^{-6}x^3 - 9\times10^{-5}x^2 + 6.2\times10^{-3}x$
	3h		$y = 4\times10^{-7}x^3 + 4\times10^{-5}x^2 + 2.1\times10^{-3}x$	$y = 7\times10^{-7}x^3 + 6\times10^{-7}x^2 + 4\times10^{-3}x$	$y = 8\times10^{-7}x^3 - 10^{-5}x^2 + 4.8\times10^{-3}x$	$y = 7\times10^{-7}x^3 - 10^{-5}x^2 + 5.4\times10^{-3}x$
	6h		$y = -2\times10^{-10}x^3 + 10^{-4}x^2 + 5\times10^{-8}x$	$y = 3\times10^{-8}x^3 + 10^{-4}x^2 + 2\times10^{-4}x$	$y = 2\times10^{-7}x^3 + 7\times10^{-5}x^2 + 1.2\times10^{-3}x$	$y = 4\times10^{-7}x^3 + 4\times10^{-5}x^2 + 2.4\times10^{-3}x$
	9h		$y = 10^{-11}x^3 + 10^{-4}x^2 + 5\times10^{-8}x$	$y = 10^{-11}x^3 + 10^{-4}x^2 + 3\times10^{-8}x$	$y = 8\times10^{-12}x^3 + 10^{-4}x^2 + 3\times10^{-8}x$	$y = 2\times10^{-8}x^3 + 10^{-4}x^2 + 9\times10^{-5}x$
	12h		$y = -2\times10^{-8}x^3 + 10^{-4}x^2 - 10^{-4}x$	$y = -5\times10^{-12}x^3 + 10^{-4}x^2 - 3\times10^{-8}x$	$y = -7\times10^{-10}x^3 + 10^{-4}x^2 - 3\times10^{-6}x$	$y = 7\times10^{-9}x^3 + 10^{-4}x^2 + 3\times10^{-5}x$

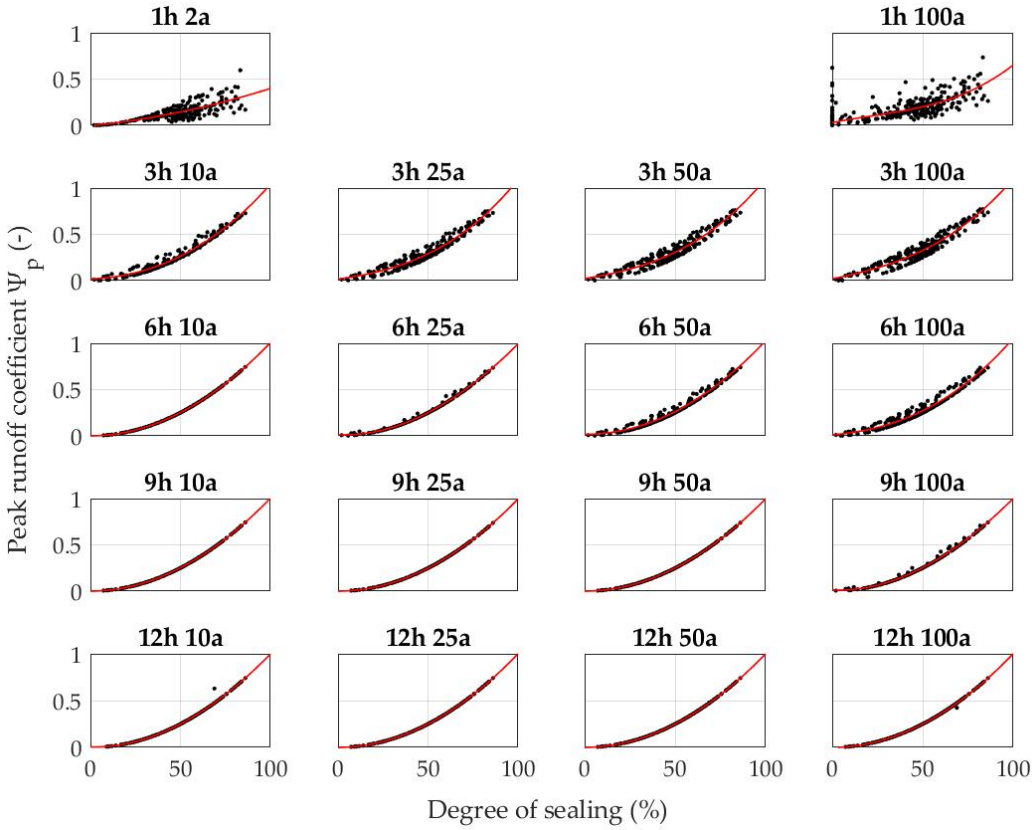

Figure 30. Correlation diagrams based on peak runoff coefficients and the degree of sealing (subheadings are composed of rainfall duration and return period).

Basically, a clear polynomial dependence of the peak runoff coefficients on the degree of sealing is visible. This is also confirmed by the coefficients of determination in Table 26. In the case of block rainfall (3 h to 12 h), the strength of the dependency increases with duration, as conditions become more and more static. Within a duration category, the dependency tends to decrease from small to large return periods (respectively small to large rain intensities). For the duration 1 h with a clear intensity gradient, the scatter of the peak runoff coefficients around the function curve is significantly greater than for the block rainfall, which suggests that other factors, such as the area size or the flow length or the soil conductivity, superimpose the influence of the degree of sealing. In the case of the most severe event (1h-100a), it is noticeable that even the unsealed areas react as if they were sealed, since the conductivity of the soil is increasingly exceeded.

Table 26. Corresponding coefficients of determination R^2 (-) for the simulated rain events.

		Return period				
		2a	10a	25a	50a	100a
Duration	1h	0.601				0.658
	3h		0.972	0.945	0.929	0.918
	6h		1.000	0.997	0.982	0.960
	9h		1.000	1.000	1.000	0.997
	12h		0.996	1.000	1.000	1.000

4.3.2 Validation of the GIS-DSS Storm Water Routine

4.3.2.1 Comparison of Model Results for Actual and Plan State in SWMM

In order to better interpret and evaluate the results of the GIS-DSS storm water routine, this section first compares the model results for the current and the planned state. To start with a less extreme event, Figure 31 shows the difference in flows ($Q_{max,plan} - Q_{max,act}$) in the planned and actual state for the rainfall event 6h-10a simulated with SWMM. The turquoise and yellow sections show on which stretches the discharge change has an effect.

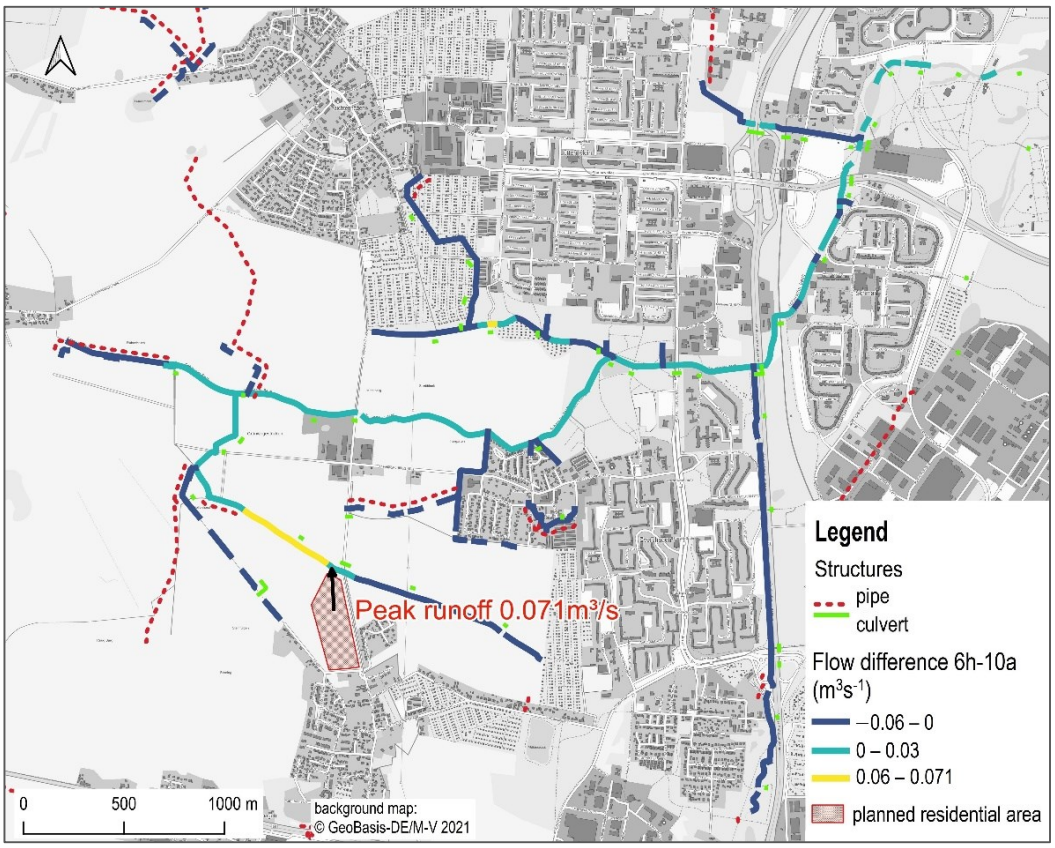

Figure 31. Difference of flows (m^3s^{-1}) in planned and current state for the rain event 6h-10a simulated with SWMM (pipes and culverts are plotted with offset to original route).

As expected, the largest differences in stream flow occur immediately downstream of the discharge point and are of the same magnitude as the peak runoff from the planned area (Figure 32). At the same time, the new runoff also affects an approx. 130 m long stretch upstream of the discharge point but with a less prominent amplitude.

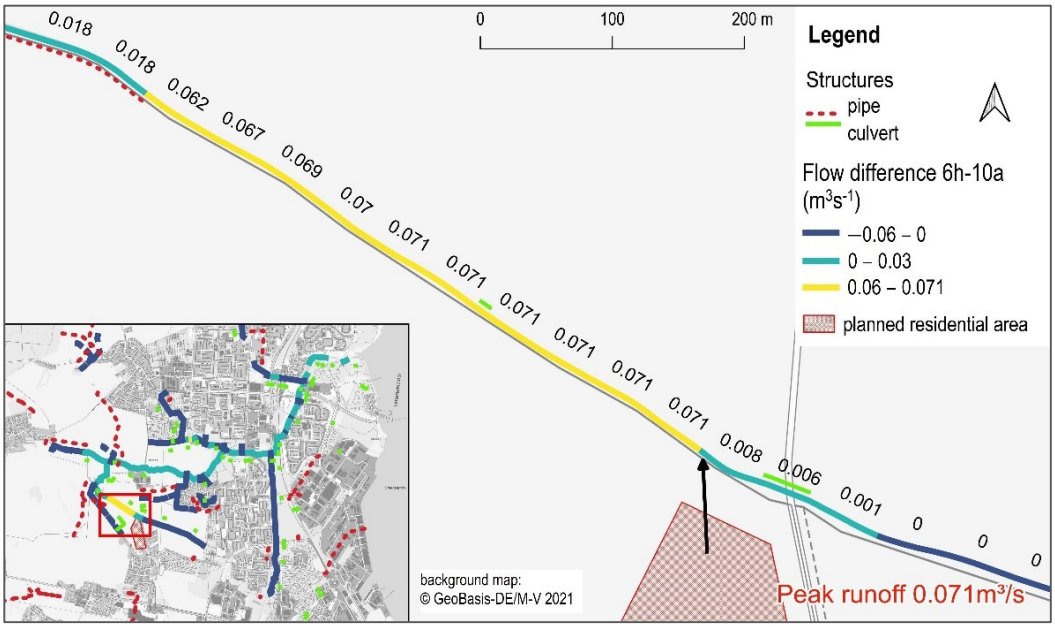

Figure 32. Flow difference (m^3s^{-1}) in the immediate area of the discharge point for the rain event 6h-10a (pipes and culverts are plotted with offset to original route).

With downstream distance from the discharge point, the flow difference flattens from 0.071 m^3s^{-1} to 0.062 m^3s^{-1}, which can be explained by the natural retention of an open channel. A pipeline section follows, which is about 95 % full in the actual state, but already overloaded in the planned state. As a result, the flows are noticeably throttled here, which is why the additional discharge of the new residential area from this section onwards has relatively little effect.

A much more intense event is the 1h-100a rainfall (Figure 33 and Figure 34). Here, 0.82 m^3s^{-1} of runoff is generated on the new residential site. Since the profile downstream can only capture 0.42 m^3s^{-1}, the conduits capacity limit is already reached. However, due to the rise in water level in the area of the discharge point and the resulting inversion of the upstream gradient, water flows in both directions: 0.42 m^3s^{-1} flows downstream and approx. 0.26 m^3s^{-1} flows upstream (Figure 35).

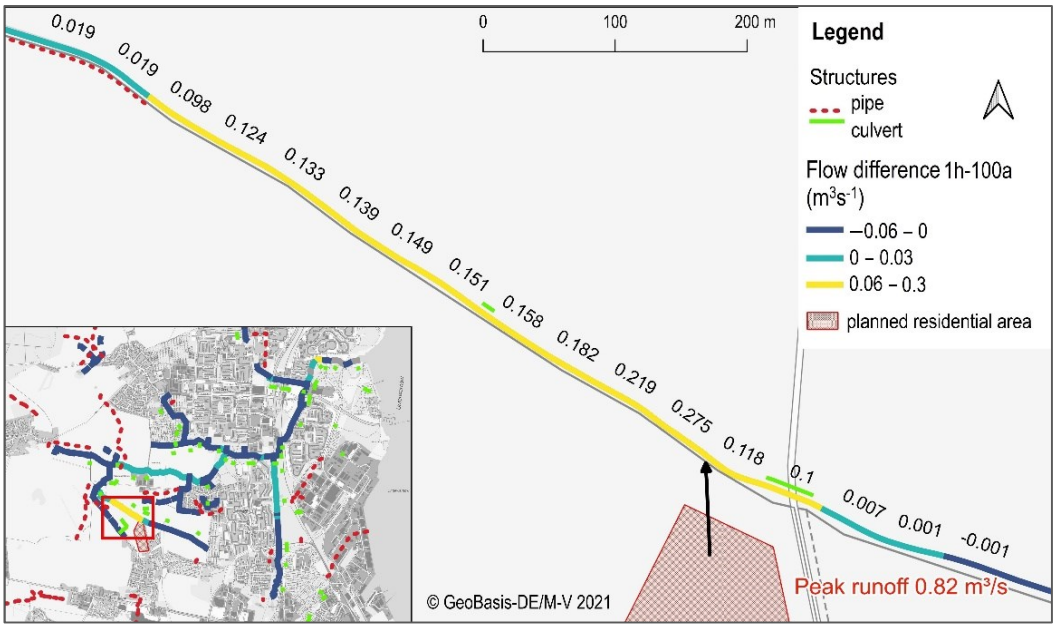

Figure 33. Flow difference (m^3s^{-1}) in the immediate area of the discharge point for the rain event 1h-100a simulated with SWMM.

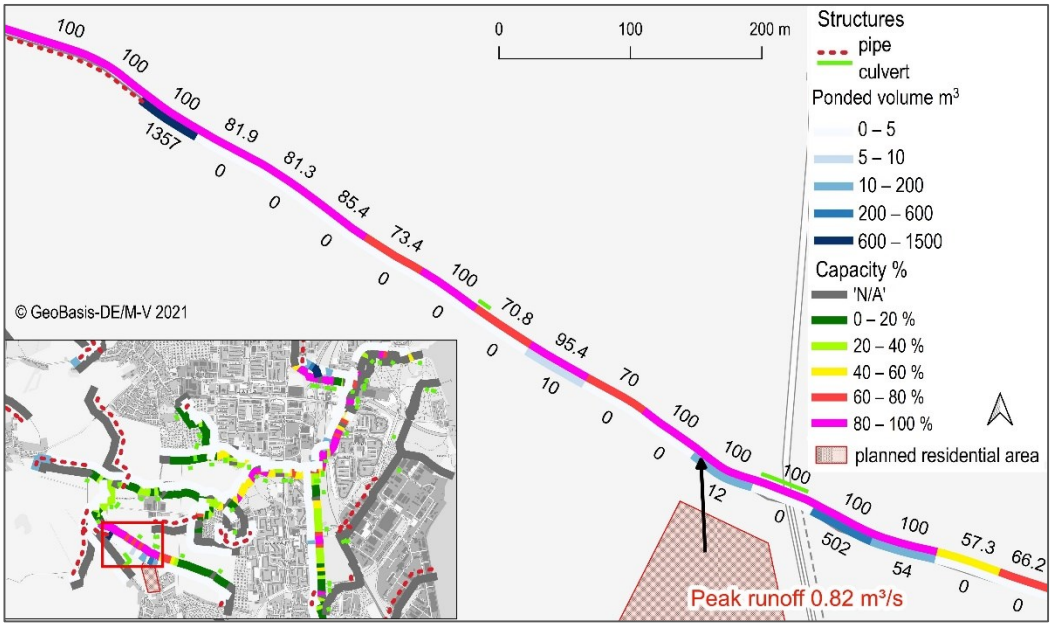

Figure 34. Maximum capacity and ponded volume in the immediate area of the discharge point for the rain event 1h-100a (plan state).

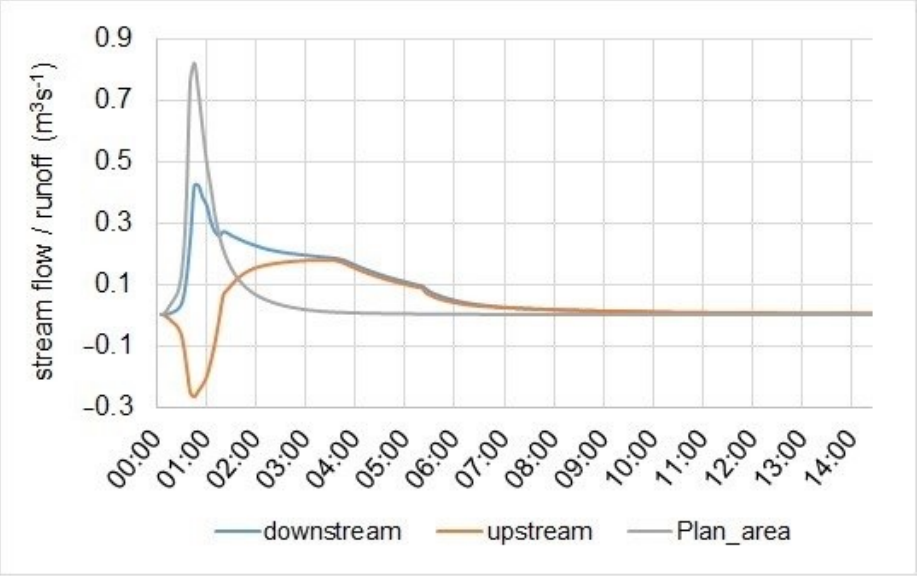

Figure 35. Runoff from plan area and simulated stream flow with rain event 1h-100a in the conduit directly downstream (max. flow = 0.42 m^3s^{-1}) and upstream (min. flow = −0.264 m^3s^{-1}) of the discharge point from the new residential site.

The remaining discharge (approximately 0.14 m^3s^{-1}) is excess water and is temporarily stored in a conceptual reservoir above the banks. In SWMM, this is called the ponded volume. The speed with which the water flows out of the reservoir back into the cross-section depends on the size of the base area of the reservoir. If the surface area is small, the hydraulic pressure in the reservoir is relatively high and the water flows back again correspondingly quickly. This in return influences the shape and the maximum value of the stream flow. Since the study area is located in the lowlands, the footprint of the reservoir was chosen to be relatively large (distance to the next cross section below multiplied by 40 m). However, this conceptual approach has uncertainties from the moment flooding occurs.

4.3.2.2 Comparison of SWR Results with Model Results for the Plan State

Regarding peak runoff, the deviations of the results achieved by the SWR from those of the model tend to be larger the shorter the event is. As validation criterion, SWR results for events with a relative deviation smaller than 10 % were classified as 'good'. As shown in Table 27, this applies to all SWR peak runoffs with a duration of 3 h and longer which have a coefficient of determination higher than 0.9.

Table 27. Comparison of the simulated (SWMM) and calculated (SWR) direct runoff of the planned residential area (70 % sealed).

Rain Event	Peak Runoff Simulated with SWMM (m^3s^{-1})	Peak Runoff Calculated with SWR (m^3s^{-1})	Runoff Difference (m^3s^{-1})	Relative Deviation (%)
1h-2a	0.209	0.309	0.100	32
1h-100a	0.820	1.169	0.349	30
3-10a	0.131	0.123	−0.008	−7
3h-25a	0.163	0.158	−0.005	−3
3h-50a	0.191	0.192	0.001	0
3h-100a	0.229	0.224	−0.005	−2
6h-10a	0.071	0.071	0.000	0
6h-25a	0.083	0.087	0.004	5
6h-50a	0.097	0.094	−0.004	−4
6h-100a	0.119	0.109	−0.009	−9
9h-10a	0.051	0.051	0.000	0
9h-25a	0.059	0.059	0.000	0
9h-50a	0.066	0.066	0.000	0
9h-100a	0.076	0.078	0.002	2
12h-10a	0.040	0.038	−0.001	−3
12h-25a	0.046	0.046	0.000	0
12h-50a	0.052	0.052	0.000	0
12h-100a	0.059	0.059	0.001	1

The two 1 h events, whose triggering rains show a varying intensity course, deviate considerably with 30 % and 32 %, respectively. It should be noted here that more accurate results for those events would have been expected if the degree of sealing for the planned area had been < 50 % (cf. correlation for 1 h events in Figure 30). However, the peak runoffs for the 1 h events calculated with SWR can be taken as the mean area response if other parameters (gradient, flow length, roughness, etc.) are still unknown in the process of planning.

Figure 36 illustrates the effect of the user-defined discharge point. The sealed residential area overlaps four subcatchments where in this precipitation scenario (6h-10a) hardly any runoff was generated in the initial state. In the planning scenario, the surface runoff increases by 0.071 m^3s^{-1} in the selected subcatchment (highlighted in yellow), while in the other three subcatchments the runoff slightly decreases or remains unchanged.

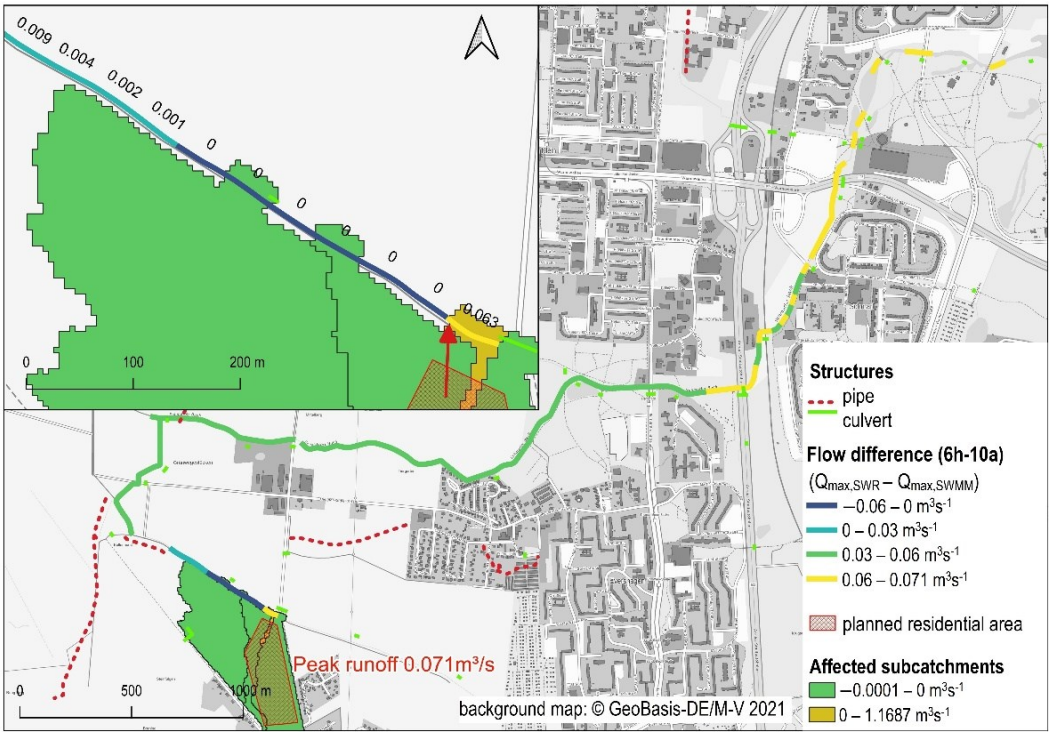

Figure 36. Peak runoff generated on the affected subcatchments and flow difference in m^3s^{-1} ($Q_{max,SWR} - Q_{max,\ SWMM}$) in plan state for the rain event 6h-10a.

When comparing SWR-calculated peak flows with those simulated by SWMM the results directly downstream of the discharge point (300 m reach) are nearly identical (cf. Figure 36). With increasing distance, however, the differences become larger. This can be explained by different hydraulic effects such as wave flattening and retention in the hydraulic model, which are not implemented in the simplified routing algorithm of the SWR. The same applies for the deviations between SWR and model directly upstream of the discharge point. Due to backwater, a part of the runoff flows upstream for a short time in the model (cf. Figure 35), which the SWR does not take into account. After heavy rainfall events, the deviations of the peak flows can be even larger than the indicated runoff difference from Table 27, due to the flow redistribution (flow direction downstream and upstream), which the SWR cannot consider.

During more extreme events such as 1h-100a (Figure 37), runoff also occurs on the unsealed subcatchments in the initial state. As the planned area drains only into the central user-defined segment (+1.169 m^3s^{-1}), the resulting difference in runoff of adjacent and intersected subcatchments is negative in the planning scenario (blue and green areas in Figure 37).

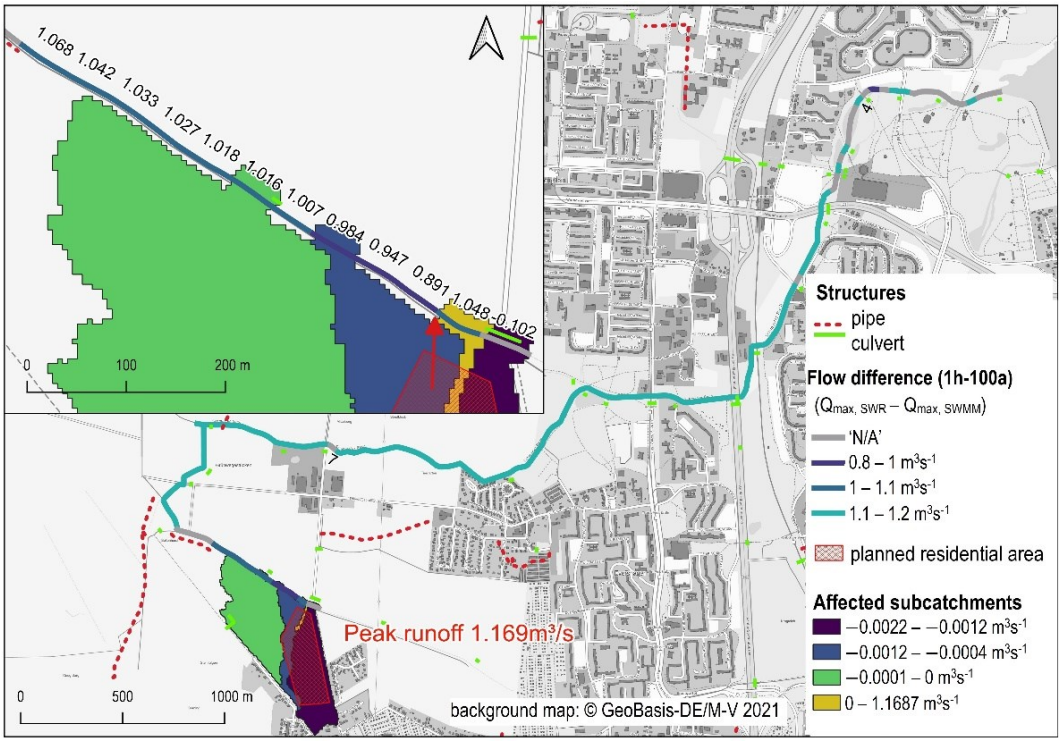

Figure 37. Peak runoff generated on the affected subcatchments and flow difference in m^3s^{-1} ($Q_{max,SWR} - Q_{max,\ SWMM}$) in plan state for the rain event 1h-100a.

Additionally, the different spatial resolutions of both approaches have an impact here: In order to be consistent with other data sets of the DSS, the SWR routes the peak runoff from the discharge point along river sections of 50 m length. By contrast, the hydraulic model in SWMM uses river segments of varying length to address any relevant changes (profile, infrastructure).

Despite the mentioned simplifying approaches, the SWR enables a rapid evaluation of the impact of land use change scenarios on flood risk. Figure 38 shows an exemplary result for flow capacities ($Q_{max,\ SWR}/Q_{full} * 100$ %) calculated by the SWR for the 6h-10a event. The colours of the stream segments indicate how critical its water level could rise in the planning scenario. Pink sections mark the areas that could potentially be affected by flooding, especially if the capacity is greater than 100 %.

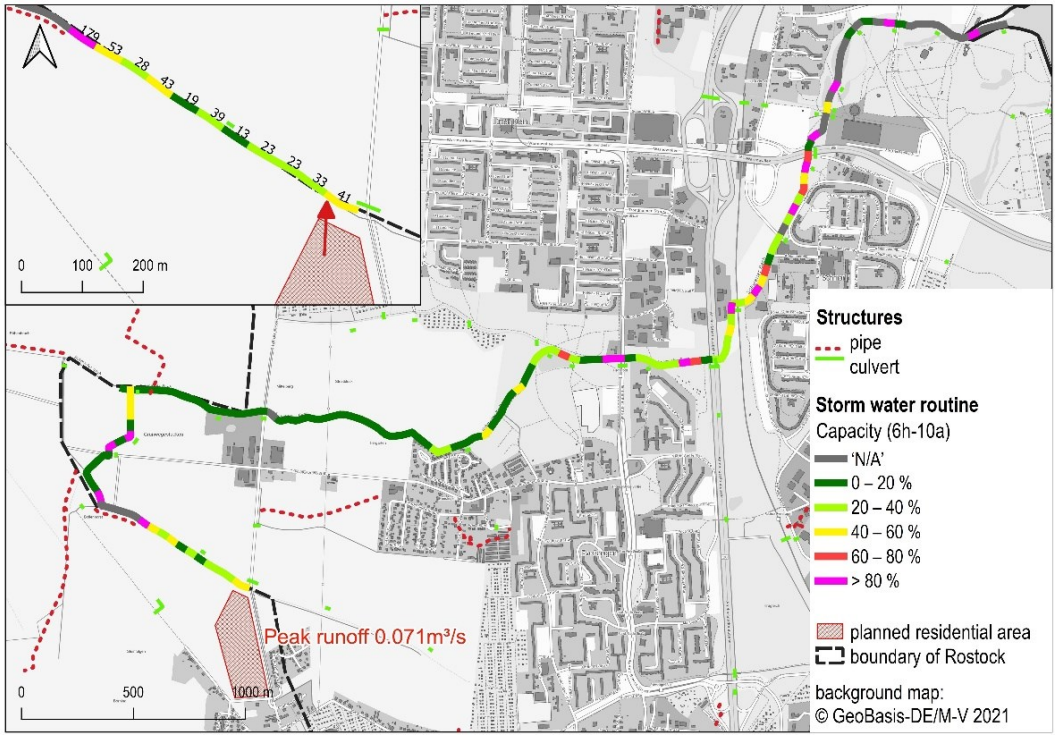

Figure 38. Stream capacity in plan state calculated with the storm water routine for the rain event 6h-10a.

4.4 Discussion

Before discussing the pros and cons of the total approach, the background and overall objectives shall be shortly remembered: The developed approach shall enable regional planners, water authorities, and other stakeholders to assess the potential impact of planned land use changes on runoff, peak flow, and related flood risk in the receiving river system. Focus water bodies are small lowland rivers, often without any monitoring data for model calibration. The often missing modelling expertise of the stakeholders is addressed replacing detailed modelling by GIS based analysis.

Summarizing parts 1 [134] and 2, the approach consists of two major steps:

1. Setup and parametrization of a detailed hydrologic/hydrodynamic model
2. Forecasting runoff change induced by land use changes and downstream flood risks applying newly developed GIS routines

For consistency, here, we shortly repeat the main findings of step 1. For the combined representation of rainfall-runoff and hydrodynamic streamflow processes, we selected the free-ware model SWMM-UrbanEVA. Since the model is physically based, it can be strictly setup and parametrized using geodata. We proposed an according workflow, including the definition of important model parameters, for lowland river

basins. The approach was shown and tested for two river basins representing two extremes of approximately 20 superior catchments in the northeast German lowlands. Even though all are located in the same climatic and geo-morphologic zone, they differ in some characteristics (e.g., average terrain slope, depth to groundwater table, dominant land use, etc.). For the here interesting peak runoff, the most hydrologically significant attribute is land use, specifically the degree of urbanity or the percentage of sealed surfaces. It was found that the model performed better at stronger urbanised river basin. As discussed there, the lower model performance is only partly due to the parametrization but rather to uncertain rain data. Though, it can be postulated that the object data of urbanised areas are in most cases better documented and the rainfall-runoff process is less complex, leading to an expectable better model performance compared to near natural river basins. Despite the proposed strict and highly automated workflow based on geodata, model setup still requires an experienced modeller.

For the flood risk analysis, model based or with the GIS tool, distinct precipitation scenarios have to be chosen. Here, we propose synthetic rains, characterised by reoccurrence interval and duration. The reoccurrence intervals have to be chosen according to the desired protection level of the different land uses. The advantages of this approach are short computation time and the availability of regionalised rain data. However, the approach is very sensitive to the initial condition of the model, when precipitation starts. Here, we pre-processed the model using rain times series to produce average flow. More detailed analysis of rain statistics may lead to more differenced settings for the initial condition according to the precipitation scenario.

Once the model exists, the analysis of land use changes can be performed by any person with basic GIS skills. As the above discussed results show, the simplified calculation of runoff, based on the rain intensity dependent peak runoff functions matches very well with the results of the physical model. Since only a static peak runoff is applied, the calculation accuracy decreases with increasing impact of dynamics, as seen here for the 1-hour precipitation scenario. The same applies for the routed stream runoff in river. For rain duration stages between 3 h to 12 h, the results of the benchmark model are met very well ($R^2 > 0.92$), while dynamic effects for short duration stages (wave flattening, backwater effects) cannot be addressed by the simplified routing algorithm. Generally, the routing tends to overestimate downstream flow effects and is, regarding the impact assessment, on the safe side.

The method presented here was specifically tailored to the study area and the available data, but if similar data sets are available, it is also very well transferable to other sites. It should be noted that the proposed peak runoff functions have been derived for the characteristics of rather flat morphology and short distances between regarded area and discharge point. In other regions or spatial conditions, the terrain gradient or the flow length may lead to deviating peak runoff coefficients. Case specific functions can be derived as described above.

A great advantage of the method is the evaluation of flood risk for planners without the setup of a complex model, as proposed by [124].

Compared to earlier approaches, assessing runoff induced by land us change in the past [115; 116], the SWR can be applied to predict runoff from future settlement areas. Additionally, not only runoff, but the actual flood risk is assessed.

For this, the method goes in two dimensions one step further: i) small scale land use change can be directly allocated and assessed; ii) the spread of runoff in the watercourse is calculated by incorporating high resolution DEM-derived stream geometry and characteristics. Considering that the method is to be used primarily in early planning phases, when it is perhaps just known that an industrial area of a certain size is to be built in a district, for example, it is a great progress if the stream hydraulic impact can be calculated immediately without prior knowledge. The method quickly shows tendencies where the water is overflowing and where additional measures may be necessary.

Following the generic framework of [127], the tool can be regarded partly as collaborative and partly as participatory modelling approach. Arguments for real collaborative modelling are:

- The modelling concept has been developed jointly
- The data for the model are accessible for or provided by the decision-makers and stakeholders
- The tool is designed interactively and embedded in a familiar GIS environment
- Results are processed and visualized for direct use (interactive planning, decision on storm water discharge applications, etc.)

However, the underlying process models set up with SWMM-UrbanEVA will require regular updates (changes of assets, land-use). Still, this requires an expert modeller.

Though the highly automated model setup strictly based on geodata (see chapter 3) simplifies model updates significantly, this task should remain in one hand to avoid inconsistent model versions at the various partners.

Currently, the tool provides one-dimensional information of flood risk. For experienced users, this is already highly informative. However, these data are less suitable for dissemination to citizens, since interpretation of an actual precise flood risk at a certain point would require well-considered 2D flood maps [129] and in best case a clear instruction, what a certain flood level means for the property and which response measures should be taken [140]. This applies even more, since information on flood risk have clear financial consequences for property owners [141]. Therefore, the main purpose of this tool is not to warn citizens, but to avoid flood risks by interactive sustainable land use planning and well-reasoned definition of tolerable storm water discharges.

In validating the results produced using the SWR tool, citizen science can be an important component (cf. [142; 143]). For example, the tool shows us stream segments that potentially spill during heavy rain events. Interviewing eyewitnesses to past flooding events can help confirm potential problem areas. More automatable is the evaluation of social media comments on flooding events (e.g., Twitter) [53]. Therefore, the latter is particularly suitable for large-scale observations.

4.5 Conclusions and Outlook

This study presents a procedure that uses a simple method to calculate the impact of planned land use changes on river flow and potential flooding. It combines a detailed hydrologic and hydrodynamic model set up for the status quo with a simplified forecast of direct runoff in the planning scenario, which is routed through the downstream watercourse network.

The SWR forecast tool is easy and intuitive to use and does not necessarily demand modelling experience. It requires only the drawing or uploading of one or more new land use polygons, the planned degree of sealing and the precipitation scenario of interest. The calculations in the GIS-DSS take only few seconds, so that several scenarios can be tested and compared efficiently — e.g., size and location of area, degree of sealing or discharge point. The advanced visualization of the results, for example the display of overloaded river sections, improves communication with stakeholders enormously [143].

The underlying physically based process model can be set-up highly automated based on available geodata. For comparable catchment characteristics, a parameter transfer from gauged to ungauged catchments is possible with tolerable loss of model accuracy.

Nevertheless, the described method is based on simplifications that may deviate more or less from reality. Three main sources of uncertainty can be mentioned here:

- Uncertainty of the input data (object data, time series of rainfall and flow) for set-up and calibration/parametrization of the process model for the current state (in the investigated river basins the resulting peak runoff error was 8 – 26 %)
- Inaccuracies in the simplified calculation of the peak runoff of a newly planned site: 0 – 32 % (depending on rain scenario)
- Inaccuracies in the propagation of additional peak runoff in the watercourse: 0 – 1.07 m^3s^{-1} downstream of discharge point and 0.06 – 1.05 m^3s^{-1} upstream (depending on rain scenario)

A flood event is a transient process, whereas the applied calculation method is stationary. Therefore, the presented method performs better for block rains of larger durations. Generally, the deviations between SWR-calculated and simulated peak flows increase with distance from the discharge point downstream due to wave attenuation and flow retention. However, this is not to be seen as a shortcoming — rather, the calculated maximum flows represent the potential changes in planned state and thus have a warning effect on the user. In the exemplary case, downstream of the imaginary discharge point, an enlargement of the pipeline was discussed, which would reduce the retention effect and might produce flooding in the lower reach.

Although the results of the SWR already provide the user with a great deal of information gain, several suggestions for improvement can be derived.

The implementation of a retention factor per stream segment would be conceivable for the routing of peak flows. These could be calculated directly from the model results as a percentage of the respective upstream flow. It would also be possible and simple to implement to stop the routing as soon as the capacity is exceeded at a point in the watercourse (typically a culvert). However, this 'improvement' has to be taken with care since it cannot be ruled out that in reality the water continues to flow on the surface of the terrain and enters the stream again at another point.

As a next step, the intersection of the flooded stream segments with the surrounding land uses (and their required level of protection/return period) would also be conceivable, e.g., by means of a 50 m buffer around the segments. The land use polygons where the required level of protection cannot be achieved could subsequently be marked with a warning colour.

What has not been addressed, yet, is the possibility of using the SWR tool for low impact design measures (LID) [144]. The required conceptual approach to link LID measures with direct runoff calculations could be derived from scenario modelling using SWMM-UrbanEVA. This upgrade of SWR would allow a fast preliminary design and allocation of LID to mitigate existing or potential flooding situations.

5 Final Discussion

5.1 Error Discussion

Modelling of the current state makes up a large part of the present work and, above all, produces the basic data for further analysis using the storm water routine. If we want to assess the model results, we must first and foremost consider the uncertainties involved. Generally, four sources of uncertainty can be distinguished regarding the (1) model concept, (2) input data, (3) parameterization and (4) initial / boundary conditions.

5.1.1 Model Concept

The choice fell on the semi-deterministic software SWMM or SWMM-UrbanEVA respectively. Besides the use of physical equations, the software contains a certain share of empirical approach. Here, we want to focus on the methods for calculating base flow and direct runoff, since these are the most important for the formation of peak flows in the stream.

In chapter 2 (article l) it was worked out that in the study area the groundwater or drainage inflows to the watercourse play a significant role across the seasons (cf. Table 9 and Figure 11). Ultimately, the groundwater or base flows in the receiving stream provide the initial condition upon which the model rainfall events are founded. We know from cross-seasonal measurement campaigns that much of the base flow comes from drainage pipes of agricultural sites. It is assumed that we are dealing with receiving surface waters only, meaning that no water percolates through the riverbed and contributes to groundwater recharge. The latter is based on the assumption that particles are deposited on the bed due to relatively low flow velocities and thus prevent bilateral exchange. The GW power function must be aligned in such a way that it does justice to these purposes.

The power function for calculating the groundwater inflow to the watercourse node (see equation 1) consists of three terms. The first term represents the influence of the distance between the groundwater table and the bottom of the stream. The second term accounts for the water depth in the stream. The third term regulates the interaction between groundwater and surface water. The terms each contain coefficients and exponents which must be calibrated by the user. By setting the coefficients of the second and third term to zero (see Table 6), they are no longer relevant for the calculations. The groundwater inflow to the stream therefore only

occurs when the groundwater level reaches a certain threshold (here 1.2 m below ground surface height, see Chap. 2.2.2.1 and Table 6) and at the same time is higher than the river bed. Strictly speaking, the chosen form of the GW function is only realistic if the drainage water has a free outlet into the receiving stream and is thus unaffected by the water level in the stream. However, this is not always and everywhere necessarily the case and becomes increasingly unlikely during flood events. This may in some rare cases contribute to a tendency towards overestimating stream flows during extreme events, although in small catchments the peaks of direct runoff and groundwater flow do not appear simultaneously. In the end, however, the chosen design of the power function resulted in the best overall cross-seasonal fit.

Direct runoff in SWMM is conceptualized using the nonlinear reservoir method, which simplifies a subcatchment as a rectangular surface that drains to a single outlet (which is part of the stream network) and has a uniform slope and flow length [69]. The surface runoff is a nonlinear differential function (based on Manning equation) of the water depth of the reservoir. The latter is solved by continuity equations. The method is relatively simple and therefore very robust. However, it has the disadvantage that no translation effects are taken into account, which means that overland flow is immediately converted to subcatchment outflow when it reaches the stream. Although the shape of the direct runoff curve can be calibrated by the area width or flow length and the Manning coefficient, the time of the peak cannot be shifted in time depending on the area size. In small catchments, such as urban areas with their branched stormwater network, this effect may be negligible. In large, near-natural agricultural catchments, however, the resulting model error becomes even larger. In fact, the agricultural catchments in the study area are generally larger than the urban catchments (cf. Figure 13 and Figure 14), suggesting that the error is particularly large in agricultural areas. But if we look at Figure 30 it can be observed that runoff is only formed on the unsealed areas during extremely high rainfall intensities (here the 1h 100a event; peak runoff coefficient is higher than zero). Therefore, the error only affects events and locations with rain intensities greater than the infiltration capacity of the soil. However, SWMM provides a workaround for the representation of runoff delay which consists in the ability to route the runoff internally between permeable and impermeable subareas. Since this would require a more complex parameterization and corresponding targeted measurements, this option was not applied within the scope of this work.

5.1.2 Input Data

5.1.2.1 Object Data

Each model is only as good as its input data. Despite the fact that the data for the study area are good in general, there are some deficiencies that need to be discussed here. This concerns in particular the input data of the hydrodynamic model as compromises had to be made here due to numerous data gaps or time consuming acquisition difficulties.

One simplification is the derivation of cross profiles (CP) from high-resolution DEM 0.2 (see Figure 39). Although it saves a lot of processing time (months to years in case of an area size of the study area) because CP do not have to be measured in the field, it has the disadvantage that the flow CP under water cannot be represented in case that water is present.

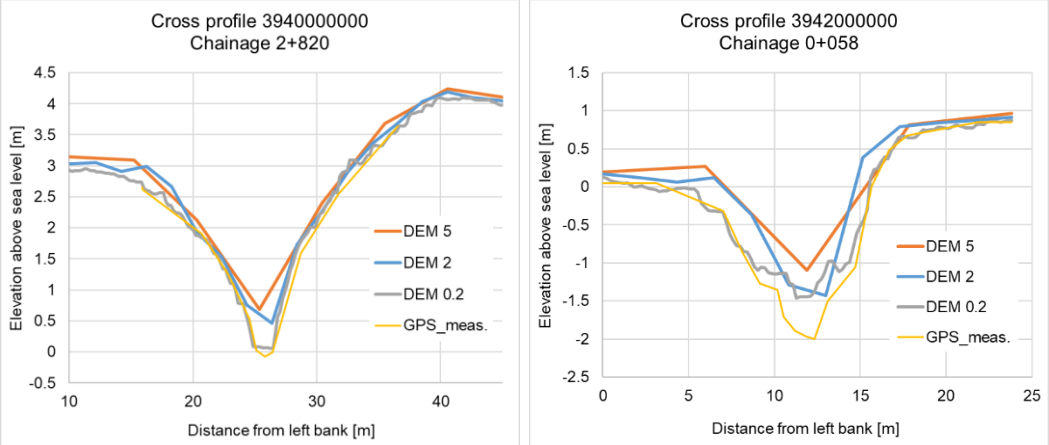

Figure 39. Examples of CP in the catchment area of the Schmarler Bach derived from DEM 5x5m, 2x2m 0,2x0,2m and measured terrestrially with GPS device; left: very good agreement of DEM_0.2 CP and CP measured terrestrially with GPS; right: deviation of about 0.5 m in bed elevation in a tributary of the Schmarler Bach (backwater effects are to be assumed).

As a result, the bed levels and thus the simulated water levels are systematically too high, especially in the medium and low flow range (see Figure 40). During flood events, the error is relativized because the missing underwater volume is distributed over a much larger base area in the upper lamella of the CP and therefore only accounts for a water level difference of a few cm (< 10 cm). This effect is attributable to the trapezoidal to parabolic shape of the cross-section.

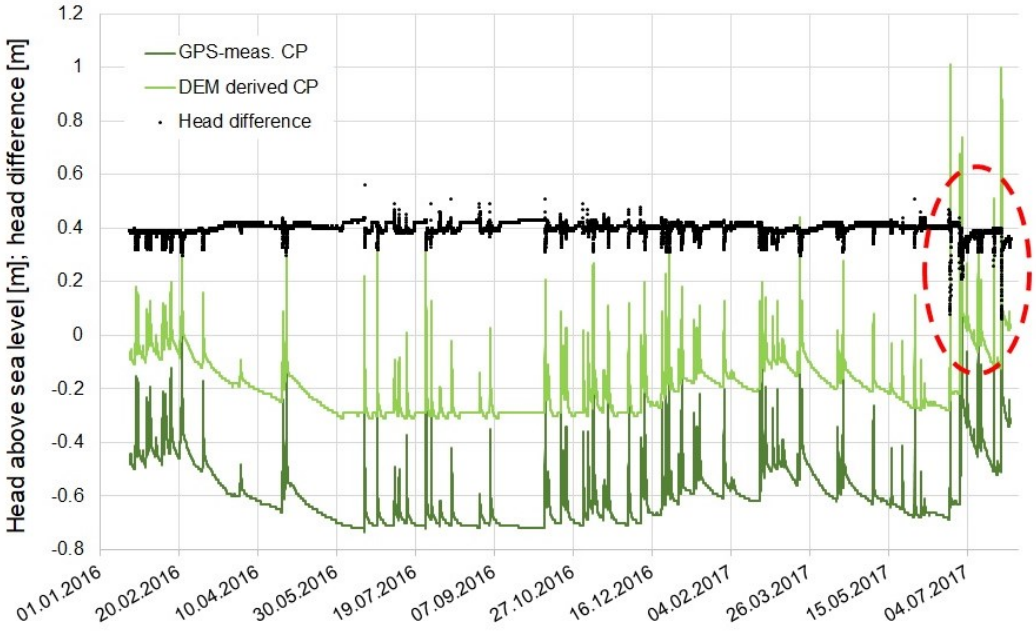

Figure 40. Simulated water level with two different Schmarler Bach models: one with CP obtained from manual GPS measurements in the field and one with CP derived from DEM_0.2 (DEM derived: chainage 2+416, invert elevation -0.31 m; GPS-measured in field, chainage 2+402.36, invert elevation -0.81 m); the red dashed ring marks the extreme events of June/July 2017 where the water level deviation is less than 10 cm.

Of course, there are ways to adjust the underwater cross profile and the bed to the real shape of the cross profile. For example, Petikas et al. [145] present an approach to edit DEM-derived cross sections whose beds appear unnaturally flat due to the fact that the transmitted beam cannot penetrate the water surface. Using the outermost measurement points of this flat plane on the left and right and the points above them, the authors construct a parabola that approximates the underwater cross-section. This way the channel's effective area and of its conveyance are increased. The algorithm is fully parametric and can be applied repeatedly [145]. However, careless use of an automated procedure can result in errors, so each (edited) CP should be verified and the user should have some knowledge of the approximate water depths of the channel in question. In the context of the present work a constructing and attaching of the underwater CP was not accomplished for different reasons:

1. A constructed bed can lead to an unrealistic zig-zag longitudinal course depending on the shape of the over water profile.
2. Overall, such procedures are considered complex and their benefit can only be quantified if the real bed elevations are known in some sections.

3. An inaccuracy of the water level of less than 10 cm at high water is sufficiently accurate for flood investigations.

For low water analyses, however, such procedures would be rewarding.

Anthropogenic stream structures, like culverts, pipes, weirs and other bed structures (riverbed slides, fish ladders, etc.) have a crucial impact on stream hydraulics, especially during flood events. In the study area, the location of these structures is known in most cases. Yet, there is often a lack of data that characterizes existing geodata more precisely (e.g., geometry data, elevation data). Regarding the diameters of culverts and pipes in the study area, we are dealing with 20 % missing values in the former case and 2 % in the latter. To close the gaps, a correlation analysis with diameter and catchment size was performed. As was to be expected, the linear relationship with a correlation coefficient of 0.3 proved not to be robust. In principle, there is a relationship between the diameter and the size of the catchment, but the size is also dependent on other overshadowing factors, including the potential for damage in the immediate vicinity of the structure. For example, a culvert under a railroad track is usually larger than one under a county road or an agricultural crossing. In addition, the shape of the profile depends on available space and the minimum cover above the structure, but also on ecological requirements. Newer culverts are often ecologically passable (containing bed sediment and otter berm if necessary) and have a larger and wider profile. In the study area, mouth profiles, rectangular and twin profiles can be found, but the standard is a circular profile, especially for pipes. In order not to pretend an accuracy or certainty that we cannot achieve due to the numerous imponderables, it was decided to determine the missing diameters nonetheless via a correlation to the catchment size. In the case that there were culverts/pipes with known diameters upstream and downstream of the structure, the constructed diameter was compared to them and corrected if necessary. If the size did not change between the known values, all pipes/culverts were assumed to be the same size between the known values, as also suggested by [146]. Still, assumed diameters should be re-measured in the field and modified in the model if detailed investigations are required. The same applies to the specification of invert heights of culverts and pipes. Nowadays, the structures are measured with tachymeter or GPS device after construction, but the data are usually stored locally in projects and not attached to the official, available geodata. For many old structures only analog data or mostly no measurement data at all are available. Since the focus

of this work was also on automating processes (and, furthermore, for the size of the study area, reviewing individual documents would have been impractical due to time constraints), the pipe / culvert inverts were constructed or interpolated as a function of surrounding streambed and terrain elevations taken from DEM. Attention must be paid here, because the slope of a pipeline is determined by the underlying invert levels and has a great influence on the water level and thus also on the filling level and the capacity of the pipe. The model results here are correspondingly vague if the slope is constructed and not measured. Nevertheless, the inclusion of the structures was necessary to route the water and to inform the stakeholders that there are structures at the respective locations that may need to be verified.

Weirs and other bed structures were not considered in the model, as no information on geometry and elevation was available. Indirectly, however, they were taken into account through the cross-sections derived from the DEM (bed slope of the model corresponds to water level slope).

In addition, eight pumping stations are operated in the study area, but information on pumps was available for only four of them. The necessary data comprises the number of pumps, startup and shutoff water levels and the flow rate depending on the head difference. Where these data were not available, an idealized pump was assumed to transfer exactly the volume flow in the inlet node, i.e. the pumping capacity is never exhausted, which is not realistic.

Some compromises also had to be made in the development of the hydrological rainfall-runoff model, more specifically in the generation of the soil model. For the mineral soils, which make up more than 90 %, hydrologically relevant parameters such as porosity, field capacity, wilting point and conductivities could be derived from the soil type. For organic soils, the determination of hydrological parameters was difficult because the degree of decomposition was not recorded, which is required for this purpose. Fortunately, some studies on the hydrological properties of peat soils have already been carried out in the study area (particularly in Pölchow, Reez and Dummerstorf). Thus, hydrological properties were adopted across the board from [147] and [148]. However, this is a gross simplification, as hydrological properties for individual sites vary greatly depending on peat type, parent substrate, genesis, drainage history and degradation. A derivation from literature values for site-specific questions is therefore very uncertain [148]. However, since peat soils largely run along the large river valleys of the Warnow and Recknitz, uncertainties associated

with this tend to affect only the lower marginal model domain and thus have less impact on the entire catchment.

5.1.2.2 Status Data

By far the most important model input variable is the rainfall in the form of a time series. It overshadows all other factors influencing the model result. The “input precipitation” has already been discussed in detail in chap. 3.3.4 and should only be listed here for the sake of completeness. Yet, it should be pointed out once again that it is of great advantage if a precipitation gauge is located directly in the calibration and validation model domain and delivers reliable, error-free values. Unfortunately, in our case a reliable gauge was not installed in those domains, which makes the assessment of the overall model error more difficult. Many scientists report that the rainfall bias is amplified into an even greater streamflow bias. In this regard, Nanding et al. provide a good tabular overview of previous studies ([149] table 1). Kobold and Sušelj [150], e.g., show at the example of two catchments in Slovenia that “an error in rainfall amount leads to 1.6 times greater error in peak discharge”. Maggioni et al. [151] predicted the propagation in flood simulation of three satellite rainfall products and report a doubling in the bias from rainfall to runoff at basin scales from 500 to 5000 km^2 in the south-eastern United States. These results once again underline the sensitivity and significance of precipitation as a key input variable. Besides the use of the time series of "conventional" precipitation gauges installed near the ground, there is also the option of using radar or satellite measurements for stream flow modelling. However, these are subject to systematic and random errors and usually have to be laboriously corrected using measured rainfall near the ground. Personal experience with radar rainfall in the study area as well as other studies show that rain gauge data nevertheless provide better results with regard to streamflow modelling. For example, Ahmed et al. [152] set up a HEC-HMS rainfall runoff model and used as input i) rain gauge data, ii) radar rainfall and iii) corrected radar rainfall. The simulated and the observed stream flows were compared and resulted in a correlation coefficient R of 0.88 for the simulation with rain gauge data, while using radar data only resulted in R = 0.75. Correcting radar data by the Mean Field Bias using rain gauge data at least improved R to 0.78. Nikolopoulos et al. [153] used three high-resolution satellite rainfall products to simulate a flash flood in the north-eastern Italian Alps and compared the results against radar-rainfall observations for the corresponding storm event. Results indicated that satellite rainfall estimates “suffered from large bias” and therefore “could not capture the basin’s hydrologic response during the flood event”

even after correction for the Mean Field Bias. Artan et al. [154] compared remotely sensed satellite and gauge-estimated rainfall data. On a daily time scale, "the two rainfall estimates were only weakly correlated", while the "match between monthly accumulated rainfall values was excellent". The authors therefore recommend the use of remotely sensed rainfall estimates for stream flow modelling only for monthly or longer time scales. Remote sensing precipitation products arguably need to be improved to be reliably used for modelling flood events. Thus, within the scope of this work, only gauge data was applied. Nevertheless, the use of remotely sensed data can be seen as a real option for sparsely gauged [154] and mountainous regions.

5.1.2.3 Spatial Discretization

Linking up with the explanations on the calculation of direct runoff (chap. 5.1.1), the spatial discretisation of the subcatchments must be discussed. For the purposes of this work, subcatchments were created so that whenever two streams meet or there is a discharge from the storm sewer network, a new subcatchment begins and is accumulated from that point upward. This has the advantage that area-specific hydrological/hydraulic information is available exactly at the points of interest (the storm sewer outfall) and at the same time not too many subcatchments arise that lead to an increase in computing time. However, the method also has the disadvantage that areas of very different sizes are created. In retrospect, it might be advisable to create the subcatchments in such a way that areas of approximately the same size are formed. Consequently, the calculation of the flow length would also have to be adjusted, otherwise all subcatchments would have the same flow length with the method used (see "Width" Table 6). Since the shape of the areas can differ greatly depending on the relief of the terrain, it would be advisable to find the average flow length for each subcatchment on the basis of DEM analysis (cf. [155]). This procedure would result in a few more calculation steps in GIS, but would strengthen the physical basis of the hydrologic runoff model and this way the derivation of model parameters based on available geodata.

5.1.3 Parameterization

In this study, the concept of parameterization is based on the consistent derivation of physical model parameters from available geodata and the transfer of calibrated model parameters to other unobserved domains where no calibration or validation is performed. The approach is primarily suitable for the use of physically based models, since their principles "are assumed to be valid for a wide range of situations, including

situations that have not yet been observed" [156]. More than half of the model parameters used are derived directly (or indirectly in case of soil properties) from geodata and, thus, are individually defined for each subcatchment. This applies in particular to parameters concerning the catchment geometry (area size, average elevation, average slope, flow length, etc.), land use, the degree of sealing, as well as the soil characteristics (average infiltration rates, porosity, etc.). Almost all parameters listed in Table 16 can be measured directly or indirectly (exceptions: crop coefficient, threshold water table elevation) and thus have a physical meaning. Therefore, the models' range of validity is expected to be wider than that of conceptual models (cf. [156]). For large areas, however, not all of these parameters can be measured for practical reasons and this is also not expedient due to the strong spatial variability; instead, they must be calibrated within plausible limits.

Within the scope of the present work, a total of 33 parameters had to be adjusted. Of these, 15 parameters had a medium or strong influence on the model result (see Table 6). The more adjusting screws a model has, the more different parameter data sets exist, which can lead to a comparable final result (problem of equifinality). This is also a consequence of the fact that mutual compensation of the influencing parameters may occur during calibration, since different parameters may have the same or opposite effects on the model result. An example of this is the crop coefficient compared to the GW loss rate. While the former increases evapotranspiration with increasing value, higher values of the latter allow more deep percolation. Both parameters have a continuous effect in each calculation step and the consequence in both cases is loss of water for the model and thus less GW inflow to the receiving stream. However, by comparing with literature values and other studies, it was possible to ensure that each individual parameter is within a plausible range of values.

There is also a potential of overparameterization resulting from the use of calibration data (for example single hydrograph of measured flow) that does not contain enough information to estimate a large number of parameters [157]. According to Wagener et al. [158], flow time series for at least one complete year are sufficient for a good calibration. Some parameters have their effect almost exclusively or primarily in the winter months (groundwater parameters), others only in summer or during certain events (maximum soil conductivity during extreme precipitation). However, the risk of overparameterization could be minimized to a large extent by choosing a cross-

seasonal calibration period that includes different and also extreme precipitation events, such as those of June/July 2017.

5.1.4 Initial and Boundary Conditions

Initial and boundary conditions are essential in numerical modelling and they also have an impact on the model result. Initial boundary conditions include all reservoir states of the individual calculation modules: the soil water content, the groundwater level and the water level in the channels of the hydraulic model. The better the initial values are estimated, the sooner the model levels out and reaches a quasi-equilibrium state. This is especially relevant for the largest reservoir in the system, the groundwater reservoir, because here it can take several (model) years to reach a realistic water level if the estimate deviates largely from the actual state. A run-in model is essential for the calibration process, otherwise the effect of the model parameters will be overshadowed, leading to wrong parameter estimates. In principle, it makes sense to set a higher initial filling level than a lower one, since filling the reservoir takes more time and thus also more computing time than emptying the reservoir. Within the scope of this study, a groundwater level of 1.3 m below ground level (and thus 10 cm below the drainage level) was assumed for each subcatchment. But even an unfavourable estimate of the initial states can be compensated by a sufficiently long model lead time. In hydrological modelling of near-natural systems, a lead time of 3 to 5 years is on the safe side. However, meteorological data must be available for the lead time and the land use must roughly correspond to that of the calibration period. Within the framework of this thesis, a negative influence of the initial conditions could be ruled out, as no drift could be seen in the fill levels anymore. Initial states are equally important for the scenario simulation, because if all reservoirs were empty, the peak flow in the stream would be comparatively lower in the case of extreme precipitation, since storage capacities must first be exhausted before discharge occurs. To avoid this, a hot start file was used, as described in chapter 3.3.5.1.

In addition to the initial system states, SWMM requires at least one boundary condition at the most downstream node of the hydrodynamic model – the outfall. The software offers several options for this. In the frame of this work, the type of outfall was not determined automatically; it was specified depending on the model constellation and the terrain conditions. A majority of the watersheds in the study area drain into the Warnow River. Since the river has a wide riverbed with a large

surface area and comparatively little water level fluctuations, it provides a good water level boundary condition for the outfalls of each sub-basin in the study area. Therefore, outfalls that drain into the Warnow were assigned the "fixed" water level of the river, taken from the DEM in the vicinity of the outfall. This means that the water level at this point cannot drop, but can rise when high flows are registered. However, the selected boundary condition at the outfall is only valid for the actual state. It is expected that the water level along the German coasts and thus also of the Lower Warnow will rise by 0.3 to 1.1 m (depending on scenario) by the end of the 21st century as a result of climate change [159]. This has not yet been taken into account by the model, but can be adjusted subsequently if necessary, especially for the rainfall scenarios with a return interval of 50 or 100 years. Nevertheless, any boundary condition set by the modeller is only an approximation to real states. However, the further one moves upstream from the boundary condition, the less significant its influence becomes. Thereby, the longitudinal slope of the hydraulic system is decisive, because the influence of the boundary condition decreases the sooner, the steeper the river bed is. The rule of thumb for the extension of the influence zone of the boundary condition is an imaginary horizontal extension of the defined fixed water level. Water levels outside this zone are considered unaffected and relatively safe.

5.2 Comparison of Modelling Concepts with External Studies

The new software extension SWMM-UrbanEVA was applied to better represent the evapotranspiration of vegetated areas and consequently to better simulate the flow in its stream system. The question now is whether the hydrological model structure of SWMM-UrbanEVA can keep up with coexisting alternatives regarding the simulation of runoff and stream flows in agricultural-urban catchments. In Chapter 1.2.2 two alternatives to SWMM have already been presented. HEC-HMS turned out to be inferior to SWMM-UrbanEva, as it only insufficiently represents groundwater discharge and also does not allow for variable (seasonal) interception storage in the evapotranspiration calculation. In contrast, the SWAT software had the highest score when comparing hydrologic rainfall-runoff components (cf. Table 2, Point 2). It was developed for predominantly agricultural catchments and therefore represents the associated hydrological processes (including surface runoff, percolation, evapotranspiration, transmission losses, pond and reservoir storage, crop growth and irrigation as well as groundwater flow) in great detail [160]. A study from Schleswig-Holstein in northern Germany presents the new SWAT+ (a revised version of the

SWAT model released in Nov 2022) based on a well comparable watershed (50 km^2 catchment size, low hydraulic gradients, near-surface groundwater, tile drainage, agricultural land use, urban influence, similar climatic conditions). An interesting finding is that, when comparing three SWAT variants, the one that achieved the best fit to the measured flow was the one that produced the lowest mean annual evapotranspiration and the largest tile drainage flow (see [161], table 4, SWAT+$_{LSU}$), as also highlighted in the frame of comparing SWMM and SWMM-UrbanEVA (Chap. 2.3.3). The SWAT+ model[3] showed "very good performance" after calibration in terms of discharge at the catchment outlet with a NSE of 0.84 [161]. The same NSE value was achieved in the present work. Thus, for a comparable catchment with a similar climate, SWMM-UrbanEVA is able to represent the relevant hydrological processes of a vegetated catchment similarly well as a representative that was developed specifically for landscapes whose dominant land use is agriculture.

With regard to the transfer of model parameters, some efforts have already been accomplished. These were introduced in chapter 1.2.1.2 (Point 3: transfer of model parameters from gauged, (neighbouring) watersheds). Three literature sources were presented that use parameter transfer for either neighbouring, internal or more distant catchments. Table 28 gives an overview of the studies and their validation results after parameter transfer (rows 1 – 3) in comparison with the results of the present study (last row).

Table 28. Comparison of NSE of different studies in model validation in the context of parameter transfer.

Study No.	Software	Location	Source	NSE [-]	Rating
1	SWMM	Norway	[39]	< 0.5[1)]	not satisfactory
				> 0.5[2)]	satisfactory
2	SWAT	Belgium	[40]	0.7[3)]	satisfactory
				0.35 – 0.5[4)]	not satisfactory
3	SWAT	Switzerland	[41]	0.49	"satisfactory" after [41]

[3] best fit was SWAT+$_{LSU}$

Study No.	Software	Location	Source	NSE [-]	Rating
Present	SWMM-UrbanEVA	north-east German lowlands	Chap. 3.3.3	0.59	satisfactory

[1)] cross validation
[2)] multi-site calibration
[3)] transfer to internal or neighbouring catchment
[4)] transfer to catchment with different environment

In the external studies, the transfer of parameters tends to lead to unsatisfactory results when parameters are transferred from a donor to a recipient catchment and the two differ in terms of climate and landscape characteristics. Transfer to internal or neighbouring catchments is less problematic. Study 1 from Norway reports that the volume error is particularly large in a long-term simulation due to inadequate evapotranspiration calculation, while study 2 reports poor fitting of base flows after parameter transfer. In the present study, in contrast, the volume error is acceptable and the fit of the base flows (see Figure 20 and Table 20) performs well. Uncertainties concern rather the discharge peaks, whereby it is assumed that the rainfall input is not fully representative for the validation area and is therefore partly responsible for the poorer model fit. However, with an NSE coefficient of 0.59, the simulation matches the measured values quite satisfactorily, even though the catchments are not contiguous and not similar in structure, yet they are located in the same region. Thus, the results of the present study turn out to be better compared to the three other studies. This could be explained by the fact that the majority of the (physical) model parameters were derived from available geodata, which enables a high spatial resolution. Only a small portion of parameters (e.g. groundwater parameters) were transferred 1:1 from one area to the other.

Web applications to provide decision support have become a trend in recent years [162]. The Storm Water Routine (SWR) represents an approach that is specifically adapted to the needs of the PROSPER-RO research project and to the existing data base. The SWR evaluation routine running in the background of the Web-GIS is based on the rational method which is relatively simple and primarily used in urban areas as well as small rural catchments. There are a variety of water management and flood related web-GIS applications with different calculation algorithms and objectives. None of these tools is directly comparable to the SWR but there are some powerful

web applications that allow similar assessments. Thus, for example, the web implementation of the Hydrological Simulation Program - FORTRAN (HSPF) [163] and also SWMM [162; 164] was realized to implement sharing and reuse of models in a network environment.

The integration of modelling software such as HSPF or SWMM into a web service framework is a very welcome advance. These web applications can be used for many different research questions; also for exploring the impact of land use changes on flood dynamics as can be done with the SWR developed in the present work. The more powerful a tool is, the more knowledge and experience is usually required to use it. That is why the application without modelling experience of the web solutions described above is questionable. Compared to these approaches the SWR method builds on high-resolution flood characteristics for the actual land use state. The method thus benefits from already calculated and validated flood characteristics and is therefore very effective, fast and reliable.

6 Final Conclusions

In this study, SWMM-UrbanEVA was used for the first time for hydrological-hydraulic modelling of an agricultural and urban influenced watershed. It turned out that due to the improved evapotranspiration calculation for different vegetation types, the model results, here related to stream flow, improved significantly compared to the official SWMM version. Above all, the base flow could be better adapted to the measured flows in the watercourse across the seasons. SWMM-UrbanEVA has consequently become an even more powerful tool, opening up new areas of application.

In particular, the use of SWMM-UrbanEVA offers great advantages in urban-rural environments, where the streamflow is characterised by both agricultural influences (tile drainage determines base flow) and stormwater discharges from sealed surfaces (which produce peak flows) – especially when the stream network and the storm sewer network mutually influence each other, as is often the case in the lowlands with shallow terrain gradients. In addition, SWMM offers the possibility of implementing blue-green measures, which are becoming increasingly important in the cities of the future.

The derivation of physical model parameters from available geodata and the transfer of the linkage between them to other areas could be successfully applied in the present study. Yet, in this process, a degradation of model performance is observed. While the base flows and smaller to moderate peak flows are met quite well even after parameter transfer, the peak flows related to heavy rainfall in the summer months in particular are overestimated and subject to uncertainty. This suggests that in principle the uncertainties concern direct runoff formation. Possible sources of error may include:

- the model concept does not consider runoff translation
- flow length is a function of area size and not derived on the basis of the digital elevation model
- shape of the subcatchment is not taken into account
- partially very different subcatchment sizes
- non-representative input precipitation (strong spatial heterogeneity during heavy rainfall in summer)

The more a donor and a receiver catchment differ in terms of climate, land use, topography, etc., the more important it is that the governing processes are physically represented and that their physical model parameters are consistently derived from geospatial data.

7 Outlook

Hydrologic/hydraulic modelling will become even more relevant in the future. Therefore, it is essential to advance digitisation and to digitally record data required for modelling (e.g. geometry and elevation data for watercourse structures) and to store and maintain it according to a standardised scheme (preferably defined on a nationwide basis via a manual or guideline). This would greatly facilitate data exchange and automation processes in the future.

Consideration should also be given to how the generated models can be further utilized. One important reuse option for the existing models is described in the Code of Practice DWA-M 102-3/BWK-M 3-3 [165]. Thus, when developing new sites and their drainage systems, but also when redesigning and revising existing systems, evidence must be provided that the hydraulic impact on the receiving stream resulting from the stormwater discharge remains within acceptable limits. Currently, many stream sections are already hydraulically overloaded due to generously granted water permits. Since the permits are reviewed every 10 years, the models can be used to strategically reduce water stress and prioritize appropriate measures. According to DWA-M 102-3/BWK-M 3-3, the flood flow of a one-year return period including stormwater discharge in the plan state should not be greater than the 2-year flood flow of the potential near-natural state, which represents an area-characteristic use of cultivated land (e.g. grassland, arable land or forest) without settlement and traffic areas. The overall objective of the approach is to maintain or restore as far as possible near-natural discharge dynamics in order to achieve the good ecological status required by the Water Framework Directive. By making minor changes to the existing models (replacing the urban land uses with, for example, grassland), the input parameters for the described procedure could be calculated with relatively little effort. Other options for subsequent use of the models are also conceivable, for example:

- Utilisation as planning tool, e.g.
  - Enlargement or reduction of pipe diameters, effects of pipe removal and watercourse renaturation
  - Installation of retention basins / profile widening
  - Effects of sealing or unsealing measures
- Simulation of different vegetation scenarios of streams and rivers by changing the Manning value

- Long-term simulation (15 - 30 years) with observed precipitation data for the generation of hydrographical characteristic values: mean flow, mean low flow[4] and mean high flow using SWMM-UrbanEVA
- Simulation of land use and/or climate scenarios (e.g. higher Baltic Sea water levels by 2021 (+ 1 m) as hydraulic boundary condition)

The SWMM-UrbanEVA models can further be upgraded to include a high-resolution urban drainage and a pollution load model, so both systems, the sewer network and the stream network, can interact and pollution can be simulated if necessary.

What SWMM models currently cannot do is predict floodplains as required by the Flood Risk Management Directive [1]. The directive stipulates the determination of parameters such as inundation extent and water depth (if relevant also flow velocity) as part of the preparation of flood hazard and flood risk maps. If it is of interest, there is the possibility to realize the floodplain analysis via a small workaround. Thus, it would be possible to expand the watercourse cross-sections generously to the left and right into the area up to a higher terrain. In this way, the stream valley can be included in the hydraulic model and the maximum water level can be read out for the different rainfall scenarios. The latter can later be intersected with the DEM in GIS to obtain the inundation area.

Another option, but one that involves more time and effort, is to couple a surface inundation model to determine floodplains, water depths and optionally overland flow velocities. Here, the coupling of a 1D [166] as well as coupling with a 2D [167] surface flooding model is possible. In contrast to the SWMM software, HEC-RAS 2D already offers the possibility for inundation simulation (e.g. [168]). This would also be desirable for SWMM, but would certainly require a few years of development work.

The models for both current and planned states can help identify the weak points in the drainage system and reveal the causes of local flooding. In this way, measures can be defined to mitigate current problems and - thinking into the future - to plan sites in such a way that their water balance is as close as possible to near natural conditions (cf. [165]) in order to prevent an aggravation of the hydraulic (and at the same time ecologic) situation.

[4] For the evaluation of low water levels, the models are less suitable due to the use of DEM cross profiles.

References

[1] European Parliament and the Council of the European Union (2007) *Directive 2007/60/EC of the European Parliament and of the Council of 23 October 2007 on the assessment and management of flood risks*.

[2] Feyen, S. &. N. [Hrsg.] (2009) *Water and urban development paradigms – Towards an integration of engineering, design and management approaches ; proceedings of the International Urban Water Conference, Heverlee, Belgium, 15-19 September, 2008*. Boca Raton, Fla.: CRC Press.

[3] Ramis, C. et al. (2019) *Climate Change and Extreme Events* in: Maurice, P. [Hrsg.] *Encyclopedia of Water*. Wiley, S. 1–17.

[4] IPCC - The Intergovernmental Panel on Climate Change (2021) *Climate Change 2021: The Physical Science Basis - Summary for Policymakers – Contribution of Working Group I to the Sixth Assessment Report of the Intergovernmental Panel on Climate Change*. https://www.ipcc.ch/report/ar6/wg1/downloads/report/IPCC_AR6_WGI_SPM_final.pdf [Zugriff am: 11. Feb. 2022].

[5] WMO - World Meteorological Organization (2021) *WMO Atlas of Mortality and Economic Losses from Weather, Climate and Water Extremes (1970 - 2019) (1970–2019)*. Geneva.

[6] Ndr (16.02.2022) *Hochwasser-Katastrophe 2002: Die Jahrhundertflut an der Elbe* [online]. https://www.ndr.de/geschichte/chronologie/Hochwasser-Katastrophe-2002-Die-Jahrhundertflut-an-der-Elbe,elbehochwasser165.html [Zugriff am: 16. Feb. 2022].

[7] RND - Redaktionsnetwerk Deutschland (19.07.2021) *Hochwasser in NRW und RLP: Vergleich mit Elbhochwasser 2002* RND RedaktionsNetzwerk Deutschland. 19. Jul. 2021.

[8] bpb - Bundeszentrale für politische Bildung (02.02.2022) *Jahrhunderthochwasser 2021 in Deutschland* Bundeszentrale für politische Bildung. 2. Feb. 2022.

[9] UNFCCC - United Nations Framework Convention on Climate Change (08.02.2022) *Climate Change Leads to More Extreme Weather, but Early Warnings Save Lives* [online]. https://unfccc.int/news/climate-change-leads-to-more-extreme-weather-but-early-warnings-save-lives [Zugriff am: 10. Feb. 2022].

[10] Umweltbundesamt (11.02.2022) *Weltweite Temperaturen und Extremwetterereignisse seit 2010* [online]. https://www.umweltbundesamt.de/themen/klima-energie/klimawandel/weltweite-temperaturen-extremwetterereignisse-seit#Chronik [Zugriff am: 11. Feb. 2022].

[11] Hall, J. et al. (2014) *Understanding flood regime changes in Europe: a state-of-the-art assessment* in: Hydrology and Earth System Sciences 18, H. 7, S. 2735–2772. https://doi.org/10.5194/hess-18-2735-2014

[12] Max-Planck-Gesellschaft (2017) *Mehr Regen im Winter, mehr Dürren im Sommer* [online]. https://www.mpg.de/11178333/klimawandel-wassersysteme [Zugriff am: 18. Feb. 2022].

[13] Regionaler Klimaatlas Deutschland (21.02.2022) *Mögliche mittlere Änderung der Starkregentage im Jahr bis Ende des 21. Jahrhunderts (2071-2100) im Vergleich zu heute (1961-1990)* [online]. https://www.regionaler-klimaatlas.de/klimaatlas/2071-2100/jahr/starkregentage/deutschland/mittlereanderung.html [Zugriff am: 21. Feb. 2022].

[14] Winkler, K. et al. (2021) *Global land use changes are four times greater than previously estimated* in: Nature communications 12, Nr. 1, p. 2501. https://doi.org/10.1038/s41467-021-22702-2

[15] EEA - European Environment Agency (11.05.2021) *Land and soil in Europe — Ever-sprawling urban concrete?* 11. Mai. 2021.

[16] EEA - European Environment Agency (2021) *Land cover country fact sheets 2000-2018 — European Environment Agency* [online]. https://www.eea.europa.eu/themes/landuse/land-cover-country-fact-sheets [Zugriff am: 23. Feb. 2022].

[17] EEA - European Environment Agency (2016) *Urban sprawl in Europe*. Luxembourg: Publications Office of the European Union.

[18] Umweltbundesamt (24.02.2022) *Bebauung und Versiegelung* [online]. https://www.umweltbundesamt.de/themen/boden-landwirtschaft/bodenbelastungen/bebauung-versiegelung [Zugriff am: 24. Feb. 2022].

[19] Copernicus Land Monitoring Service. (24.02.2022) *Sealed surface per country and NUT3 region in 2018 — Copernicus Land Monitoring Service* [online]. https://land.copernicus.eu/dashboards/imp_country_nut3_2018 [Zugriff am: 24. Feb. 2022].

[20] Europäische Kommission (24.02.2022) *Übereinkommen von Paris* [online]. https://ec.europa.eu/clima/eu-action/international-action-climate-change/climate-negotiations/paris-agreement_de [Zugriff am: 25. Feb. 2022].

[21] United Nation (25.02.2022) *United Nations Treaty Collection* [online]. https://treaties.un.org/Pages/ViewDetails.aspx?src=IND&mtdsg_no=XXVII-7-d&chapter=27&clang=_en [Zugriff am: 25. Feb. 2022].

[22] bpb - Bundeszentrale für politische Bildung (2020) *Fünf Jahre Pariser Klimaabkommen* [online]. Bundeszentrale für politische Bildung. https://www.bpb.de/kurz-knapp/hintergrund-aktuell/322749/fuenf-jahre-pariser-klimaabkommen/ [Zugriff am: 25. Feb. 2022].

[23] Bundesamt für Justiz (02.03.2022) *Verordnung über die bauliche Nutzung der Grundstücke (Baunutzungsverordnung - BauNVO)* [online]. https://www.gesetze-im-internet.de/baunvo/__19.html [Zugriff am: 2. Mrz. 2022].

[24] DWA und BWK *Arbeitsblatt DWA-A 102-1/BWK-A 3-1 Grundsätze zur Bewirtschaftung und Behandlung von Regenwetterabflüssen zur Einleitung in Oberflächengewässer – Teil 1: Allgemeines*. 2020. Aufl. DWA-Arbeitsblatt.

[25] Razavi, T.; Coulibaly, P. (2013) *Streamflow Prediction in Ungauged Basins: Review of Regionalization Methods* in: Journal of Hydrologic Engineering 18, Nr. 8, pp. 958–975. https://doi.org/10.1061/(ASCE)HE.1943-5584.0000690

[26] European Parliament and the Council of the European Union (23.10.2000) *Directive 2000/60/EC of the European Parliament and of the Council of 23 October 2000 establishing a framework for Community action in the field of water policy – WFD*.

[27] Bundesanstalt für Gewässerkunde (2020) *Fließgewässermodellierung – Wasserstandsinformation für Bundeswasserstraßen – auch zwischen Pegeln möglich?* [online]. https://www.bafg.de/DE/08_Ref/M2/03_Fliessgewmod/fliessgewmod_node.html;jsessionid=0BE087C9EDE1A35F4DE0D300B2080747.live11314 [Zugriff am: 3. Mrz. 2022].

[28] Universität Rostock Wasserwirtschaft (24.11.2022) *PROSPER-RO* [online]. https://prosper-ro.auf.uni-rostock.de [Zugriff am: 24. Nov. 2022].

[29] Brahmer, G. (2008) *Regionalisierung von Hochwasserkennwerten für Hessen*. Jahresbericht 2008. https://www.hlnug.de/fileadmin/dokumente/das_hlug/jahresbericht/2008/Jb_2008_043-050_screen.pdf [Zugriff am: 2. Sep. 2022].

[30] Ihringer, J.; Liebert, J. (2015) *Abfluss-BW, Regionalisierte Abfluss-Kennwerte Baden-Württemberg*. https://udo.lubw.baden-wuerttemberg.de/projekte/themes/bwabfl/images/custom/dokumente/bwabfl/bwabfl_151012_Doku_HQ.pdf [Zugriff am: 2. Sep. 2022].

[31] Tim G. Hoffmann; Konrad Miegel; Dietmar Mehl (2017) *Regionalisierung der Hochwasserkennwerte für das Land Mecklenburg-Vorpommern: Aktualisierung und methodische Neuerungen*. https://doi.org/10.5675/HyWa_2018,2_3

[32] Merz, R.; Blöschl, G. (2004) *Regionalisation of catchment model parameters* in: Journal of Hydrology 287, 1-4, S. 95–123. https://doi.org/10.1016/j.jhydrol.2003.09.028

[33] Zehe, E. et al. (2001) *Modeling water flow and mass transport in a loess catchment* in: Physics and Chemistry of the Earth, Part B: Hydrology, Oceans and Atmosphere 26, 7-8, S. 487–507. https://doi.org/10.1016/S1464-1909(01)00041-7

[34] Guse, B. et al. (2019) *Charakterisierung und Analyse hydrologischer Modelle im deutschsprachigen Raum* in: Wasser und Abfall 21, H. 5, S. 43–52. https://doi.org/10.1007/s35152-019-0043-x

[35] Parajka, J. et al. (2013) *Prediction of runoff hydrographs in ungauged basins* in: Blöschl, G. et al. [Hrsg.] *Runoff Prediction in Ungauged Basins*. Cambridge University Press, S. 227–269.

[36] Duan, Q. et al. (2006) *Model Parameter Estimation Experiment (MOPEX): An overview of science strategy and major results from the second and third workshops* in: Journal of Hydrology 320, 1-2, S. 3–17. https://doi.org/10.1016/j.jhydrol.2005.07.031

[37] Sun, W.; Ishidaira, H.; Bastola, S. (2012) *Calibration of hydrological models in ungauged basins based on satellite radar altimetry observations of river water level* in: Hydrological Processes 26, H. 23, S. 3524–3537. https://doi.org/10.1002/hyp.8429

[38] Waseem, M. et al. (2020) *Suitability of a Coupled Hydrologic and Hydraulic Model to Simulate Surface Water and Groundwater Hydrology in a Typical North-Eastern Germany Lowland Catchment* in: Applied Sciences 10, Nr. 4, p. 1281. https://doi.org/10.3390/app10041281

[39] Johannessen, B. G. et al. (2019) *The transferability of SWMM model parameters between green roofs with similar build-up* in: Journal of Hydrology 569, S. 816–828. https://doi.org/10.1016/j.jhydrol.2019.01.004

[40] Heuvelmans, G.; Muys, B.; Feyen, J. (2004) *Evaluation of hydrological model parameter transferability for simulating the impact of land use on catchment hydrology* in: Physics and Chemistry of the Earth, Parts A/B/C 29, 11-12, S. 739–747. https://doi.org/10.1016/j.pce.2004.05.002

[41] Andrianaki, M. et al. (2019) *Assessment of SWAT spatial and temporal transferability for a high-altitude glacierized catchment* in: Hydrology and Earth System Sciences 23, Nr. 8, pp. 3219–3232. https://doi.org/10.5194/hess-23-3219-2019

[42] US Army Corps of Engineers - Hydrologic Engineering Center (2021) *HEC-HMS (Hydrologic Modeling System)4.8* [Software]. https://www.hec.usace.army.mil/software/hec-hms/ [Zugriff am: 28. Jun. 2021].

[43] US Army Corps of Engineers - Hydrologic Engineering Center (2021) *HEC-RAS (River Analysis System)6.0* [Software]. https://www.hec.usace.army.mil/software/hec-ras/ [Zugriff am: 28. Jun. 2021].

[44] Arnold, J. G. et al. (1998) *LARGE AREA HYDROLOGIC MODELING AND ASSESSMENT PART I: MODEL DEVELOPMENT* in: JAWRA Journal of the American Water Resources Association 34, Nr. 1, pp. 73–89. https://doi.org/10.1111/j.1752-1688.1998.tb05961.x

[45] Rautenberg, K. (05.04.2019) *Automatisierte, geodatenbasierte Modellierung am Beispiel des Schmarler Baches (Engl.: Automated, geodata-based modeling using the example of the Schmarler Bach)* [Master's thesis]. University of Rostock.

[46] Gassman, P. W.; Yingkuan, W. (2015) *IJABE SWAT Special Issue: Innovative modeling solutions for water resource problems* in: Int J Agric & Biol Eng, S. 1–8.

[47] Betrie, G. D. et al. (2011) *Linking SWAT and SOBEK Using Open Modeling Interface (OpenMI) for Sediment Transport Simulation in the Blue Nile River Basin* in: Transactions of the ASABE 54, Nr. 5, pp. 1749–1757. https://doi.org/10.13031/2013.39847

[48] Rai, P. K.; Dhanya, C. T.; Chahar, B. R. (2018) *Coupling of 1D models (SWAT and SWMM) with 2D model (iRIC) for mapping inundation in Brahmani and Baitarani river delta* in: Natural Hazards 92, H. 3, S. 1821–1840. https://doi.org/10.1007/s11069-018-3281-4

[49] Zhang, L. et al. (2017) *Stream flow simulation and verification in ungauged zones by coupling hydrological and hydrodynamic models: a case study of the Poyang Lake ungauged zone* in: Hydrology and Earth System Sciences 21, H. 11, S. 5847–5861. https://doi.org/10.5194/hess-21-5847-2017

[50] Tränckner, J. et al. (2018) *KOGGE: Kommunale Gewässer gemeinschaftlich entwickeln – Ein Handlungskonzept für kleine urbane Gewässer am Beispiel der Hanse- und Universitätsstadt Rostock*. Rostock: Universität Rostock, Professur für Wasserwirtschaft, Agrar- und Umweltwissenschaftliche Fakultät.

[51] Gregersen, J. B.; Gijsbers, P. J. A.; Westen, S. J. P. (2007) *OpenMI: Open modelling interface* in: Journal of Hydroinformatics 9, H. 3, S. 175–191. https://doi.org/10.2166/hydro.2007.023

[52] Hörnschemeyer, B.; Henrichs, M.; Uhl, M. (2021) *SWMM-UrbanEVA: A Model for the Evapotranspiration of Urban Vegetation* in: Water 13, Nr. 2, p. 243. https://doi.org/10.3390/w13020243

[53] Vettermann, F.; Weinzierl, T.; Bill, R. (2018) *Monitoring Twitter Messages for Spatio-Temporal and Thematic Analysis – Twittermonitor Rostock* in: gis.Science, H. 1, S. 1–9.

[54] Rossman, L. (2015) *Storm Water Management Model – User's Manual Version 5.1* [online]. https://www.epa.gov/sites/production/files/2019-02/documents/epaswmm5_1_manual_master_8-2-15.pdf [Zugriff am: 29. Jun. 2020].

[55] Feldman, A. D. (2000) *Hydrologic Modeling System HEC-HMS Technical Reference Manual*. https://www.hec.usace.army.mil/software/hec-hms/documentation/HEC-HMS_Technical%20Reference%20Manual_(CPD-74B).pdf [Zugriff am: 26. Okt. 2020].

[56] Moynihan, K.; Vasconcelos, J. (2014) *SWMM Modeling of a Rural Watershed in the Lower Coastal Plains of the United States* in: Journal of Water Management Modeling. https://doi.org/10.14796/JWMM.C372

[57] Davis, J. P.; Rohrer, C. A.; Roesner, L. A. (2012) *Calibration of Rural Watershed Models in the North Carolina Piedmont Ecoregion | World Environmental and Water Resources Congress 2007* [online]. https://ascelibrary.org/doi/10.1061/40927%28243%29574 [Zugriff am: 22. Okt. 2020].

[58] Talbot, M. et al. (2016) *Parameterization and Application of Agricultural Best Management Practices in a Rural Ontario Watershed Using PCSWMM* in: Journal of Water Management Modeling. https://doi.org/10.14796/JWMM.C400

[59] Pretorius, H.; James, W.; Smit, J. (2013) *A Strategy for Managing Deficiencies of SWMM Modeling for Large Undeveloped Semi-Arid Watersheds* in: Journal of Water Management Modeling. https://doi.org/10.14796/JWMM.R246-01

[60] Tsai, L.-Y. et al. (2017) *Using the HSPF and SWMM Models in a High Pervious Watershed and Estimating Their Parameter Sensitivity* in: Water 9, H. 10, S. 1–16. https://doi.org/10.3390/w9100780

[61] Tu, M.-C.; Wadzuk, B.; Traver, R. (2020) *Methodology to simulate unsaturated zone hydrology in Storm Water Management Model (SWMM) for green infrastructure design and evaluation* in: PLOS ONE 15, Nr. 7, e0235528. https://doi.org/10.1371/journal.pone.0235528

[62] Feng, Y.; Burian, S. (2016) *Improving Evapotranspiration Mechanisms in the U.S. Environmental Protection Agency's Storm Water Management Model* in: Journal of Hydrologic Engineering 21, H. 10, S. 6016007. https://doi.org/10.1061/(ASCE)HE.1943-5584.0001419

[63] Hörnschemeyer, B.; Henrichs, M.; Uhl, M. *Setting up a SWMM-integrated model for the evapotranspiration of urban vegetation* in: *NOVATECH 2019*, S. 1–4.

[64] Hörnschemeyer, B. *Modellierung der Verdunstung urbaner Vegetation – Weiterentwicklung des LID-Bausteins im US EPA Storm Water Management Model*.

[65] Hörnschemeyer, B.; Henrichs, M.; Uhl, M. *Ein SWMM-Baustein für die Berechnung der Evapotranspiration von urbaner Vegetation* in: *Tagungsband Aqua Urbanica 2019*, S. 133–140.

[66] Allan, R. et al. (1998) *FAO Irrigation and Drainage Paper No. 56* [online]. http://www.fao.org/3/X0490E/x0490e00.htm [Zugriff am: 24. Sep. 2020].

[67] *Hydrologischer Atlas Deutschland – Teil 2: Hydrometeorologie*. Bundesamt für Gewässerkunde (BfG).

[68] Pettyjohn W. A.; Henning R. (1979) *Preliminary estimate of ground-water recharge rates, related streamflow and water quality in Ohio*. Ohio.

[69] Rossman, L.; Huber, W. (2016) *Storm Water Management Model – Reference Manual Volume I - Hydrology (Revised)* [online]. https://nepis.epa.gov/Exe/ZyPDF.cgi/P100NYRA.PDF?Dockey=P100NYRA.PDF [Zugriff am: 24. Sep. 2020].

[70] Hossain, S.; Hewa, G. A.; Wella-Hewage, S. (2019) *A Comparison of Continuous and Event-Based Rainfall–Runoff (RR) Modelling Using EPA-SWMM* in: Water 11, H. 3, S. 611. https://doi.org/10.3390/w11030611

[71] Rossman, L. (2017) *Storm Water Management Model – Reference Manual Volume II - Hydraulics* [online]. https://nepis.epa.gov/Exe/ZyPDF.cgi?Dockey=P100S9AS.pdf [Zugriff am: 24. Sep. 2020].

[72] Bremicker, M. (1998) *Aufbau eines Wasserhaushaltsmodells für das Weser-und das Ostsee-Einzugsgebiet als Baustein eines Atmosphären-Hydrologie-Modells* [Dissertation]. Albert-Ludwigs-Universität Freiburg.

[73] Bremicker, M. (2000) *Das Wasserhaushaltsmodell LARSIM – Modellgrundlagen und Anwendungsbeispiele* in: Freiburger Schriften für Hydrologie, H. 11, S. 1–130.

[74] Braden, H. (1985) *Ein Energiehaushalts- und Verdunstungsmodell für Wasser und Stoffhaushaltsuntersuchungen landwirtschaftlich genutzter Einzugsgebiete*. 42.

[75] Deardorff, J. W. (1978) *Efficient prediction of ground surface temperature and moisture, with inclusion of a layer of vegetation* [online]. https://doi.org/10.1029/JC083iC04p01889 [Zugriff am: 20. Okt. 2020].

[76] Dickinson, R. E. (1984) *Modeling evapotranspiration for three-dimensional global climate models*. Washington, D. C.: Geophysical Monograph Series.

[77] Kroes, J.G., van Dam, J.C., Groenendijk, P., Hendriks, R.F.A., Jacobs, C.M.J. (2008) *SWAP version 3.2 - Theory description and user manual*.

[78] Schulla, J. (2012) *Model Description WaSiM (Water balance Simulation Model)*. Zürich.

[79] Madsen H. (2000) *Automatic calibration of a conceptual rainfall–runoff model using multiple objectives* in: Journal of Hydrology, H. 235, S. 276–288.

[80] Barco, J.; Wong, K. M.; Stenstrom, M. K. (2008) *Automatic Calibration of the U.S. EPA SWMM Model for a Large Urban Catchment* in: Journal of Hydraulic Engineering 134, H. 4, S. 466–474. https://doi.org/10.1061/(ASCE)0733-9429(2008)134:4(466)

[81] Krause, P., Boyle, D., & Bäse, F. (2005) *Comparison of different efficiency criteria for hydrological model assessment* in: Advances in Geoscience 5, S. 89–97.

[82] Chiew, F. H.; McMahon, T. A. (1993) *Assessing the adequacy of catchment streamflow yield estimates* in: Australian Journal of Soil Research 31, H. 5, S. 665–680.

[83] Moriasi, D. et al. (2015) *Hydrologic and Water Quality Models: Performance Measures and Evaluation Criteria* in: Transactions of the ASABE 58, H. 6, S. 1763–1785. https://doi.org/10.13031/trans.58.10715

[84] Zenker, T. (2003) *Verdunstungswiderstände und Gras-Referenzverdunstung : Lysimeteruntersuchungen zum Penman-Monteith-Ansatz im Berliner Raum* [Doctoral Thesis]. Technische Universität Berlin, ehemalige Fakultät VII - Architektur Umwelt Gesellschaft.

[85] Zhou, T.; Endreny, T. (2020) *The Straightening of a River Meander Leads to Extensive Losses in Flow Complexity and Ecosystem Services* in: Water 12, H. 6, S. 1680. https://doi.org/10.3390/w12061680

[86] Poelmans, L.; van Rompaey, A.; Batelaan, O. (2010) *Coupling urban expansion models and hydrological models: How important are spatial patterns?* in: Land Use Policy 27, H. 3, S. 965–975. https://doi.org/10.1016/j.landusepol.2009.12.010

[87] Handayani, W. et al. (2020) *Urbanization and Increasing Flood Risk in the Northern Coast of Central Java—Indonesia: An Assessment towards Better Land Use Policy and Flood Management* in: Land 9, H. 10, S. 343. https://doi.org/10.3390/land9100343

[88] Park, G.; Park, H. (2018) *Influence analysis of land use by population growth on urban flood risk using system dynamics using system dynamics* in: Casares, J.; Passerini, G.; Perillo, G. [Hrsg.] *ENVIRONMENTAL IMPACT 2018*. Naples, Italy. WIT PressSouthampton UK, S. 195–205.

[89] Ungaro, F. et al. (2014) *Modelling the impact of increasing soil sealing on runoff coefficients at regional scale: a hydropedological approach* in: Journal of Hydrology and Hydromechanics 62, H. 1, S. 33–42. https://doi.org/10.2478/johh-2014-0005

[90] Miller, J. D.; Hutchins, M. (2017) *The impacts of urbanisation and climate change on urban flooding and urban water quality: A review of the evidence concerning the United Kingdom* in: Journal of Hydrology: Regional Studies 12, S. 345–362. https://doi.org/10.1016/j.ejrh.2017.06.006

[91] Semadeni-Davies, A. et al. (2008) *The impacts of climate change and urbanisation on drainage in Helsingborg, Sweden: Combined sewer system* in: Journal of Hydrology 350, 1-2, S. 100–113. https://doi.org/10.1016/j.jhydrol.2007.05.028

[92] Alexakis, D. D. et al. (2014) *GIS and remote sensing techniques for the assessment of land use change impact on flood hydrology: the case study of Yialias basin in Cyprus* in: Natural Hazards and Earth System Sciences 14, Nr. 2, pp. 413–426. https://doi.org/10.5194/nhess-14-413-2014

[93] U.S. Geological Survey *The 100-Year Flood* [online]. USGS - U.S. Geological Survey. https://www.usgs.gov/special-topic/water-science-school/science/100-year-flood?qt-science_center_objects=0#qt-science_center_objects [Zugriff am: 28. Jun. 2021].

[94] Song, J.-H. et al. (2019) *Regionalization of a Rainfall-Runoff Model: Limitations and Potentials* in: Water 11, Nr. 11, p. 2257. https://doi.org/10.3390/w11112257

[95] Seibert, J. (1999) *Regionalisation of parameters for a conceptual rainfall-runoff model* in: Agricultural and Forest Meteorology 98-99, S. 279–293. https://doi.org/10.1016/S0168-1923(99)00105-7

[96] Servat, E.; Dezetter, A. (1993) *Rainfall-runoff modelling and water resources assessment in northwestern Ivory Coast. Tentative extension to ungauged catchments* in: Journal of Hydrology 148, 1-4, S. 231–248. https://doi.org/10.1016/0022-1694(93)90262-8

[97] Ibrahim, A. B.; Cordery, I. (1995) *Estimation of recharge and runoff volumes from ungauged catchments in eastern Australia* in: Hydrological Sciences Journal 40, H. 4, S. 499–515. https://doi.org/10.1080/02626669509491435

[98] Garambois, P. A. et al. (2015) *Parameter regionalization for a process-oriented distributed model dedicated to flash floods* in: Journal of Hydrology 525, S. 383–399. https://doi.org/10.1016/j.jhydrol.2015.03.052

[99] Kachholz, F.; Tränckner, J. (2020) *Long-Term Modelling of an Agricultural and Urban River Catchment with SWMM Upgraded by the Evapotranspiration Model UrbanEVA* in: Water 12, Nr. 11, p. 3089. https://doi.org/10.3390/w12113089

[100] QGIS Association (2021) *QGIS Geographic Information System3.10.2* [Software]. http://www.qgis.org [Zugriff am: 10. Mrz. 2021].

[101] QGIS.org (2019) *QGIS User Guide – Release 2.18* [online]. https://docs.qgis.org/2.18/pdf/en/QGIS-2.18-UserGuide-en.pdf [Zugriff am: 9. Apr. 2021].

[102] Microsoft Ireland Operations Limited (2019) *Microsoft Excel* [Software]. https://office.microsoft.com/excel [Zugriff am: 11. Mrz. 2021].

[103] The Document Foundation (2020) *LibreOffice Calc6.2.8.2 (x64)* [Software]. https://de.libreoffice.org/discover/calc/ [Zugriff am: 11. Mrz. 2021].

[104] Waseem, M.; Kachholz, F.; Tränckner, J. (2018) *Suitability of common models to estimate hydrology and diffuse water pollution in North-eastern German lowland catchments with intensive agricultural land use* in: Frontiers of Agricultural Science and Engineering 0, H. 0, S. 0. https://doi.org/10.15302/J-FASE-2018243

[105] U.S. EPA - United States Environmental Protection Agency (2020) *Storm Water Management Model (SWMM)5.1.013* [Software]. https://www.epa.gov/water-research/storm-water-management-model-swmm [Zugriff am: 15. Mrz. 2021].

[106] Rossman, L. (2015) *Storm Water Management Model – User's Manual Version 5.1* [online]. https://www.epa.gov/sites/production/files/2019-02/documents/epaswmm5_1_manual_master_8-2-15.pdf [Zugriff am: 23. Jun. 2021].

[107] Mehl, D. et al. *Integraler Entwässerungsleitplan (IELP) für die Hansestadt Rostock – Definition von Hauptentwässerungsachsen (HEA)*. https://rathaus.rostock.de/media/rostock_01.a.4984.de/datei/Endbericht_IELP_20161108.pdf [Zugriff am: 29. Apr. 2021].

[108] Otter, J.; Königer, W. (1986) *Bemessungsregen für Kanalnetz, Regenüberläufe und Regenbecken* in: Gas-Wasser-Abwasser 66, H. 3, S. 124–128.

[109] DWA - Deutsche Vereinigung für Wasserwirtschaft, Abwasser und Abfall *Arbeitsblatt DWA-A 118. Hydraulische Bemessung und Nachweis von Entwässerungssystemen*. 2006. Aufl. DWA-Regelwerk.

[110] Junghänel, T.; Ertel, H.; Deutschländer, T. (2017) *KOSTRA-DWD-2010R Deutscher Wetterdienst – Bericht zur Revision der koordinierten Starkregenregionalisierung und -auswertung des Deutschen Wetterdienstes in der Version 2010*. https://www.dwd.de/DE/leistungen/kostra_dwd_rasterwerte/download/bericht_revision_kostra_dwd_2010.pdf?__blob=publicationFile&v=6 [Zugriff am: 7. Jul. 2021].

[111] Tretropp, S. (20.07.2017) *Unwetter in Rostock: Straßen gesperrt, Keller voll, Autos abgesoffen* svz.de. 20. Jul. 2017.

[112] Schmidtbauer, B. (04.01.2018) *Starkregen verschärft Gefahren an den Steilküsten in MV* Ostsee-Zeitung. 4. Jan. 2018.

[113] Henrichs, M. (2015) *Einfluss von Unsicherheiten auf die Kalibrierung urban-hydrologischer Modelle* [Dissertation]. Technische Universität Dresden. https://tud.qucosa.de/api/qucosa%3A28938/attachment/ATT-1/?L=1 [Zugriff am: 27. Jan. 2023].

[114] Julia Ewert (2016) *Durchführung und Auswertung von Durchflussmessungen in gefällearmen, kleinen Fließgewässern nahe der Ostseeküste (engl.: Flow measurements in low gradient, small streams near the Baltic Sea coast)* [Master's thesis]. Universität Rostock.

[115] Shi, P.-J. et al. (2007) *The effect of land use/cover change on surface runoff in Shenzhen region, China* in: CATENA 69, H. 1, S. 31–35. https://doi.org/10.1016/j.catena.2006.04.015

[116] Weng, Q. (2001) *Modeling urban growth effects on surface runoff with the integration of remote sensing and GIS* in: Environmental management 28, Nr. 6, pp. 737–748. https://doi.org/10.1007/s002670010258

[117] Kind, J.; Wouter Botzen, W. J.; Aerts, J. C. (2017) *Accounting for risk aversion, income distribution and social welfare in cost-benefit analysis for flood risk management* in: Wiley Interdisciplinary Reviews: Climate Change 8, H. 2, e446. https://doi.org/10.1002/wcc.446

[118] Deguid, K. (2021) *Here's what flood damage is predicted to cost America by 2051* [online]. https://www.weforum.org/agenda/2021/02/cost-of-flood-damage-to-u-s-homes-will-increase-by-61-in-30-years/ [Zugriff am: 19. Jul. 2021].

[119] Pit, M. (2008) *The Pitt Review - Learning lessons from the 2007 floods* [online]. Cabinet Office. https://webarchive.nationalarchives.gov.uk/20100812084907/http://archive.cabinetoffice.gov.uk/pittreview/_/media/assets/www.cabinetoffice.gov.uk/flooding_review/pitt_review_full%20pdf.pdf [Zugriff am: 2. Feb. 2021].

[120] Tsatsaris, A. et al. (2021) *Geoinformation Technologies in Support of Environmental Hazards Monitoring under Climate Change: An Extensive Review* in: ISPRS International Journal of Geo-Information 10, H. 2, S. 94. https://doi.org/10.3390/ijgi10020094

[121] Mysiak, J.; Giupponi, C.; Rosato, P. (2005) *Towards the development of a decision support system for water resource management* in: Environmental Modelling & Software 20, H. 2, S. 203–214. https://doi.org/10.1016/j.envsoft.2003.12.019

[122] Levy, J. K. (2005) *Multiple criteria decision making and decision support systems for flood risk management* in: Stochastic Environmental Research and Risk Assessment 19, H. 6, S. 438–447. https://doi.org/10.1007/s00477-005-0009-2

[123] Mysiak, J.; Giupponi, C.; Rosato, P. (2005) *Towards the development of a decision support system for water resource management* in: Environmental Modelling & Software 20, H. 2, S. 203–214. https://doi.org/10.1016/j.envsoft.2003.12.019

[124] Wang, L.; Cheng, Q. (072007) *Design and implementation of a web-based spatial decision support system for flood forecasting and flood risk mapping* in: *2007 IEEE International Geoscience and Remote Sensing Symposium*. Barcelona, Spain. IEEE, S. 4588–4591.

[125] Todini, E. (1999) *An operational decision support system for flood risk mapping, forecasting and management* in: Urban Water 1, H. 2, S. 131–143. https://doi.org/10.1016/S1462-0758(00)00010-8

[126] Mahmoud, S. H.; Gan, T. Y. (2018) *Urbanization and climate change implications in flood risk management: Developing an efficient decision support system for flood susceptibility mapping* in: The Science of the total environment 636, pp. 152–167. https://doi.org/10.1016/j.scitotenv.2018.04.282

[127] Basco-Carrera, L. et al. (2017) *Collaborative modelling or participatory modelling? A framework for water resources management* in: Environmental Modelling & Software 91, S. 95–110. https://doi.org/10.1016/j.envsoft.2017.01.014

[128] Maskrey, S. A. et al. (2016) *Participatory modelling for stakeholder involvement in the development of flood risk management intervention options* in: Environmental Modelling & Software 82, S. 275–294. https://doi.org/10.1016/j.envsoft.2016.04.027

[129] Luke, A. et al. (2018) *Going beyond the flood insurance rate map: insights from flood hazard map co-production* in: Natural Hazards and Earth System Sciences 18, H. 4, S. 1097–1120. https://doi.org/10.5194/nhess-18-1097-2018

[130] Costabile, P. et al. (2021) *Terrestrial and airborne laser scanning and 2-D modelling for 3-D flood hazard maps in urban areas: new opportunities and perspectives* in: Environmental Modelling & Software 135, S. 104889. https://doi.org/10.1016/j.envsoft.2020.104889

[131] Macchione, F. et al. (2019) *Moving to 3-D flood hazard maps for enhancing risk communication* in: Environmental Modelling & Software 111, S. 510–522. https://doi.org/10.1016/j.envsoft.2018.11.005

[132] Sanders, B. F. et al. (2020) *Collaborative Modeling With Fine-Resolution Data Enhances Flood Awareness, Minimizes Differences in Flood Perception, and Produces Actionable Flood Maps* in: Earth's Future 8, H. 1. https://doi.org/10.1029/2019EF001391

[133] Hoffmann, T. et al. (2021) *GIS-basiertes Entscheidungsunterstützungssystem für die prospektive synergistische Planung von Entwicklungsoptionen in Regiopolen am Beispiel des Stadt-Umland-Raums Rostock* in: gis.Science.

[134] Kachholz, F.; Tränckner, J. (2021) *A Model-Based Tool for Assessing the Impact of Land Use Change Scenarios on Flood Risk in Small-Scale River Systems—Part 1: Pre-Processing of Scenario Based Flood Characteristics for the Current State of Land Use* in: Hydrology 8, H. 3, S. 102. https://doi.org/10.3390/hydrology8030102

[135] Kunze, U. (2021) *Die Geschichte der Hansestadt* [online]. https://www.rostock.de/kultur/historisches/geschichte-der-hansestadt.html [Zugriff am: 11. Mai. 2021].

[136] Olaf (2019) *Rostock wächst langsamer als erwartet – Die tatsächliche Bevölkerungsentwicklung liegt in Rostock deutlich unter der Prognose von 2016 – die Grünen wollen mehr Grünflächen erhalten* [online]. https://www.rostock-heute.de/rostock-einwohnerzahl-bevoelkerungsprognose/105402 [Zugriff am: 12. Mai. 2021].

[137] Wimes – Stadt- und Regionalentwicklung (2017) *Bevölkerungsprognose 2030 für den LK Rostock – Endfassung*. http://213.254.33.168/landkreis/daten_fakten/Bevxlkerungsprognose_2030_LK_Rostock.pdf [Zugriff am: 12. Mai. 2021].

[138] Chen, S.; Hoffmann, T. G.; Mehl, D. (2021) *Digitale Gewässerkataster – Grundlage von system- und prozessorientierter Raumanalyse und -planung* in: RaumPlanung, H. 211, S. 44–51.

[139] Tränckner, J.; Mehl, D. (2017) *Überflutungsvorsorge – kommunale Gemeinschaftsaufgabe und verteilte Zuständigkeiten* in: Wasser & Abfall, 9/2017, S. 34–38.

[140] Rollason, E. et al. (2018) *Rethinking flood risk communication* in: Natural Hazards 92, H. 3, S. 1665–1686. https://doi.org/10.1007/s11069-018-3273-4

[141] Pilla, F.; Gharbia, S. S.; Lyons, R. (2019) *How do households perceive flood-risk? The impact of flooding on the cost of accommodation in Dublin, Ireland* in: The Science of the total environment 650, Pt 1, pp. 144–154. https://doi.org/10.1016/j.scitotenv.2018.08.439

[142] Sy, B. et al. (2019) *Flood hazard assessment and the role of citizen science* in: Journal of Flood Risk Management 12, S2. https://doi.org/10.1111/jfr3.12519

[143] Voinov, A. et al. (2016) *Modelling with stakeholders – Next generation* in: Environmental Modelling & Software 77, S. 196–220. https://doi.org/10.1016/j.envsoft.2015.11.016

[144] Eckart, K.; McPhee, Z.; Bolisetti, T. (2018) *Multiobjective optimization of low impact development stormwater controls* in: Journal of Hydrology 562, S. 564–576. https://doi.org/10.1016/j.jhydrol.2018.04.068

[145] Petikas, I.; Keramaris, E.; Kanakoudis, V. (2020) *A Novel Method for the Automatic Extraction of Quality Non-Planar River Cross-Sections from Digital Elevation Models* in: Water 12, Nr. 12, p. 3553. https://doi.org/10.3390/w12123553

[146] Titterington, J. et al. (2017) *Code of Practice for the Hydraulic Modelling of Urban Drainage Systems 2017 – Version 01* [online]. https://www.ciwem.org/assets/pdf/Special%20Interest%20Groups/Urban%20Drainage%20Group/Code%20of%20Practice%20for%20the%20Hydraulic%20Modelling%20of%20Ur.pdf [Zugriff am: 24. Jan. 2023].

[147] Liu, H.; Lennartz, B. (2015) *Visualization of Flow Pathways in Degraded Peat Soils Using Titanium Dioxide* in: Soil Science Society of America Journal 79, H. 3, S. 757–765. https://doi.org/10.2136/sssaj2014.04.0153

[148] Tiemeyer, B. et al. (2015) *Moorschutz in Deutschland – Instrumente und Indikatoren zu Bewertung von Biodiversität und Ökosystemleistungen*.

[149] Nanding, N. et al. (2021) *Assessment of Precipitation Error Propagation in Discharge Simulations over the Contiguous United States* in: Journal of Hydrometeorology. https://doi.org/10.1175/JHM-D-20-0213.1

[150] Kobold, M.; Sušelj, K. (2005) *Precipitation forecasts and their uncertainty as input into hydrological models* in: Hydrology and Earth System Sciences 9, H. 4, S. 322–332. https://doi.org/10.5194/hess-9-322-2005

[151] Maggioni, V. et al. (2013) *Investigating the Applicability of Error Correction Ensembles of Satellite Rainfall Products in River Flow Simulations* in: Journal of Hydrometeorology 14, H. 4, S. 1194–1211. https://doi.org/10.1175/JHM-D-12-074.1

[152] Ahmed, S. I. et al. (2022) *A Comparative Evaluation of Using Rain Gauge and NEXRAD Radar-Estimated Rainfall Data for Simulating Streamflow* in: Hydrology 9, Nr. 8, p. 133. https://doi.org/10.3390/hydrology9080133

[153] Nikolopoulos, E. I.; Anagnostou, E. N.; Borga, M. (2013) *Using High-Resolution Satellite Rainfall Products to Simulate a Major Flash Flood Event in Northern Italy* in: Journal of Hydrometeorology 14, H. 1, S. 171–185. https://doi.org/10.1175/JHM-D-12-09.1

[154] Artan, G. et al. (2007) *Adequacy of satellite derived rainfall data for stream flow modeling* in: Natural Hazards 43, H. 2, S. 167–185. https://doi.org/10.1007/s11069-007-9121-6

[155] Prodanović, D. et al. (2009) *DEM-Based GIS Algorithms for Automatic Creation of Hydrological Models Data* in: Journal of the Serbian Society for Computational Mechanics, H. 3, S. 64–85.

[156] Guinot, V.; Gourbesville, P. (2003) *Calibration of physically based models: back to basics?* in: Journal of Hydroinformatics 5, H. 4, S. 233–244. https://doi.org/10.2166/hydro.2003.0020

[157] Jakeman, A. J.; Hornberger, G. M. (1993) *How much complexity is warranted in a rainfall-runoff model?* in: Water Resources Research 29, Nr. 8, pp. 2637–2649. https://doi.org/10.1029/93WR00877

[158] Wagener, T.; Gupta, H. V.; Wheater, H. (2008) *Rainfall-Runoff modelling in gauged and ungauged catchments*. London, Singapore: Imperial College Press; World Scientific.

[159] Jensen, J. et al. (2019) *Zukunft der Meeresspiegel* [online]. https://www.deutsches-klima-konsortium.de/fileadmin/user_upload/pdfs/Publikationen_DKK/dkk-kdm-meeresspiegelbroschuere-web.pdf [Zugriff am: 27. Jan. 2023].

[160] FAO - Food and Agriculture Organization of the United Nations (28.04.2023) *Soil and Water Assessment Tool (SWAT)* [online]. https://www.fao.org/land-water/land/land-governance/land-resources-planning-toolbox/category/details/en/c/1111246/ [Zugriff am: 28. Apr. 2023].

[161] Wagner, P. D. et al. (2022) *Representation of hydrological processes in a rural lowland catchment in Northern Germany using SWAT and SWAT +* in: Hydrological Processes 36, H. 5. https://doi.org/10.1002/hyp.14589

[162] Zeng, Z. et al. (2021) *Designing and implementing an SWMM-based web service framework to provide decision support for real-time urban stormwater management* in: Environmental Modelling & Software 135, S. 104887. https://doi.org/10.1016/j.envsoft.2020.104887

[163] Lohani, V.; Kibler, D. F.; Chanat, J. (2002) *CONSTRUCTING A PROBLEM SOLVING ENVIRONMENT TOOL FOR HYDROLOGIC ASSESSMENT OF LAND USE CHANGE* in: Journal of the American Water Resources Association 38, H. 2, S. 439–452. https://doi.org/10.1111/j.1752-1688.2002.tb04328.x

[164] Xiao, D. et al. (2019) *Research on the Construction Method of the Service-Oriented Web-SWMM System* in: ISPRS International Journal of Geo-Information 8, Nr. 6, p. 268. https://doi.org/10.3390/ijgi8060268

[165] DWA und BWK *Grundsätze zur Bewirtschaftung und Behandlung von Regenwetterabflüssen zur Einleitung in Oberflächengewässer – Teil 3: Immissionsbezogene Bewertungen und Regelungen*.

[166] Chen, W.; Huang, G.; Zhang, H. (2017) *Urban stormwater inundation simulation based on SWMM and diffusive overland-flow model* in: Water Science and Technology 76, H. 12, S. 3392–3403. https://doi.org/10.2166/wst.2017.504

[167] Leandro, J.; Martins, R. (2016) *A methodology for linking 2D overland flow models with the sewer network model SWMM 5.1 based on dynamic link libraries* in: Water Science and Technology 73, Nr. 12, pp. 3017–3026. https://doi.org/10.2166/wst.2016.171

[168] Meena, R. S.; Jha, R. (2022) *Flood Inundation Modeling Using Coupled 1D–2D HEC-RAS Model in Lower Kosi River Basin, India with Limited Data* in: Chembolu, V.; Dutta, S. [Eds.] *Recent Trends in River Corridor Management: Select Proceedings of RCRM 2021*. Singapore: Springer Nature Singapore; Imprint Springer, pp. 177–188.